

**DESIGN AND IMPLEMENTATION OF MAXIMUM
POWER POINT TRACKING CONTROLLER FOR
PHOTOVOLTAIC SYSTEMS**

BY

MUHAMMAD SHERAZ

A Thesis Presented to the
DEANSHIP OF GRADUATE STUDIES

KING FAHD UNIVERSITY OF PETROLEUM & MINERALS

DHAHRAN, SAUDI ARABIA

In Partial Fulfillment of the
Requirements for the Degree of

MASTER OF SCIENCE

In

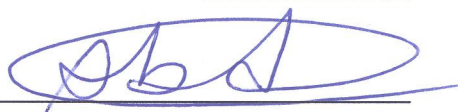
ELECTRICAL ENGINEERING

APRIL 2013

KING FAHD UNIVERSITY OF PETROLEUM & MINERALS
DHAHRAN, SAUDI ARABIA
DEANSHIP OF GRADUATE STUDIES

This thesis, written by **Muhammad Sheraz Khalid** under the direction of his thesis advisor and approved by his thesis committee, has been presented to and accepted by the Dean of Graduate Studies, in partial fulfillment of the requirements for the degree of **MASTER OF SCIENCE in ELECTRICAL ENGINEERING**.

Thesis Committee



Thesis Advisor

Prof. Mohammed A. Abido



Member

Dr. Ibrahim Mohamed El-Amin



Department Chairman

Dr. Ali Ahmad Al-Shaikhi



Member

Dr. Ali T. Al-Awami


Dean of Graduate Studies

Prof. Salam A. Zummo



21/5/13
Date

بِسْمِ اللَّهِ الرَّحْمَنِ الرَّحِيمِ

Dedicated to

My Beloved Parents

My Beloved Bhai and Bhabi

And

My best friend and Twin brother Waqas Khalid

ACKNOWLEDGMENT

In the Name of Allah, the Most Beneficent, the Most Merciful.

Praise belongs to Allah, the Lord of all the worlds (2) The All Merciful, the Very-Merciful. (3) The Master of the Day of Requital. (4) You alone do we worship, and from You alone do we seek help. (5) Take us on the straight path (6) The path of those on whom You have bestowed Your Grace, Not of those who have incurred Your wrath, nor of those who have gone astray. (7)

Al-Fatiha

In the name of Allah, the most Merciful, the most Gracious. All praise is due to Allah; we praise Him, seek His help, and ask for forgiveness. Peace be upon the Prophet Mohammad, his family, his companions, and all those who followed him until the Day of Judgment.

I then would like to show my deepest gratitude and respect to my family, especially my parents, the ones to whom I owe all the success in my life. No words can express my gratitude to them, but I pray God to bless them and reward them. Any success in my life so far is mostly charged to them and consequently any success in the future will have their signature as well.

Acknowledgements are due to King Fahd University of Petroleum and Minerals which gave me the opportunity to pursue a graduate degree and also for all the support I received in carrying out this research.

I would like to thank my research and academic supervisor Dr. Mohammed A. Abido for his continuous supervision, advice, and guidance from the very beginning of this research. He taught me how to think, analyze, and solve problems independently in a professional and friendly manner. My appreciations are also extended to my committee members: Dr. Ibrahim Mohamed El-Amin and Dr. Ali T. Al-Awami for their useful discussions. Also, many thanks to my colleagues in the Electrical Engineering department for their help and support.

I would also like to thank all my colleagues, friends and seniors at KFUPM for providing the moral support and a pleasant atmosphere. Special thanks to my best friends Waqas Khalid, Bilal Tanweer, Osama Hasan, Adnan Saeed, Khalid Naseem, Waqas Akram, Ibrar Hussain for making my time in KFUPM memorable and unforgettable.

For everyone who had helped and supported me:

Thank you very much...!!

TABLE OF CONTENTS

ACKNOWLEDGMENT	v
TABLE OF CONTENTS	vii
LIST OF TABLES	xii
LIST OF FIGURES	xiii
THESIS ABSTRACT (English).....	xix
THESIS ABSTRACT (Arabic).....	xxi
 CHAPTER 1 INTRODUCTION	 1
1.1 Background.....	1
1.2 Motivation and Problem Description.....	3
1.3 Thesis Objectives	6
1.4 Thesis Approach	7
1.4.1 Modeling of PV system	7
1.4.2 Design and implementation of MPPT controller	7
1.5 Thesis Organization	8
 CHAPTER 2 LITERATURE SURVEY	 10
2.1 PV Electrical Modeling.....	10
2.2 Maximum Power Point Tracking.....	16
 CHAPTER 3 PARAMETER ESTIMATION OF A PV MODEL	 23
3.1 Introduction.....	23
3.2 PV Electric Circuit Model	25

3.2.1 Modeling of PV Panel.....	25
3.2.2 Modeling of PV Array	28
3.3 Effect of Parameters on PV characteristics.....	31
3.4 Parameter Estimation	33
3.4.1 Proposed Approach for Parameter Estimation using DE.....	33
3.4.2 Differential Evolution (DE)	34
3.5 Implementation of PV Model in MATLAB/Simulink.....	39
3.6 Results and Discussion	41
3.6.1 Test 1: Analysis of proposed parameter estimation method.....	41
3.6.2 Test 2: Performance as a large PV array.....	51
3.6.3 Test 3: PV performance under partial shaded condition.....	53
3.6.4 Test 4: Interfacing with converter and MPPT controller	54
3.7 Conclusion	56
CHAPTER 4 PROPOSED MPPT CONTROLLER DESIGN	57
4.1 Introduction.....	57
4.2 Conventional Incremental Conductance Method.....	58
4.3 Proposed ANFIS-based MPPT	61
4.3.1 Adaptive Network-Based fuzzy Inference System (ANFIS).....	61
4.3.2 Application of ANFIS for MPPT.....	65
4.3.3 Testing of ANFIS.....	69

4.4 Result and Discussion	70
4.4.1 Test 1: Step-up change in irradiation	71
4.4.2 Test 2: Step-down change in irradiation	75
4.4.3 Test 3: Step-up change in temperature.....	79
4.4.4 Test 4: Step-down change in temperature.....	83
4.4.5 Test 5: Linear change in irradiation	87
4.4.6 Test 6: Comparison of ANFIS and FUZZY based MPPT controllers.....	90
4.4.7: Robustness of the Proposed Controller.....	94
4.5 Conclusion	95
CHAPTER 5 EXPERIMENTAL SETUP	96
5.1 Introduction.....	96
5.2 Experimental Setup Components.....	96
5.2.1 Real Time Digital Simulator (RTDS)	96
5.2.2 dSPACE Controller.....	99
5.3 Building PV model using RTDS.....	102
5.3.1 PV array	103
5.3.2 Buck Converter	104
5.3.3 Gigabit Transceiver Analogue Output (GTAO)	104
5.3.4 Gigabit Transceiver Analogue Input (GTAI)	106
5.3.5 PV system in RSCAD	109

5.4 Building MPPT in dSPACE	113
5.5 Integrating dSPACE with RTDS	114
CHAPTER 6 EXPERIMENTAL VERIFICATION OF PROPOSED ANFIS- BASED MPPT	117
6.1 Introduction.....	117
6.2 Experimental Results	117
6.2.1 Test 1: Step-up change in irradiation level	117
6.2.2 Test 2: Step-down change in irradiation level	120
6.2.3 Test 3: Step-up change in temperature level.....	123
6.2.4 Test 4: Step-down change in temperature level.....	125
6.3 Comparison of Simulation and Experimental Results	128
6.3.1 Test 1: Step-up change in irradiation level	128
6.3.2 Test 2: Step-down change in irradiation level	131
6.3.3 Test 3: Step-up change in temperature level.....	133
6.3.4 Test 4: Step-down change in temperature level.....	136
6.4 Conclusion	138
CHAPTER 7 CONCLUSION AND FUTURE WORK.....	139
7.1 Conclusion	139
7.1.1 Parameter Estimation for PV Electrical Model	139
7.1.2 Proposed ANFIS-Based MPPT controller	140
7.2 Future Work	141

APPENDIX-A: SOLAR PANEL DATASHEETS	143
APPENDIX-B: DATA EXTRACT FROM PV PANEL DATASHEETS.....	155
NOMENCLATURE AND SYMBOLS	159
ACRONYMS AND ABBREVIATIONS.....	161
REFERENCES.....	163
LIST OF PUBLICATIONS	175
VITAE.....	176

LIST OF TABLES

Table 3.1: Array parameters in relation with panel parameters.....	30
Table 3.2: Estimated values of the five parameters at STC using proposed method..	43
Table 4.2: Specification of PV panel at STC.....	69

LIST OF FIGURES

Figure 2.1: Equivalent electric circuit model of PV device.....	12
Figure 3.1: Five parameter equivalent electric circuit model of PV device.	26
Figure 3.2: Panels connected in series in an array.	29
Figure 3.3: Panels connected in parallel in an array.	30
Figure 3.4: Effect of five parameters on I-V curve.....	32
Figure 3.5: Flowchart for parameter estimation method using DE.	38
Figure 3.6: Implementation of PV array simulator in simulink.....	40
Figure 3.7: Block parameters window of PV array simulator in Simulink.	41
Figure 3.8: Partial shaded implementation of PV array simulator in simulink.	41
Figure 3.9: key points on I-V curve [113].	42
Figure 3.10: I-V characteristics for mono-crystalline technology (Sunpower 230W) (a) different irradiation level and (b) different temperature.	45
Figure 3.11: I-V characteristics for poly-crystalline technology (BP Solar 3230N) (a) different irradiation level and (b) different temperature.	46
Figure 3.12: I-V characteristics for thin-film technology (Shell ST36) (a) different irradiation level and (b) different temperature.	47
Figure 3.13: RMSE, MBE, MAE for different irradiation and temperature (a) mono- crystalline (m-Si) and (b) thin film (CIS).....	49
Figure 3.14: Cumulative error for power and current of mono-crystalline silicon technology (a) Sunpower 230W (b) SunForte PM318B00.....	50

Figure 3.15: Cumulative error for power and current of ploy-crystalline silicon technology (a) BP Solar 3230N (b) Lorentz120W LC120-12P	50
Figure 3.16: Cumulative error for power and current of thin-film technology (a) Shell ST36 (b) Kaneka U-EA110W.....	51
Figure 3.17: I-V characteristics of PV array at different irradiation (W/m^2) and constant temperature of 25^0C	52
Figure 3.18: I-V characteristics of PV array at different temperatures (^0C) and constant irradiation of 1000W/m^2	52
Figure 3.19: I-V curve for partial shaded PV array of Fig. 3.8.....	53
Figure 3.20: P-V curve for partial shaded PV array of Fig. 3.8.....	53
Figure 3.21: PV system used in test 4.....	54
Figure 3.22: Irradiation pattern used in test.....	55
Figure 3.23: Plot of PV panel power (P_{PV}) vs time.	55
Figure 4.1: Flowchart for incremental conductance method.	60
Figure 4.2: ANFIS architecture.....	61
Figure 4.3: Proposed method to generate input output data set for ANFIS training	66
Figure 4.4: PV system.....	68
Figure 4.5: Training error versus epochs for the ANFIS	70
Figure 4.6: Setup-up irradiation pattern.....	71
Figure 4.7: PV curve under normal and low irradiation conditions.	71
Figure 4.8: Characteristics of PV power output under step-up irradiation change.....	72
Figure 4.9: Plot of duty ratio under step-up change in irradiation.....	73

Figure 4.10: Characteristics of PV voltage under step-up irradiation change.	74
Figure 4.11: Characteristics of PV current under step-up irradiation change.....	74
Figure 4.12: Setup-down irradiation pattern.	75
Figure 4.13: PV curve under normal and low irradiation conditions.	75
Figure 4.14: Characteristics of PV power output under step-down irradiation change....	76
Figure 4.15: Plot of duty ratio under step-down irradiation change.	77
Figure 4.16: Characteristics of PV voltage under step-up irradiation change.	78
Figure 4.17: Characteristics of PV current under step-up irradiation change.....	78
Figure 4.18: Step-up temperature pattern.	79
Figure 4.19: PV curve under normal and low temperature conditions.	79
Figure 4.20: Characteristics of PV power output under step-up temperature change.	80
Figure 4.21: Plot of duty ratio under step-up temperature change.	81
Figure 4.22: Characteristics of PV voltage under step-up temperature change.....	82
Figure 4.23: Characteristics of PV voltage under step-up temperature change.....	82
Figure 4.24: Step-down temperature pattern.	83
Figure 4.25: PV curve under normal and low temperature conditions.	83
Figure 4.26: Characteristics of PV power output under step-down temperature change.	84
Figure 4.27: Plot of duty ratio under step-down temperature change.....	85
Figure 4.28: Characteristics of PV voltage under step-down temperature change.....	86
Figure 4.29: Characteristics of PV current under step-down temperature change.	86
Figure 4.30: linear change in irradiation.....	87
Figure 4.31: PV curve under normal and low irradiation conditions.	87

Figure 4.32: Characteristics of PV power output under linear irradiation change	88
Figure 4.33: Plot of duty ratio under linear irradiation change.....	89
Figure 4.34: Characteristics of PV voltage under linear irradiation change.....	89
Figure 4.35: Characteristics of PV current under linear irradiation change.	90
Figure 4.36: Step-down change in irradiation.....	91
Figure 4.37: PV curve under normal and low irradiation conditions.	91
Figure 4.38: Characteristics of PV power output under step-down irradiation change....	92
Figure 4.39: Plot of duty ratio under step-down irradiation change	92
Figure 4.40: Characteristics of PV voltage under step-up irradiation change	93
Figure 4.41: Characteristics of PV current under step-up irradiation change.....	93
Figure 4.42: Percentage error in P_{MP} at different irradiation level and constant temperature.....	94
Figure 4.43: Percentage error in P_{MP} at different temperature and constant irradiation...	94
Figure 5.1: Real Time Digital Simulator (RTDS) rack.....	98
Figure 5.2: dSPACE controller card.	100
Figure 5.3: dSPACE panel connector board.	102
Figure 5.4: PV array model in RTDS.	103
Figure 5.5: Buck converter in RTDS.	104
Figure 5.6: Gigabit Transceiver Analogue Output (GTAO) card.....	105
Figure 5.7: GTAO component in RSCAD.....	106
Figure 5.8: Gigabit Transceiver Analogue Input (GTAI) Card.	107
Figure 5.9: GTAI component in RSCAD.	108

Figure 5.10: PV system in RSCAD.	110
Figure 5.11: Buck converter, triangular wave generator and comparator block in RSCAD.	110
Figure 5.12: Measurement and control unit in RSCAD.	111
Figure 5.13: Arrangement of GTAO and GTAI in interfacing the RTDS with external controller.	112
Figure 5.14: ANFIS-based MPPT controller in simulink to build in dSPACE.	113
Figure 5.15: Closed loop control system.	115
Figure 5.16: A complete experimental setup.	116
Figure 6.1: PV output power (P_{PV}) for step-up change in irradiation.	118
Figure 6.2: Plot of duty ratio for step-up change in irradiation.	119
Figure 6.3: PV voltage (V_{PV}) for step-up change in irradiation.	119
Figure 6.4: PV current (I_{PV}) for step-up change in irradiation.	120
Figure 6.5: PV output power (P_{PV}) for step-down change in irradiation.	121
Figure 6.6: Plot of duty ratio for step-down change in irradiation.	121
Figure 6.7: PV voltage (V_{PV}) for step-down change in irradiation.	122
Figure 6.8: PV current (I_{PV}) for step-down change in irradiation.	122
Figure 6.9: PV output power (P_{PV}) for step-up change in temperature.	123
Figure 6.10: Plot of duty ratio for step-up change in temperature.	124
Figure 6.11: PV voltage (V_{PV}) for step-up change in temperature.	124
Figure 6.12: PV current (I_{PV}) for step-up change in temperature.	125
Figure 6.13: PV output power (P_{PV}) for step-down change in temperature.	126

Figure 6.14: Plot of duty ratio for step-down change in temperature.	126
Figure 6.15: PV voltage (V_{PV}) for step- down change in temperature.	127
Figure 6.16: PV current (I_{PV}) for step- down change in temperature.	127
Figure 6.17: Comparison of PV power (P_{PV}) for step-up change in irradiation.	129
Figure 6.18: Comparison of duty ratio for step-up change in irradiation.	129
Figure 6.19: Comparison of PV voltage (V_{PV}) for step-up change in irradiation.	130
Figure 6.20: Comparison of PV current (I_{PV}) for step-up change in irradiation.	130
Figure 6.21: Comparison of PV power (P_{PV}) for step-down change in irradiation.	131
Figure 6.22: Comparison of duty ratio for step-down change in irradiation.	132
Figure 6.23: Comparison of PV voltage (V_{PV}) for step-down change in irradiation.	132
Figure 6.24: Comparison of PV current (I_{PV}) for step-down change in irradiation.	133
Figure 6.25: Comparison of PV power (P_{PV}) for step-up change in temperature.	134
Figure 6.26: Comparison of duty ratio for step-up change in temperature.	134
Figure 6.27: Comparison of PV voltage (V_{PV}) for step-up change in temperature.	135
Figure 6.28: Comparison of PV current (I_{PV}) for step-up change in temperature.	135
Figure 6.29: Comparison of PV power (P_{PV}) for step-down change in temperature.	136
Figure 6.30: Comparison of duty ratio for step-down change in temperature.	137
Figure 6.31: Comparison of PV voltage (V_{PV}) for step-down change in temperature.	137
Figure 6.32: Comparison of PV current (I_{PV}) for step-down change in temperature.	138

THESIS ABSTRACT (ENGLISH)

Name	Muhammad Sheraz Khalid
Title	Design and Implementation of Maximum Power Point Tracking Controller for Photovoltaic Systems
Degree	Master in Science
Major Field	Electrical Engineering
Date of Degree	April 2013

In this thesis, work is done in two-fold. First, a generalized Photovoltaic (PV) array simulator is developed in MATLAB/Simulink based on the five parameters equivalent electric circuit model. The values of the five unknown parameters are estimated using a stochastic optimization technique. Estimation problem is converted into an optimization problem where Differential Evolution (DE) as an efficient optimizing technique is employed to identify the model parameters at Standard Test Condition (STC) using only the data provided by the manufacturer. The effectiveness of the proposed method is analyzed by estimating the parameters of six PV panels of three different technologies and comparing the determined I-V curves with the experimental curves given in the datasheets. These identified parameters are then used to develop a precise PV simulator which is flexible enough to simulate any number of PV panels connected in series and parallel. The robustness of the proposed simulator is demonstrated under partial shaded conditions and its performance is verified by interfacing it with an actual power electronics converter and Maximum Power Point Tracking (MPPT) controller.

Second, an efficient Adaptive Neuro-Fuzzy Inference System (ANFIS) based MPPT controller is proposed that extract maximum possible power from PV under all operating condition. The proposed ANFIS-based MPPT controller has the capacity to track the optimum point under rapidly changing irradiation conditions with less fluctuations in steady state as compared to the conventional MPPT methods. Nonlinear time domain simulations have been carried out to assess the effectiveness of the proposed controllers under different disturbances and compared with the performance of conventional Incremental Conductance (InCond) method. The obtained results demonstrate that the proposed ANFIS-based MPPT controller has better dynamic and steady state performance than the conventional method. Finally, its performance is investigated experimentally where Real Time Digital Simulator (RTDS) is utilized to simulate a PV system in real time and proposed ANFIS-based MPPT controller is developed in dSPACE DS1104. The experimental results are compared with those obtained from MATLAB simulation to assess the validity and accuracy of the proposed controller. Simulation and experimental results show that the proposed ANFIS-based MPPT has fast dynamic response and fewer fluctuations in the steady state as compare to conventional InCond method.

THESIS ABSTRACT (ARABIC)

اسم الطالب: محمد شيراز خالد

عنوان الرسالة: تصميم وتنفيذ وحدة تحكم لتتبع النقطة العظمى للطاقة الكهربية المولدة عن طريق استخدام نظم الخلايا الشمسية.

الدرجة العلمية : ماجستير العلوم

مجال التخصص الرئيسي: الهندسة الكهربائية

تاريخ الحصول علي الدرجة: أبريل 2013

في هذه الأطروحة، ويتم العمل في شقين:

أولاً، يقترح محاكاة عامة لمجموعة من نظم الخلايا الكهروضوئية (PV) وتطويرها في برنامج الماتلاب سيمولينك (MATLAB / SIMULINK) على أساس خمسة عوامل تعادل نموذج الدائرة الكهربائية المكافئة. تقدر قيم الخمسة معاملات المجهولة باستخدام تقنية التحسين لمؤشر ستوكاستيك. يتم تحويل مشكلة التقدير لمشكلة التحسين الأمثل حيث يعمل التفاضلية المتطورة (DE) كتقنية فعالة للتحسين الأمثل لتحديد عوامل النموذج في ظروف الاختبار المعاييرة (STC) فقط باستخدام البيانات المقدمة من قبل الشركة المصنعة. ويتم تحليل فعالية الطريقة المقترحة عن طريق تقدير العوامل من ستة ألواح الكهروضوئية من ثلاث تقنيات مختلفة ومقارنة منحنيات التيار الكهربي والجهد (I-V) مع منحنيات التجريبية الواردة في البيانات التصنيعية. ثم يتم استخدام هذه العوامل المحددة لتطوير محاكاة دقيقة للخلايا الكهروضوئية (PV) التي هي مرنة بما فيه الكفاية لمحاكاة أي عدد من الألواح الكهروضوئية في سلسلة متصلة علي التوالي والتوازي. ويتجلى مدى متانة هذه المحاكاة المقترحة وفقاً للشرط المظلة جزئياً ويتم التحقق من أدائها من خلال التواصل مع الكترونياات القدرة الفعلية ووحدة تحكم لتتبع النقطة العظمى للطاقة الكهربية للتحكم (MPPT).

ثانياً، يقترح تقديم نظام كفاءة الاستدلال العصبية الضبابي (ANFIS) و المستند علي وحدة التحكم MPPT والذي يستند إلى استخراج أقصى قدرة ممكنة من PV الخلايا الكهروضوئية تحت جميع ظروف التشغيل. وحدة تحكم

MPPT المستندة إلى ANFIS المقترحة لديه القدرة على تتبع النقطة المثلى في ظل ظروف الإشعاع المتغيرة سريعا مع أقل تقلبات في الحالة المستقرة. وقد تم تنفيذ محاكاة المجال الوقتي غير الخطية لتقييم فعالية وحدات تحكم المقترحة في إطار اضطرابات مختلفة ومقارنة مع أداء طريقة الموصلية التزايدية التقليدية (InCond).

النتائج المتحصل عليها أظهرت أن ANFIS المستندة إلى وحدة التحكم MPPT المقترحة لديه أداء أفضل من الناحية الديناميكية والمستقره عن الطريقة التقليدية.

وأخيرا، يتم التحقيق من أدائها تجريبيا حيث يتم استغلال محاكاة رقمية للوقت الحقيقي (RTDS) لمحاكاة نظام الخلايا الشمسية PV في الوقت الحقيقي، ويتم تطوير ANFIS المقترح القائم على وحدة تحكم MPPT في الدي سببس DS1104.

لتقييم صحة ودقة لبرنامج الماتلاب تتم مقارنة النتائج التجريبية مع تلك التي تم الحصول عليها من المحاكاة لديه MPPT وحدة تحكم المقترح القائم على ANFIS تظهر المحاكاة والنتائج التجريبية أن وحدة تحكم المقترحة استجابة ديناميكية سريعة وأقل تقلبات في الحالة المستقرة

CHAPTER 1 INTRODUCTION

1.1 BACKGROUND

In the near future, the demand of electric energy is expected to increase rapidly due to the global population growth and industrialization. This increase in energy demand requires electric utilities to increase their generation. Recent studies predict that the world's net electricity generation is expected to rise from 17.3 trillion kilowatt-hours in 2005 to 24.4 trillion kilowatt-hours (an increase of 41%) in 2015 and 33.3 trillion kilowatt-hours (an increase of 92.5%) in 2030 [1]. Currently, a large share of electricity is generated from fossil fuels, especially coal due to its low prices. However, the increasing use of fossil fuels accounts for a significant portion of environmental pollution and greenhouse gas emissions, which are considered the main reason behind global warming. For example, the emissions of carbon dioxide and mercury are expected to increase by 35% and 8%, respectively, by the year 2020 due to the expected increase in electricity generation [2]. Moreover, possible depletion of fossil fuel reserves and unstable price of oil are two main concerns for industrialized countries.

To overcome the problems associated with generation of electricity from fossil fuels, Renewable Energy Sources (RES) can participate in the energy mix. Also the

deregulation in electricity markets and the development of the distributed generation (DG) technologies are promoting the use of RES in power generation [3]. Among the renewable energy sources (RES), solar energy is the promising and photovoltaic (PV) system provides the most direct method to convert solar energy into electrical energy without environmental contamination. As PV cells are semiconductor devices, they are quite, static, having no moving or rotating parts, require very little maintenance and have very low operational cost as compared to other RES like wind energy. Despite the intermittency of sunlight, numerous PV systems have been developed in many countries around the world because of their long term benefits, benevolent fed in tariff initiatives and other schemes offered by governments to encourage the use of renewable energy sources (RES). The use of photovoltaic (PV) systems for electricity generation started in the seventies of the 20th century and is currently growing rapidly worldwide. In fact, many organizations expect a bright future for these systems because it is abundant, ubiquitous, sustainable, environmental friendly and free of cost. The world's cumulative installed capacity of PV was 23GW in year 2009. In 2011, more than 69GW of PV power is installed worldwide that can generate 85TWh of electricity per year. Among all the RES the growth rate of PV power is incomparable and reached almost 70% in year 2011 [4]. The European Photovoltaic Industry Association (EPIA) expects that the global cumulative PV capacity will reach 200 GW by the year 2020 and 800 GW by the year 2030 [4]. This large increase in the deployment of PV generation has led the researchers to work on the different issues of photovoltaic like PV cells material, modeling of the PV

panel, maximum power point tracking algorithms, power electronics converter used to integrate PV array with grid and its impact on power system etc.

1.2 MOTIVATION AND PROBLEM DESCRIPTION

PV panels are usually used in three main fields: Satellite applications, where the solar arrays provide power to satellites, Off-grid applications, where solar arrays are used to power remote loads that are not connected to the electric grid, and On-grid or grid connected applications, in which solar arrays are used to supply energy to local loads as well as to the electric grid [6]. In addition, PV panels can be used in battery chargers, solar hybrid vehicles and solar powered water pumping system. Grid-connected PV systems currently dominate the PV market and can be installed on the facades and rooftops of buildings, on the shades of parking lots or they can also be installed as power plants that inject all produced power into the grid.

Large penetration of PV power into the electricity grid would have adverse effects on the transmission\distribution network and also on the other connected generators due to the uncertainty of the irradiation. It may cause security and stability issues of power system especially in the case of disturbances. An accurate PV array model is required that can simulate its output characteristics with the change in atmosphere conditions, i.e irradiation and cell temperature, to study and analyze the impact of PV generation on the utility power grid.

The energy production of the PV generation system can be increased in two ways; one is to build a larger Photovoltaic (PV) array generation system and the other is to achieve higher efficiency in converting incident solar energy into electrical energy. Once the construction of the generation system has been completed, the only viable solution is to maximize the conversion efficiency. The output of PV array generation system depends upon factors such as sun light intensity (irradiation), ambient temperature and the configuration of PV array; each of these factors is either a fixed or natural condition and thus generally cannot be controlled. Therefore, extracting the largest amount of power under a certain given set of operating conditions becomes very important for the total economics of the PV generation system.

The output characteristics of PV device are representing by I-V and P-V curves and shown in Figure 1.1. For an arbitrary PV array configuration and set of operating conditions, it is possible to plot an I-V curve showing the array's output current as a function of its output voltage. The array's P-V curve shows the output power as a function of the output voltage. Figure 1.1 shows two such curves for an arbitrary operating condition; the solid line shows the I-V curve of a PV array while the dotted line shows the power output of that same array. The small dot marked on the P-V curve is known as the Maximum Power Point (MPP) and it represents the maximum power that can be delivered by the PV array under a specific set of operating conditions. This is the point where the PV device is most efficient in converting the solar energy into electrical energy. The MPP is not a fixed point but actually varies throughout the day depending upon the environmental conditions, i.e solar radiation and cell temperature. These

conditions are commonly known as operating conditions for PV device and are always changing with time which keeps varying the MPP. Therefore maximum power point tracking (MPPT) controller is of a great importance and an integral part of all kinds of PV systems that forces the PV system to operate at its maximum efficiency. Despite the increasing use of PV, this technology still faces a major obstacle due to its high capital cost and the low efficiency. Overall efficiency of the PV system depends upon the efficiencies of PV panels, power electronics converters and maximum power point algorithm. PV panels have efficiency around 8-20% only, converters have 95-98% and MPPT algorithm has more than 98%. The efficiencies of electronic converters and PV arrays depend on technology but MPPT efficiency can be increased by improving its tracking methods. These efficient and superior techniques can easily be installed in the previously existed PV systems by updating their software with less cost.

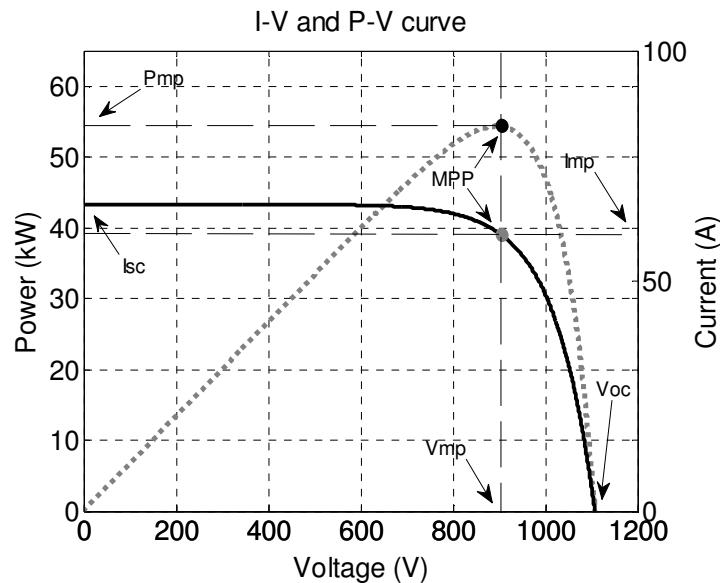


Figure 1.1: I-V and P-V curve of PV device showing key points.

1.3 THESIS OBJECTIVES

The aim of this research is to develop the efficient PV array model by optimizing its electric circuit parameters that is able to accurately simulate output characteristics, I-V and P-V curves, under all environmental conditions. This modeled PV panel will be used to analyze the effectiveness and robustness of the proposed Maximum Power Point Tracking (MPPT) controller.

Following are the major objectives that are considered in this thesis:

- 1) Developing a five-parameter PV array model that is robust to simulate the array under different conditions.
- 2) Designing optimally a proficient Maximum Power Point Tracking (MPPT) controller.
- 3) Integrating the proposed MPPT to PV array model.
- 4) Building a laboratory prototype of PV array with the proposed MPPT controller on Real Time Digital Simulator (RTDS).

1.4 THESIS APPROACH

The approach that is used to fulfill the objectives is comprised two major phases:

1.4.1 Modeling of PV system

- 1) The non-linear model of the PV panel using the five parameter equivalent electric circuit model is developed.
- 2) Behavior of the PV panel output characteristics with respect to these parameters is investigated.
- 3) Optimal values of the parameters are estimated at Standard Test conditions (STC) using the Differential Evolution (DE) technique to simulate the exact output characteristics of PV panel.
- 4) MATLAB/Simulink model of the PV array is developed that is flexible enough to simulate any number of series and parallel connected panels.
- 5) Robustness of the developed model is verified using simulation study at different operating conditions.
- 6) PV panels of three different technologies are used to verify the effectiveness of the proposed modeling.

1.4.2 Design and implementation of MPPT controller

- 1) The complete non-linear model of the PV array, DC-DC converter, Maximum power point tracking (MPPT) controller and load is developed.
- 2) Assessment of the conventional MPPT techniques is investigated and merits and demerits are studied.

- 3) A proficient Adaptive Neuro-Fuzzy Inference System (ANFIS) based Maximum power point tracker (MPPT) is developed to overcome the shortcomings of the conventional techniques.
- 4) Time domain simulations of a PV system are carried out to verify the robustness of the proposed controller under different operating conditions.
- 5) The dynamic performance of the complete system is investigated under different disturbances such as sudden change in irradiation scenario.
- 6) The proposed ANFIS-based MPPT is implemented on dSPACE DS1104.
- 7) Practical validation of the proposed controller is verified using the Real Time Digital Simulator (RTDS).

1.5 THESIS ORGANIZATION

This thesis is organized as follows:

Chapter 2 contains the brief description of PV technology and extensive literature survey on PV modeling and maximum power point tracking (MPPT) techniques.

In Chapter 3 electrical modeling of PV has been described based on a five-parameter equivalent electric circuit model and a novel method of parameters estimation has been proposed using Differential Evolution (DE).

In chapter 4 an efficient Adaptive Neuro-Fuzzy Inference System (ANFIS) based MPPT controller has been proposed and developed and its effectiveness is compared with

the conventional Incremental Conductance (InCond) method in the MATLAB/Simulink environment.

Chapter 5 describes the experimental setup used to verify the correctness of proposed ANFIS-based MPPT practically. Interfacing of the Real Time Digital Simulator (RTDS) and dSPACE DS1104 is explained. RTDS is utilized to work as a PV system and proposed ANFIS-based MPPT controller is developed in dSPACE DS4011.

Chapter 6 investigates the performance of proposed ANFIS-based MPPT experimentally. Comparison between the experimental and simulation results have been carried to validate the effectiveness of the proposed controller.

Chapter 7 presents the conclusions drawn from this research work and directions for the possible future work.

CHAPTER 2 LITERATURE SURVEY

Photovoltaic (PV) system is one of the promising RES and can provide clean energy to the electricity grid and distant loads connected through the power electronic devices. This chapter presents a detailed literature review on the PV array modeling and MPPT techniques.

2.1 PV ELECTRICAL MODELING

For the simulation study of a power system, the system designers require an efficient and regimented PV array electrical model that is capable of generating electrical characteristics, i.e I-V and P-V relationship of PV panel under different radiation and cell temperature. The output characteristic of PV devices (panels or arrays) is extremely nonlinear and it is not suitable to represent them with constant or controlled voltage/current source. Several PV electrical models have been proposed and developed by the researchers [7]-[47] including models that use experimental correlations, models that are based on analytical information of PV cell structure and models that merge both of the methods. Some of these models are described vaguely and some of them are too complex for simple power system studies.

The simplest model is temperature and radiation scaling of maximum power point [7] it requires the temperature and irradiation coefficient of the maximum power point and predicts the performance of the PV device only at one point. In [8] and [9] a method of translation of I-V curve from one environmental condition to other is adopted. In [9] bilinear interpolation method is presented that requires four practically determined I-V curves, two at different irradiances and two at different temperatures. Behavior of the PV panel at any ambient condition is determined by interpolating the four I-V curves with short circuit current and open circuit voltage to check for solar irradiance and temperature respectively. These model are quite complex and require a large amount of data that is not usually provided from the manufacturer. The most efficient and practical model for PV array simulation is developed in [10], Sandia Lab PV model. This model takes three inputs that is ambient temperature, solar radiation and wind speed and computes the voltage and current of PV array at five main points on the I-V. This model requires thirty practically determined constants to simulate the behavior of any PV panel. The values of these coefficients are available for a large number of commercial PV modules [11]. Due to the complexity of these models power system studies like load flow, maximum power point tracking, load frequency match become difficult and requires large computational time.

Electrical characteristics of the PV panel can be modeled by representing it with equivalent electrical circuit [12]. This model has the advantage over the other models due to its electrical circuit nature and the behavior of the PV array can easily be

understood in the circuit connected. This model is best suited for the dynamic and transient study of the power electronics converters.

The electric circuit based model of the PV device is further classified as an ideal diode model (three parameters model), four parameters model (R_S model), five parameters model (R_{SH} model) and double diode model (seven parameters model) as shown in Figure 2.1.

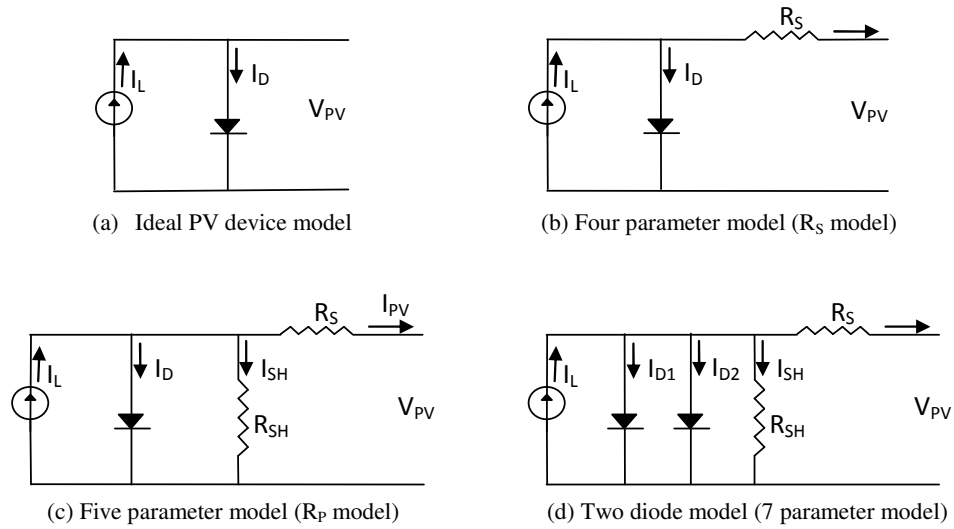


Figure 2.1: Equivalent electric circuit model of PV device.

The simplest among these models is the ideal diode model it consist of a single diode and irradiation dependant current source [13–15] as shown in Figure 2.1(a). This model needs three parameters, i.e I_L light current, I_0 saturation current of diode and “a” ideality factor of diode to generate the complete output characteristics of a PV device. Performance of this ideal model is enhanced by adding a resistance in series and it is

generally known as four parameter model (R_s -model) [12], [16–20] as shown in Figure 2.1(b). This model requires one additional parameter (R_s series resistance) to be known to characterize the I-V curve. In [20] model is implemented in MATLAB programming and examines the modeling process and illustrates the PV panel's output characteristics with the varying ambient conditions. This model is easy in implementation and provides acceptable results but its performance deteriorates at high temperatures and low irradiation [21] and also for thin film technology based PV panels [22]. Considering this issue an improved circuit based model is developed in [22–25] widely known as five parameters model (R_{SH} model) as shown in Figure 2.1(c). An additional parameter, shunt resistance, is considered which was neglected in four parameter model. Comparison of four and five parameter model is done in [18] for the mono crystalline PV panel and showed that the five parameters model is more efficient in estimating the operating current and power at different atmospheric conditions. To further improve the efficiency of the circuit based model some authors used the two diode model (seven parameters model) [21], [26–28] as shown in Figure 2.1(d). The number of parameters to be computed during simulation is increased by inclusion of an extra diode that will make the model computationally inefficient. The competency of the two diode model over R_s -model and R_{SH} -model is shown in [21]. To make the model computational efficient values of some parameters are assumed to be constant which deteriorates its performance under the partial shading condition. The authors in [23] suggested that the five parameters model is a good compromise between accuracy and simplicity and it is the most widely used model in the literature. Behavior of the PV device under the partial shaded condition

has been studied by various researchers [29–32]. This situation may happen due to passing clouds, dust or snow covering the PV panel, shadows of trees or birds litters. In partial shading state the un-shaded cells of the PV panel become more forward biased and the shaded cells become reverse bias. When the reverse voltage increases beyond the breakdown voltage of the cell the “hot-spot” phenomenon take place and causes irreparable damage to the cell. This problem is solved by using by-pass diodes [29]. Due to by-pass diodes, multiple peaks occur in the P-V characteristics, which add additional complexity in modeling the PV array. In [30] impact on the I-V curve and output of the PV panel due to the partial shading condition is studied. Experimental work on panel shading was performed in [31] . A comprehensive MATLAB based modeling of the shaded PV array is carried out in [32].

The most challenging part in the implementation of equivalent circuit based models is to identify the values of these parameters as their values are not provided in the solar panel catalogues. The performance and competence of these models are entirely dependent on these parameters and their values should be estimated using accurate and efficient algorithms. Two approaches are widely used for the estimation, one approach approximate the original I-V and P-V characteristics using the selected key points, i.e. the short circuit point, open circuit point and maximum power point [33], [34] while the other approach works on the curve fitting principle [35–37]. Both methods have their own pros and cons. The latter have the advantage that it considers all the experimental data. However, it has the difficulty of artificial solutions [33] and requires large number of experimental data which is not usually provided by the manufacturer. The preceding

method is simple and fast as compared to the curve fitting method and adopted in this study. However, it optimizes the values of parameters only at the selected key points[36].

Several algorithms have been utilized by the researchers for the identifications of these parameters. The simplest method is to assume the value of one parameter and calculate other parameters using analytical equations and iterative methods [16], [20], [25], [38], [39] [40]. In [38] authors suppose the value of “ a ” and find the values of R_S and R_{SH} concurrently by numerical technique and values of I_o and I_L analytically. An iterative technique is utilized in [20][16] to find the valued of R_S and “ a ” by neglecting the effect of R_{SH} . In [39] R_{SH} is ignored by considering it to be infinite and value of “ a ” is taken constant and compute other parameters by solving the analytical equations. In Ref. [40] authors have solved the non-linear I-V characteristics equation of PV by simplifying the highly complex diode current equation. These assumptions degrade the efficiency of these methods and limit their scope [20]. In [22][41] authors used a nonlinear equation solver software for the solution of non-linear equations to find the model parameters. These softwares packages have limitation and cannot provide result for all the PV panels. To estimate the values of these parameters accurate and efficient algorithms should be used for the optimization process. In [42] authors present a novel scheme for determination of the five parameters. Their method works on the principle of adjusting the I-V and P-V curve at three key point short circuit point, open circuit point and maximum power point and find out the best values of model parameters that result in the slightest error at these three key points. An iterative method is implemented in [43] for

the estimation of parameters. This method uses simplified I-V equation and results in fast convergence.

In recent year some intelligent techniques like fuzzy Logic [44] and artificial neural network [45][46] have been employed to identify the values of these parameters. The results of these techniques are quite promising but they show problems when parameter identification method is integrated in PV simulator. As fuzzy logic controllers have fuzzification, rule base table and defuzzification which require large memory and neural network requires large amount of training data. Optimization technique can be used for the prediction of model parameters. Ikegami et al. [35] minimized the error in the operating current using the empirically calculated current and voltage points by means of Levenberg-Marquardt optimization technique. Evolutionary Algorithm (EA) techniques are very effective stochastic optimization methods as they have the ability to deal with non-linear objective functions. Genetic algorithm (GA) [47] and particle swarm optimization (PSO) [48] are utilized to optimize the model parameters.

2.2 MAXIMUM POWER POINT TRACKING

Maximum power point tracking (MPPT) controller is a crucial part of the PV system. It tracks and extracts the maximum possible power from the PV array under different operating conditions and improves the overall efficiency of a complete PV system. The idea of MPPT is not new, many MPPT methods have been proposed by researchers [47]-[105]. These methods differ in cost, sensor required, complexity, reliability, convergence speed, efficiency and hardware implementation. A comprehensive analysis of nineteen

MPPT techniques have been presented in [49–52]. Among these techniques Perturb and Observe (P&O) method [53][54] and Hill Climbing (HC) method [55] are most popular and practically available because of their simplicity and satisfactory results. Both methods work on the same principle of perturbing the PV system and observing its effect on the PV panel power output. Difference lies in the method of perturbation, in P&O panel output voltage/current is perturbed while in Hill climbing duty cycle of DC-DC-converter is perturbed. But these methods have drawbacks associated with them like large convergence time, fluctuations in the steady state and possible failure to track MPP in rapidly changing conditions[49][50]. To overcome these shortcoming and to improve the efficiency of these methods many modified P&O and HC methods have been proposed. Predictive and adaptive P&O method is proposed in [56]; prediction is undertaken by parabolic interpolation of last three operating points. Adaptive change in voltage is provided depending upon the measured power. Authors show that the proposed method has less convergence time than the simple P&O technique. A survey on P&O and modified P&O methods has been carried out in [57] and a modified P&O method is proposed, named PI-P&O, based on the adaptive tracking and ensures no steady state fluctuations and do not require any preset system dependent constants. Comparison with already existed adaptive methods is presented and results showed the effectiveness of the proposed method. Femia N. et al. [58] developed the optimized P&O method based on the dynamics of the particular converter used. In [59–61] a superior P&O method has been proposed that can track the MPP in the rapidly varying irradiation situation; known as dP-P&O. An extra measurement has to perform to calculate the PV power within the

MPPT sampling time. dP-P&O method separates the effects of insolation and perturbation change and then optimizes the tracker according to the change in irradiation. To improve the speed and reduce the steady state oscillations, Ishaque et al. proposed an improved particle swarm optimization technique [62]. In [63], [64] an adaptive hill climbing technique is presented in which control mode switching and automatic parameter tuning is implemented to improve the steady state and dynamic response of the PV system. Reference [65] presents the Incremental Conductance (InCond) method that considers the inability of P&O and Hill climbing methods to relate the change in PV power to the change in irradiation in the rapidly varying environment condition. This algorithm can be assumed as an improvement of the P&O method. As the name implies, the algorithm uses the incremental conductance as background of operation, which is the current divided by the voltage (inverted resistance). Comparative study of the MPPT techniques is carried out in [66] [67] and it is demonstrated using MATLAB/Simulink based simulation that InCond can outperforms the P&O method in rapidly changing environmental condition. Hardware implementation of this method with direct control method is demonstrated in [68]. Analog maximum power point tracking technique (AMPPT) is proposed for fast tracking and high efficiency in [69]. Authors used a wide range current multiplier to find the PV panel power gradient situation and then track the MPP. Maximum power point controller for low power PV application is discussed in [70] [71] and for the stand alone PV water pumping system in [72]. The simplest MPPT methods are based on approximation and known as fractional open circuit voltage and fractional short circuit current. In [73][74] fractional open circuit voltage method is

implemented based on the fact that the ratio of the maximum power voltage (V_{mp}) and the open circuit voltage (V_{oc}) are approximately linearly proportional under varying weather conditions. The yielded power from PV panel definitely is less than the real power at MPP because of the obvious reason that this method is based on approximation. Following the same pattern fractional short circuit current method is shown in [75], [76] which uses the fact that the ratio of maximum power current (I_{mp}) and short circuit current (I_{sc}) are linearly proportional. This method has the same drawbacks and weakness as that of fractional open circuit voltage method.

In recent years some Evolutionary Algorithm (EA) [77] and Artificial Intelligence Techniques (AIT) like Artificial Neural Network (ANN) [78] and Fuzzy Logic [79] have been implemented to prevail over these problems as they have the ability to deal with non-linear objective functions. The Evolutionary programming techniques like tabu search, differential evolution, evolutionary programming, particle swarm optimization and genetic algorithm have been implemented in [62], [80–86]. Results show that the use of these techniques along with the conventional methods improves the dynamic and steady state response of the MPPT controllers. The use of artificial neural network (ANN) technique for the MPPT controller design is given in [84], [87–90]. Results and comparison demonstrated by the authors showed that ANN based MPPT controller has much better tracking than other MPPT algorithms [51]. ANN can map the input output nonlinear functions but it does not have heuristic nature and work as a black box that restricts its use in MPPT design. The fuzzy-inference system (FIS) based MPPT has been proposed in [79], [91–98]. Almost all proposed FIS in the literature have the same output

that is change in duty cycle (dD), but they differ in their input variables, linguistic rules and membership functions. Most of the FIS based MPP controllers have error and change in error as input variables. Basically this error and change in error represent the slope and change in slope of the P-V curve. The problem with such inputs is that, as the duty cycle is not considered as input, operating point moves away from the original MPP in the varying atmospheric condition [91].

In [94] a fuzzy controller is presented with the inputs of array power variation and duty cycle. The dynamic behavior is improved in changing ambient conditions but this method added the steady state oscillation in the PV output which causes the power loss. Fuzzy cognitive networks are used in [98] to improve the efficiency of the fuzzy-based MPP tracker but it added complexity in the hardware design. In [79], [97] drawbacks of Hill Climbing method have been discussed in detail and improvement in the conventional Hill climbing method is demonstrated by fuzzifying its rules. In [99–101] Fuzzy Logic based MPPT controller optimized by evolutionary programming techniques are proposed. These techniques are used to optimize the membership function values of FIS MPPT with the objective function to minimize the tracking speed and reduce steady state oscillations.

FIS has two major advantages one is that it allows setting the fuzzy rules that are quite close to the real world processes and the other is their interpretability, i.e it can explain the reason of particular output occurrence. On the other hand it has some inadequacies like it requires expert knowledge in defining the fuzzy rule base and requires lot of effort and time in tuning the membership function parameters. While in the case of ANN situation is completely converse, it can be trained but cannot give details about the

performance of a system for an output and act as a black box. Combining FIS with ANN results in a powerful AI technique known as Adaptive Network-Based Fuzzy Inference System (ANFIS) [102], [103].

To build ANFIS-based MPPT controller major challenge lies in gathering a large amount of training data. In [104] authors have used the actual field data for training of ANFIS-based MPPT and show that it has better performance than the conventional methods. But several problems are associated with the practical data, i.e it does not cover a wide dynamic range, only appropriate for a particular geographical location and a time consuming task as large amount of data is required for better performance of ANFIS. In Ref. [104], ANFIS inputs are open circuit voltage (V_{OC}) and short circuit current (I_{SC}) of the PV at certain operating condition and these values are calculated depending upon environmental conditions while in the proposed MPPT controller irradiation and temperature are taken as inputs whose values can directly be taken from the sensors.

On the other hand, easy and better way of getting training data is by simulation of PV model and as utilized in [105], [106]. In [105] effectiveness of PV model used to generate training data is not discussed, hence raising a concern about the incompetency of training data and so the MPPT controller. In this study, an accurate input-output data set is used for the training of the ANFIS-based MPPT controller. An accurate training data is gathered from the simulation studies using the developed PV model. This results in an efficient, simple structure of MPPT controller. In [106] working of ANFIS-based MPPT is shown in single-stage topology of power converter (with the inverter only). Unlike in [106] two-stage topology is used that provide the flexibility in designing the control

architecture since it has more control variables and multiple control objectives can be achieved like MPPT, VAR compensating, active filtering etc. Two-stage scheme also offer further advantage by providing the constant dc-link voltage to the inverter which will be beneficial especially in the case of temperature variations (as temperature change effects on the PV output voltage considerably). Additionally, a novel experimental verification of the proposed ANFIS-based MPPT controller is shown by interfacing the RTDS and dSPACE controller.

CHAPTER 3 PARAMETER ESTIMATION OF A PV MODEL

3.1 INTRODUCTION

The main objective in modeling the Photovoltaic (PV) is that the model should be able to regenerate the output characteristics of the PV panel at different ambient condition with high precision. Several PV electrical models have been proposed and developed by researchers including the models that are based on the simple idealized model and the models that replicate the actual physics of the PV cell [107]. Some of these models are described vaguely and some of them are too complex for power system studies like load flow, maximum power point tracking, load frequency match etc. These models also have implementation issues on several software packages. Electrical characteristics of the PV panel can be modeled by representing it with equivalent electrical circuit. This model has the advantage over other models due to its electric circuit nature and behavior of the PV array can easily be understood in the circuit connected. Power electronics design engineers require an efficient PV panel model for the simulation study of the power electronics before any experimental verification. This model is best suited for the dynamic and transient study of the power electronics converters.

In this chapter a generalized PV array model simulator is proposed and developed in the MATLAB/Simulink. The simulator is designed based on the five parameters equivalent electric circuit model. The major challenge in the implementation of this model lies in the estimation of the model parameters. The exact values of these parameters are required to regenerate the output characteristics of PV panel accurately. An efficient approach is introduced to identify the values of five electrical model parameters at Standard Test Condition (STC) by converting the estimation problem into optimization problem and using the Differential Evolution (DE) as an efficient optimizing technique. The proposed estimation approach does not require any experimental data as required by other methods [35] [37] and can work only with the data provided by the manufacturer. These estimated parameters are utilized to design an efficient PV array simulator. The simulator is designed as a masked block and allows the user to enter the desired number of PV panels connected in series and parallel to have prescribed power output. The effectiveness of the developed simulator is investigated under different operating conditions including harsh partial shaded condition. Results show that the proposed model can regenerate the I-V curves at STC as well as at other operating condition with acceptable errors. Furthermore, the robustness of the proposed simulator is analyzed in conjunction with the DC-DC converter and MPPT controller. It is envisaged that the developed PV array simulator can be very helpful for the power system design engineers in the simulation study of the power systems before any experimental verification.

3.2 PV ELECTRIC CIRCUIT MODEL

Commercially available PV devices are in the form of PV panels consist of series connected PV cells. Maximum output power of a single PV panel is in the range of tens of watts to some hundreds of watts that would be acceptable for the small scale applications. But for large scale applications, such as PV power stations, series and parallel combinations of these panels are needed to enhance the required PV output power. Connecting the PV panels in series increases the current capability of PV source and parallel connection increases the voltage rating of PV source. This series/parallel combination of PV panels is commonly known as PV array. Considering the importance of PV panel as a basic unit of PV array the model of the PV panel is developed which is then modified to stand for a complete PV array.

3.2.1 Modeling of PV Panel

The well known five parameters electric circuit model of PV device is used and shown in Figure 3.1 [107], [108]. It consists of light dependent current source, a p-n junction diode and two resistances one in series and the other in parallel. The current source (I_L) represents charge carrier generation in the semiconductor caused by incident radiation. The shunt diode represents recombination of these charge carriers at a high forward-bias voltage ($V+I*R_s$). The shunt resistor (R_{SH}) signifies high-current paths through the semiconductor along mechanical defects and material dislocations [109].

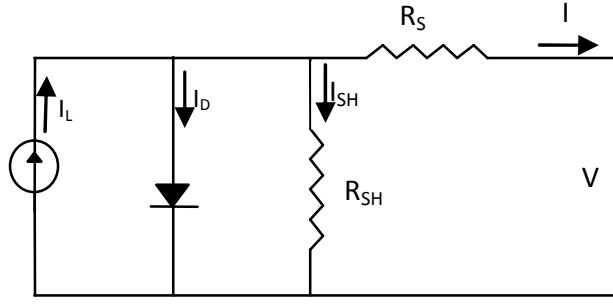


Figure 3.1: Five parameter equivalent electric circuit model of PV device.

Using simple Kirchhoff's current law following relationship can be found;

$$I = I_L - I_D - I_{SH} \quad (3.1)$$

I_D and I_{SH} depicts the diode current and shunt branch current, respectively and given by;

$$I_D = I_0 \left\{ \exp \left[\frac{(V + IR_S)}{a} \right] - 1 \right\} \quad (3.2)$$

$$I_{SH} = \frac{V + IR_S}{R_{SH}} \quad (3.3)$$

Putting these expressions of I_D and I_{SH} into Eq. (3.1) gives the complete I-V characteristics of a PV panel;

$$I = I_L - I_0 \left\{ \exp \left[\frac{(V + IR_S)}{a} \right] - 1 \right\} - \frac{V + IR_S}{R_{SH}} \quad (3.4)$$

Where; I and V represent the current and voltage generated from the PV panel. I_L is the light generated current, I_0 is the diode saturation current, R_S and R_{SH} are the series and parallel resistance respectively and factor “ a ” is the diode modified ideality factor and it is given by;

$$a = \frac{N_S n k T}{q} \quad (3.5)$$

Where, N_S is the number of cells in the PV panel, n is the ideality factor (it has a value between 1 to 2 for real diode), k is the Boltzmann's constant, T is the cell temperature and

q is the electronic charge. Eq. (3.4) shows the I-V characteristics of a PV device and governed by five parameters (I_L , I_0 , R_S , R_{SH} and “ a ”). Modeling of the PV device is quite complex because of the transcendental non-linear characteristics of Eq. (3.4). The unknown values of these parameters and their dependence on the operating condition (temperature and irradiation) add more complexity in the modeling. Data usually supplied by the manufacturer is the values of I-V pair at short-circuit condition (SC), open-circuit conditions (OC) and maximum power conditions (MP) at STC (1000 W/m² and 25⁰C). I-V characteristic at these key points is given by following equations;

At short circuit condition, voltage becomes zero, $V=0$ and $I=I_{SC, ref}$

$$I_{SC, ref} = I_{L, ref} - I_{0, ref} \left\{ \exp \left[\frac{I_{SC, ref} \cdot R_{S, ref}}{a_{ref}} \right] - 1 \right\} - \frac{I_{SC, ref} \cdot R_{S, ref}}{R_{SH, ref}} \quad (3.6)$$

At open circuit condition, current becomes zero, $I=0$ and $V=V_{OC, ref}$

$$I_{L, ref} = I_{0, ref} \left\{ \exp \left[\frac{V_{OC, ref}}{a_{ref}} \right] - 1 \right\} + \frac{V_{OC, ref}}{R_{SH, ref}} \quad (3.7)$$

At maximum power condition, $V=V_{MP, ref}$ and $I=I_{MP, ref}$

$$I_{MP, ref} = I_{L, ref} - I_{0, ref} \left\{ \exp \left[\frac{V_{MP, ref} + I_{MP, ref} \cdot R_{S, ref}}{a_{ref}} \right] - 1 \right\} - \frac{V_{MP, ref} + I_{MP, ref} \cdot R_{S, ref}}{R_{SH, ref}} \quad (3.8)$$

Having the five parameters (I_L , I_0 , R_S , R_{SH} , “ a ”) known, Eq. (3.4) can be solved. With different atmospheric conditions, these parameters have different values that can be calculated at any ambient condition using equations (3.9)-(3.13) assuming their values at STC are known.

$$a = a_{ref} \left(\frac{T_c}{T_{c, ref}} \right) \quad (3.9)$$

$$I_L = \frac{S}{S_{ref}} [I_{L, ref} + \mu_{I, sc} (T_c - T_{c, ref})] \quad (3.10)$$

$$R_{SH} = R_{SH,ref} \frac{S_{ref}}{S} \quad (3.11)$$

$$R_S = R_{S,ref} \quad (3.12)$$

$$\frac{I_0}{I_{0,ref}} = \left(\frac{T_c}{T_{c,ref}} \right)^3 \exp \left(\left(\frac{N_s * T_{ref}}{a_{ref}} \right) * \left(\frac{E_{g,ref}}{T_{ref}} \left| - \frac{E_g}{T} \right| \right) \right) \quad (3.13a)$$

$$\frac{E_g}{E_{g,ref}} = 1 - C(T - T_{ref}) \quad (3.13b)$$

Where; S and T_c represent the solar radiation and temperature of the PV panel, respectively. $\mu_{I,sc}$ and N_s are the coefficient of short circuit current and number of cells in the panel, respectively (both of these quantities is provided by the manufacturer). E_g is the band-gap energy of the PV cell material and $C=0.0003174$ [22]. Quantities with the subscript “ ref ” represent their values at the STC.

3.2.2 Modeling of PV Array

As discussed earlier PV panels can be grouped in different modes to form PV arrays. Some topologies are series array (panels are connected in series), parallel array (panels are connected in parallel), series-parallel (SP) array (panels are connected in both series and parallel) and total cross tied (TCT) array. Among these topologies SP array is most commonly used because of its flexibility in maintaining the required output voltage and current and better performance in the partial shaded conditions [110]. Eq. (3.4) can be modified to represent the I-V relationship of SP array and written as;

$$I = Npp * I_L - Npp * I_0 \left\{ \exp \left[\frac{(V + IR_S * \mathbb{N})}{Nss * a} \right] - 1 \right\} - \left(\frac{V + IR_S * \mathbb{N}}{R_{SH} * \mathbb{N}} \right) \quad (3.14)$$

$$\mathbb{N} = \frac{Nss}{Npp} \quad (3.15)$$

Where; N_{SS} and N_{PP} represent the number of panels connected in series and parallel, respectively. It can be noticed in Eq. (3.14) that N_{PP} is multiplied with the current associated terms to enhance the current output of PV system and similarly N_{SS} is multiplied with voltage related terms increase to voltage output of PV panel.

A theoretical illustration of a series connection and parallel connection of PV panels is shown in Figure 3.2 and Figure3.3, respectively. These figures depicts that the circuit elements of combined panels can be merged together to form a single equivalent model that is similar to circuit of one PV panel [40]. But the values of the parameters will transform depending upon the number of panels coupled in series and parallel. Expressions for the array parameters in relation with the panel parameters are shown in Table 3.1.

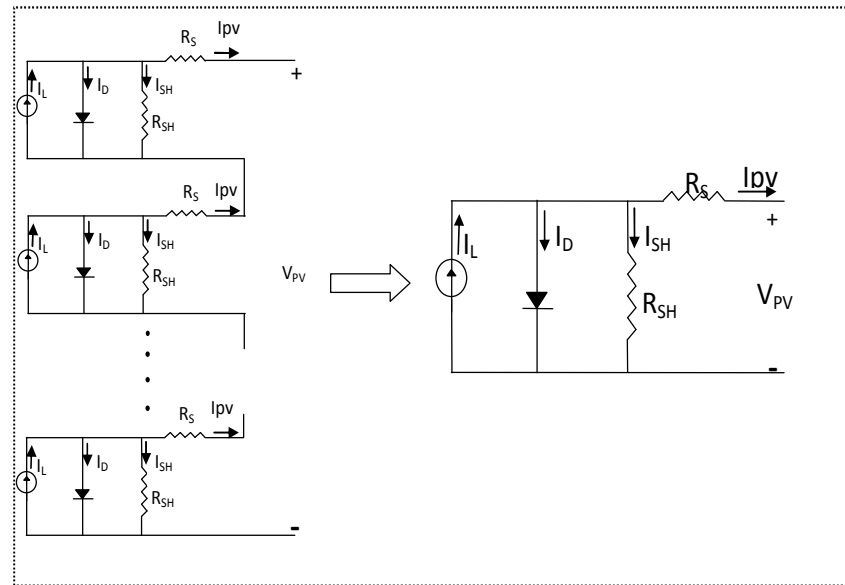


Figure 3.2: Panels connected in series in an array.

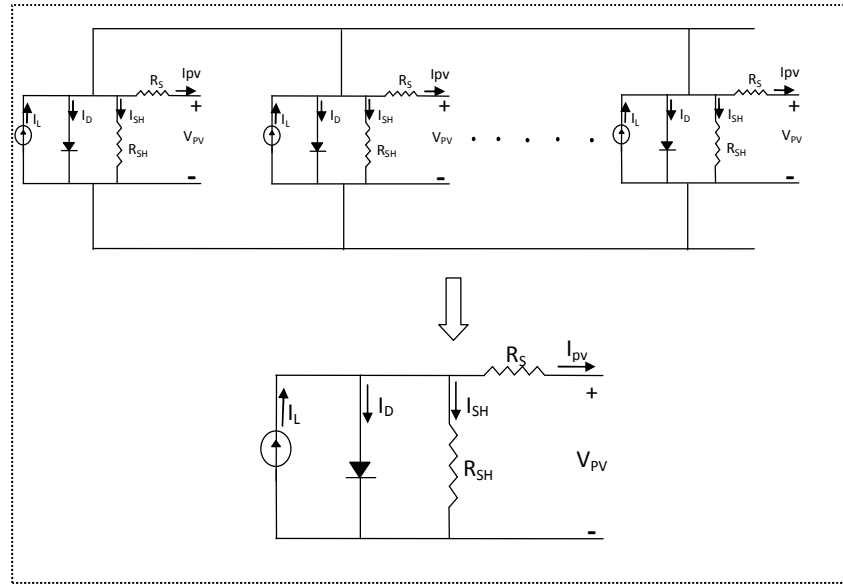


Figure 3.3: Panels connected in parallel in an array.

Table 3.1: Array parameters in relation with panel parameters.

Panel parameter	Modified array parameters		PV Model parameter	Modified array parameters
V_{OC}	$V_{OC} * N_{SS}$		I_L	$I_L * N_{PP}$
I_{SC}	$I_{SC} * N_{PP}$		I_0	$I_0 * N_{PP}$
V_{MP}	$V_{MP} * N_{SS}$		R_S	$R_S * (N_{SS} / N_{PP})$
I_{MP}	$I_{MP} * N_{PP}$		R_{SH}	$R_{SH} * (N_{SS} / N_{PP})$
n	$n * N_{SS}$		a	$a * N_{SS}$

When panels are linked in parallel to increase current rating, the values of I_{SH} (short circuit current), I_{MP} (current at maximum power point), I_L (light generated current) and I_0 (diode saturation current) are altered and multiplied with a number of parallel connected panels. The factor “ a ” (diode ideality factor), V_{OC} (open circuit voltage), V_{MP} (voltage at

maximum power point) remains unchanged. While the R_S (series resistance) and R_{SH} (shunt resistance) are get divided by the number of panels connected in parallel.

Similarly, for panels connected in series to enhance voltage rating, values of V_{OC} (open circuit voltage), V_{MP} (voltage at maximum power point) and factor “ a ” (diode ideality factor) are get multiplied with the number of series connected panels. Values of I_{SH} (short circuit current), I_{MP} (current at maximum power point), I_L (light generated current) and I_0 (dark saturation current) remain unaltered and R_S (series resistance) and R_{SH} (shunt resistance) are get multiplied by the number of series connected panels.

3.3 EFFECT OF PARAMETERS ON PV CHARACTERISTICS

The effect of each of the five parameters on the behavior of the I-V curve is shown in Figure3.4. The effect is shown for the Copper Indium Diselenide (CIS) solar panel [111] around the STC condition, although the effect of each parameter on the I-V curve is similar for all panels and operating conditions. The bold I-V curve in each of the following plots is the result of using parameters calculated at STC data while the other two are the result of adjusting one specified parameter above and below the original value. The following figures show that both “ a ” and “ I_0 ” adjust the predicted voltage at all points on the I-V curve and I_L adjusts the predicted current. R_S and R_{SH} have a more localized influence around the maximum power point; R_S adjusts the maximum power voltage and R_{SH} adjusts the maximum power current.

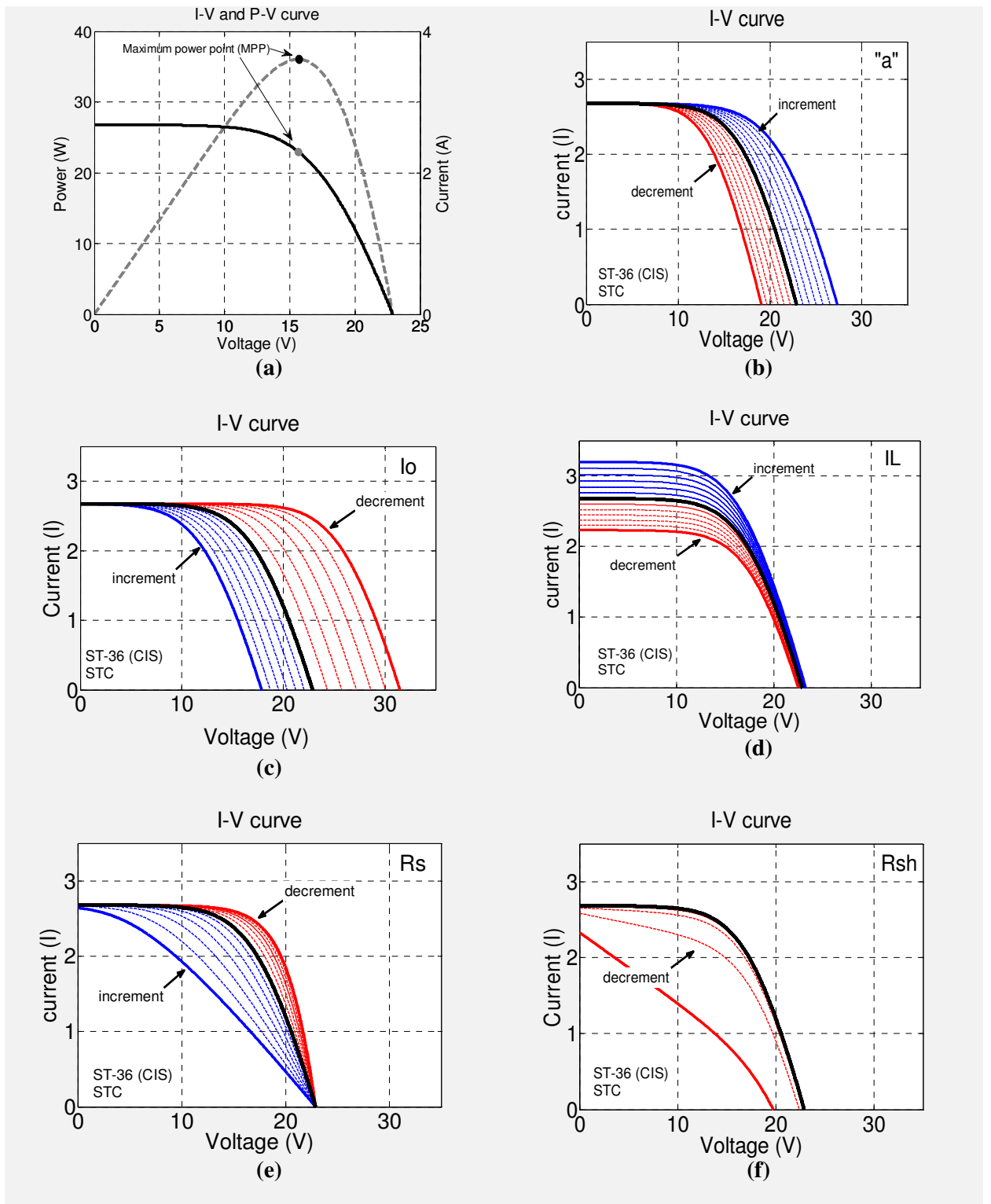


Figure 3.4: Effect of five parameters on I-V curve.

3.4 PARAMETER ESTIMATION

Values of five parameters (I_L , I_o , R_s , R_{sh} , “ a ”) are required for the solution of I-V characteristics of PV panel given in Eq. (3.4). These parameters have very significant effect on the I-V curve as discussed in section 3.3. Mostly, value of one parameter is assumed to be constant and other parameters are calculated based on this assumption [41]. But for precise PV panel modeling it is imperative to calculate their values simultaneously. In this study DE is utilized as an efficient optimization technique to identify the values of these parameters. Unlike the reported methods that need the PV panel experimental data, the proposed scheme requires only the data supplied in the manufacturer provided catalogues. This data gives the values of I-V pair at short-circuit condition (SC), open-circuit conditions (OC) and maximum power conditions (MP) at STC (1000 W/m^2 and 25°C). Figure 3.4: Effect of five parameters on I-V curve.

(a) shows these points on the typical I-V and P-V curve. The aim of the study is to use only the values of these points in estimating the parameters that can redraw the I-V and P-V curves of PV panels with high precision.

3.4.1 Proposed Approach for Parameter Estimation using DE

Similar to other optimizing techniques, DE optimization requires an objective function that needs to be minimized or maximized. An appropriate objective function is needed for this purpose that should be dependent on the optimizing parameters (I_L , I_o , R_s , R_{sh} , “ a ”). Objective function used in this work is based on the error calculation and given by the following equation;

$$J = Error_{MPP}^{V,I,P} + Error_{OC \text{ and } SC}^{V,I} \quad (3.16)$$

$$Error_X = \frac{X_{Meas} - X_{Exp}}{X_{Exp}} \quad (3.17)$$

Where; V_{MP} , I_{MP} and P_{MP} represent the voltage, current and power at maximum power point, respectively. V_{OC} and I_{SC} are voltage at open circuit point and current at short circuit point, respectively. Values of these points are given in the PV panel datasheet. V_{SC} and I_{OC} are the voltage at short circuit condition and current at open circuit condition, respectively, having values equal to zero. X represents any of the above mentioned point. X_{meas} is calculated using Eq. (3.6) to (3.8) and X_{exp} is taken from datasheet. *Error* represents the deviation of the measured value from the experimental value given in the data sheet.

3.4.2 Differential Evolution (DE)

Differential evolution (DE) is population based optimization technique and first introduced in [112]. It is renowned for its robustness, simplicity, rapid convergence, less control variables and ability to search global optimum regardless of the initial values of parameters. DE is suitable for non differentiable and non linear optimization. Like other evolutionary algorithm and search techniques DE needs to form a population (G_i) having a number (NP) of candidate solution, usually called individuals (X_n^i), and depending upon the dimension (D) of the problem each individual have control variables, called the optimizing parameters (x_n).

$$G^i = [X_1, X_2, X_3, \dots \dots X_{NP}] \quad (3.18)$$

$$X_n^i = [x_{n1}, x_{n2}, x_{n3}, \dots \dots x_{nj}] \quad (3.19)$$

Where; i represents number of generation (iteration) and usually used in a stopping criterion, NP number of individuals or population size, n describes the dimension of the problem.

In all search algorithms the key step is to form the trail vector (variant vector) from the parent vector. The stratagem employed by DE to generate a trail vector is based on the difference between randomly chosen individuals. A trail (new) individual is generated for every parent (old) individual using the operation of mutation and crossover. The best individual is selected for the next generation (iteration) by comparing the objective function of old and new individual. DE optimization process has resemblance with the genetic algorithm (GA) with little difference; GA utilizes crossover operation as a search method while DE employs mutation operation as a search mechanism. DE includes following steps;

Step 1: Initialization

As a first step DE needs to initialize its following control parameters;

G_{max} , number of generation (iteration) usually used as a stopping criterion.

NP , population size (number of candidate solution)

D , problem dimension, number of control variables (optimizing parameters)

$x_{j,min}$ and $x_{j,max}$, lower and upper bound of control variable j .

F , mutation factor, range $[0, 1]$

CR , cross over rate, range $[0, 1]$

It starts the optimization process by generating initial population containing the NP candidate solution, each having D number control variables. Values of these variables are selected randomly using the their minimum (x_{\min}) and maximum limits (x_{\max}) by following equation;

$$x_{i,j} = x_{j,\min} + rand * (x_{j,\max} - x_{j,\min}) \quad (3.20)$$

$$i = 1, 2 \dots, NP \text{ and } j = 1, 2 \dots D \quad (3.21)$$

Step 2: Locating the best solution

After initialization, the objective function value of all individuals is calculated and evaluated to get the best solution (individual). This best solution is then updated by comparing their value with the next generation best solution to locate the global optima.

Step 3: Mutation

Mutation means a perturbation with a random element. It is a first operation that is utilized to generate a trail (variant) vector and creates a “mutant vector” for all individuals in the current generation. For every individual of parent vector ($X_i^{(G)}$) in a current generation (G) two individuals ($X_{r1}^{(G)}, X_{r2}^{(G)}$) are randomly selected from the population (NP). A mutant vector $V_i^{(G)}$ is then generated by adding a weighted difference of a best vector ($X_{best}^{(G)}$) and a parent vector ($X_i^{(G)}$), and a weighted difference of two randomly selected vectors ($X_{r1}^{(G)}, X_{r2}^{(G)}$) with a base individual using the following equation.

$$V_i^{(G)} = X_i^{(G)} + F(X_{best}^{(G)} - X_i^{(G)}) + F(X_{r1}^{(G)} - X_{r2}^{(G)}) \quad (3.22)$$

Where; F represents the mutation factor having real value between $[0, 1]$ and effect the speed of convergence.

Step 4: Crossover

To further improve the diversity and add more perturbation, crossover operation is applied. In this operation mutant vector ($V_i^{(G)}$) and its parent vector ($X_i^{(G)}$) are combined to form a trial solution ($U_i^{(G)}$). Control variables (optimizing parameters) of both the vectors are mixed in this step based on the crossover factor (CR) to form the trail solution. Crossover process can be specified by following equation;

$$U_{j,i}^{(G)} = \begin{cases} V_{j,i}^{(G)}, & \text{if } rand \leq CR \\ X_{j,i}^{(G)}, & \text{otherwise} \end{cases} \quad (3.23)$$

$$j = [1, 2, \dots, D], \quad D \text{ number of control variables}$$

Where, CR is the crossover factor having value between $[0, 1]$.

Step 5: Selection

Selection operation is considered to be the last step in the formation of new population. In this stage objective function value of generated trail vector is reckoned and comparison is made with the corresponding value of the parent vector. If the individuals of the trail vector have better objective value than the corresponding individuals of parent vector they will replace them, otherwise parent vector will be retained. Selection operation for the minimizing problem can be given by;

$$X_i^{(G+1)} = \begin{cases} U_i^{(G)}, & \text{if } J(U_i^{(G)}) \leq J(X_i^{(G)}) \\ X_i^{(G)}, & \text{otherwise} \end{cases} \quad (3.24)$$

Where, J is the objective function.

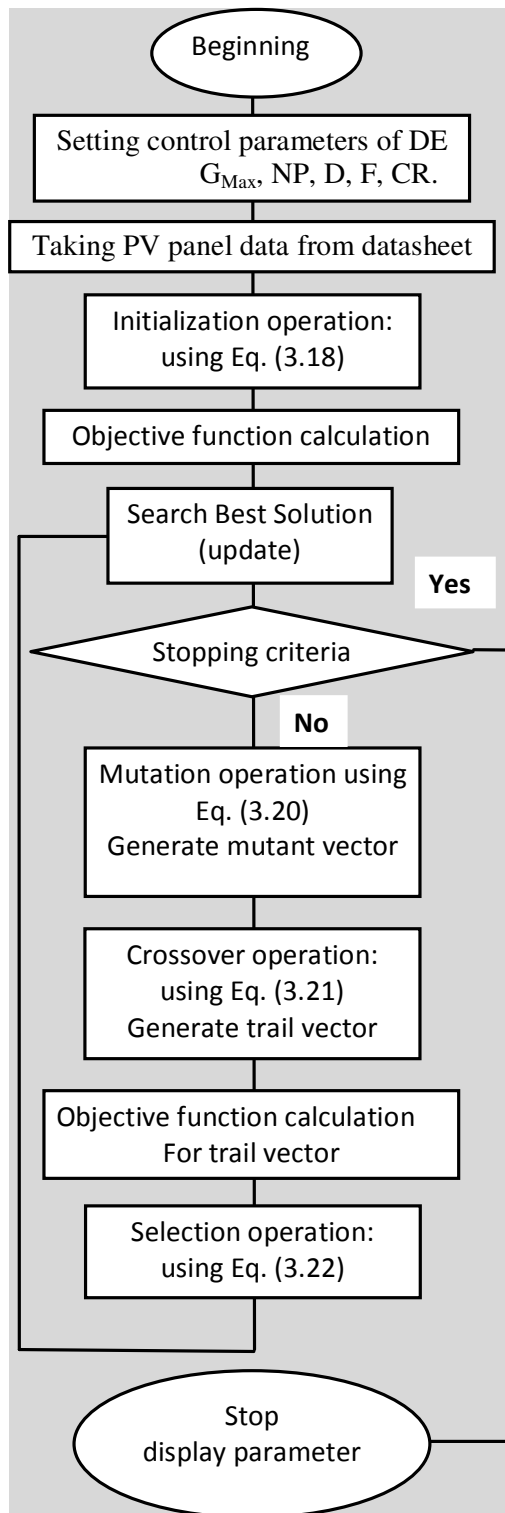


Figure 3.5: Flowchart for parameter estimation method using DE.

Step 6: Stopping Criteria

As DE is the iteration based technique it needs certain stopping criteria to end the iterative process. Usually a predefined value of maximum number of generation (iteration) or tolerance in the error is used for the purpose. It can be any user defined condition. In this study, stopping criteria is based on objective function value and stops the iteration process when its value remains same for the prescribed number of generations.

Goal of this optimization problem is to identify the optimum values of the five parameters (I_L , I_0 , R_S , R_{SH} , “ a ”) at STC by minimizing the objective function given in Eq. (3.16) which will basically reduce the error at the above mentioned key points. The parameters determined at STC can then be used to calculate the values at other operating conditions using the equations (3.9)-(3.13) as stated in section 3.2. Flowchart for the proposed parameter estimation method using DE is shown in Figure3.5.

3.5 IMPLEMENTATION OF PV MODEL IN MATLAB/SIMULINK

A generalized PV array simulator model is implemented in MATLAB/Simulink using Equations (3.1) to (3.13). The inputs to the simulator are irradiation and cell temperature and it is flexible enough to simulate any number of series (N_{SS}) and parallel (N_{PP}) connected PV panels using only the data provided by the manufacturer. Figure 3.6 shows the last stage of the modeling and it depicts that the implemented circuit is quite similar to the equivalent circuit of PV array shown in Figure 3.6.

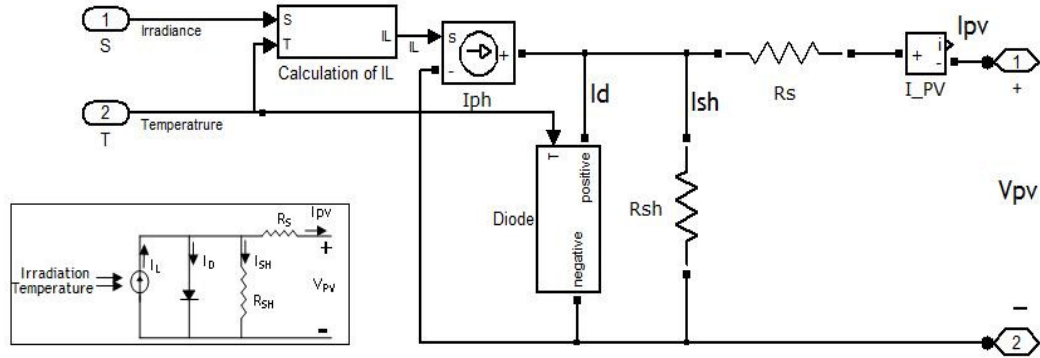


Figure 3.6: Implementation of PV array simulator in simulink

It consists of light dependent current source, p-n junction diode, series and parallel resistance. This stage contains other sub systems that are connected together to execute I-V characteristics of PV array. These sub systems are not shown for brevity. The PV simulator is implemented as a mask block that prompts the user to enter the necessary parameters of the array to be executed. Parameters required are number of cell in the panel (N_C) open circuit voltage (V_{OC}), short circuit current (I_{SH}), voltage at maximum power point (V_{MP}), current at maximum power point (I_{MP}), temperature coefficients for voltage and current (K_V and K_I), number of series (N_{SS}) and parallel (N_{PP}) connected panels in an array and the estimated values of the five parameters. A sample of parameter's block of generalized PV array simulator is shown in Figure 3.7.

The partial shaded condition of PV can be implemented by placing simulator block in series with each other and having an anti-parallel diode connected to each block as shown in Figure 3.8. The number of series connected simulator blocks required depend on the number of shaded pattern needs to be executed. For instance Figure 3.8 shows three PV

array simulator blocks connected in series and can carry out the simulation of three different shading patterns. This generalizes the proposed simulator that can simulate a single PV panel, a group of PV panels connected in series and parallel (PV array) and partially shaded arrays with user defined shading patterns.

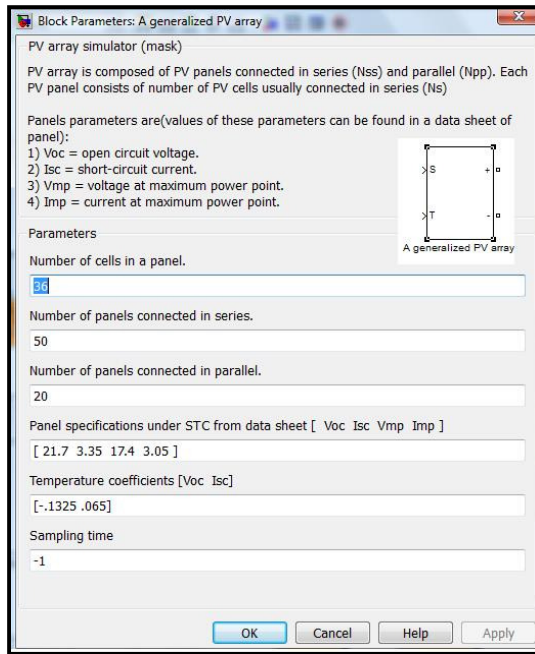


Figure 3.7: Block parameters window of PV array simulator in Simulink.

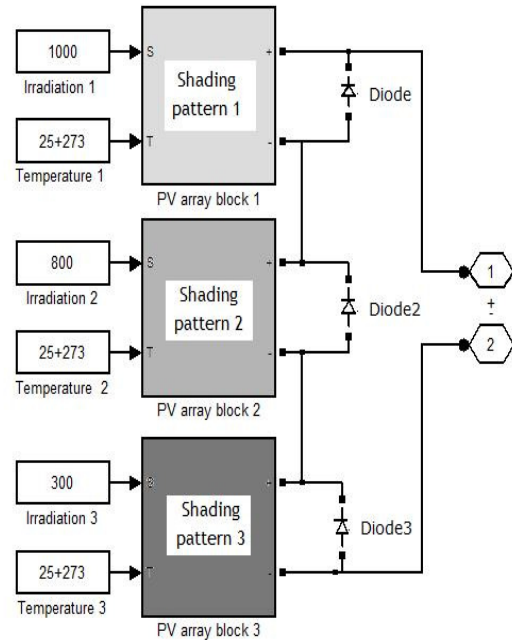


Figure 3.8: Partial shaded implementation of PV array simulator in simulink.

3.6 RESULTS AND DISCUSSION

3.6.1 Test 1: Analysis of proposed parameter estimation method

In this test, analysis of the parameter estimation method proposed is carried out. For this purpose, six PV panels of three different technologies, two mono-crystalline; two poly-crystalline and two thin-film technologies, are selected. To carry out this study, the I-V curves generated by estimated parameters are compared with the experimental curves

given in the datasheet. The efficiency of the determined curves is investigated by measuring the errors between experimental and modeled values at five key points [113] shown in Figure 3.9.

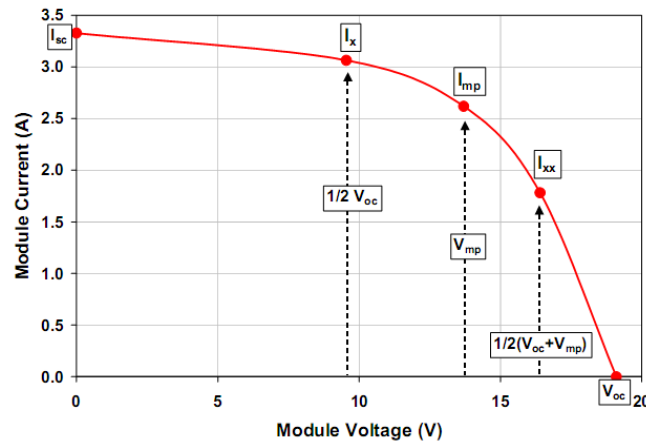


Figure 3.9: key points on I-V curve [113].

These five key points on the I-V curve are short circuit (*SC*), open circuit (*OC*), maximum power point (*MPP*), point with voltage equal to half the voltage at maximum power point (*X*) and point with voltage equal to the average of maximum power point voltage and open circuit voltage (*XX*). Result and analysis show that the proposed method can simulate the output characteristics of all technologies efficiently.

Selected PV Panels

PV panels selected to undergo this study are;

1. Sunpower 230W (mc-Si)
2. SunForte PM318B00 (mc-Si)

3. Lorentz120W LC120-12P (pc-Si)
4. BP Solar 3230N (pc-Si)
5. Shell ST36 (CIS)
6. Kaneka U-EA110W (a-Si)

The manufacturer provided electrical data for the selected PV panels at STC is shown in Appendix A. Five key points are obtained from the experimental I-V curves provided in the data sheet. These experimental curves are digitized using the digitizer software and values of these points are extracted from each curve and given in appendix A.

Estimated values of model parameter

Values of the five unknown parameters (I_L , I_0 , R_S , R_{SH} and “ a ”) are identified using the proposed parameter estimation method for all the selected PV panels and are shown in Table 3.2.

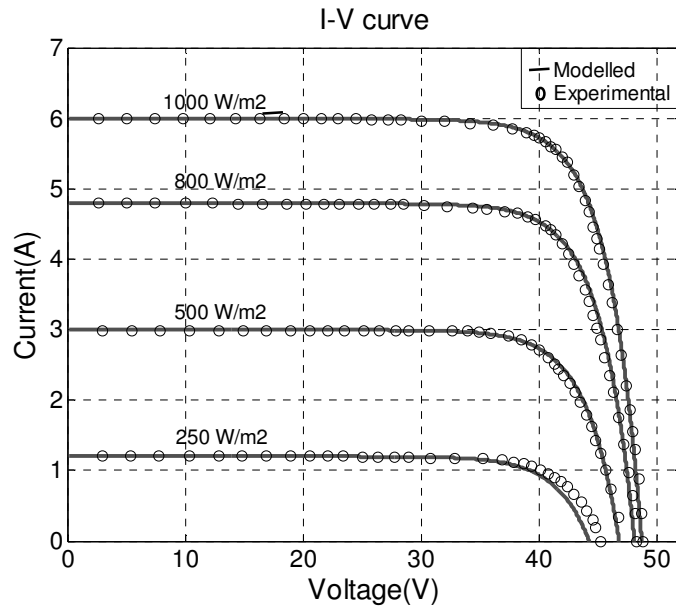
Table 3.2: Estimated values of the five parameters at STC using proposed method.

	Mono crystalline (mc-Si)		Poly crystalline (pc-Si)		Thin film	
	Sunpower 230W	SunForte PM318B0 0	Lorentz12 0W	PB solar	Kaneka U- EA110W (a- Si)	Shell ST36 (CIS)
Light Current (I_L)	5.99	6.2	7.7	8.4	2.519	2.6803
Diode Saturation current (I_0)	1.40E-07	7.76E-08	2.14E-05	8.20E-06	4.77E-06	4.12E-05
Series Resistance (R_S)	0.008686	0.01092	1.75E-04	0.0146	3.1375	1.3901
Shunt Resistance (R_{SH})	95658.604	6.15E+04	75.7418	5.63E+04	4.09E+02	3.85E+04
Modified Ideality factor (a)	2.7715	3.5559	1.7091	2.651	5.4173	2.0662

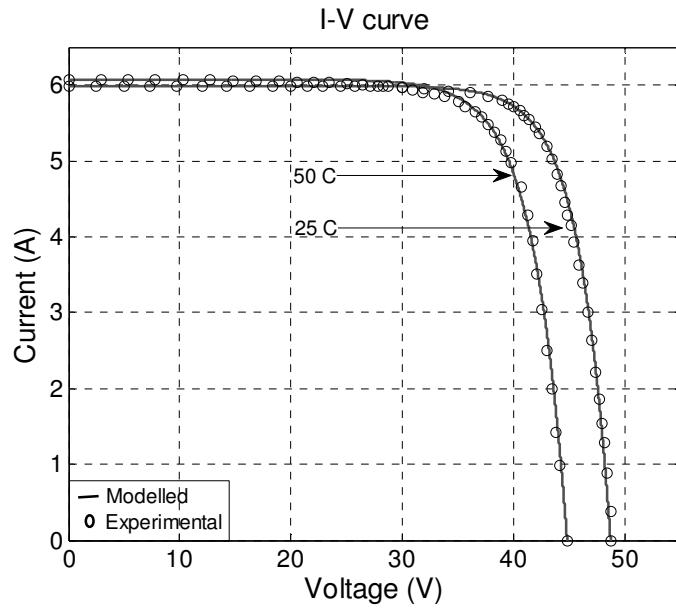
It can be noticed that the series resistance (R_S) of thin-film technology is quite higher than crystalline technology panels. Such behavior is expected and in accordance with [109][42]. Series resistance has a central job in finding the curvature of the I-V curve as shown in Figure 3.4 and its large value depicts a smoother curvature which is a usual behavior of I-V curves of thin film technologies [114].

Comparison with Experimental curves

The electrical characteristics of the selected PV panels are simulated using the estimated parameters and the proposed approach is validated by comparing the determined curves (generated by estimated parameters) with the experimental curves. The experimental curves data is extracted from the PV panel datasheets using digitizer software. Figure 3.10(a) shows the determined I-V curves (solid lines) along with the experimental curves (circles) for the mono-crystalline technology (Sunpower 230W) for different irradiation levels and constant temperature of 25⁰C. It illustrates that the I-V curves obtained from the proposed method are in great accordance with the experimental curves for all the irradiation levels, particularly for STC. The verification of the proposed method encountered with temperature change and constant irradiation level of 1000 W/m² is shown in Figure 3.10(b). It can be seen that the curves generated from the proposed method matches with the experimental curves under all the temperature variations. Similarly, Figure 3.11 and Figure 3.12 show the comparison of modeled and experimental I-V curves for other poly-crystalline and thin-film PV technologies, respectively. These figures show that the parameters estimated by the proposed approach can regenerate the I-V curves at different operating conditions accurately.



(a)



(b)

Figure 3.10: I-V characteristics for mono-crystalline technology (Sunpower 230W)

(a) different irradiation level and (b) different temperature.

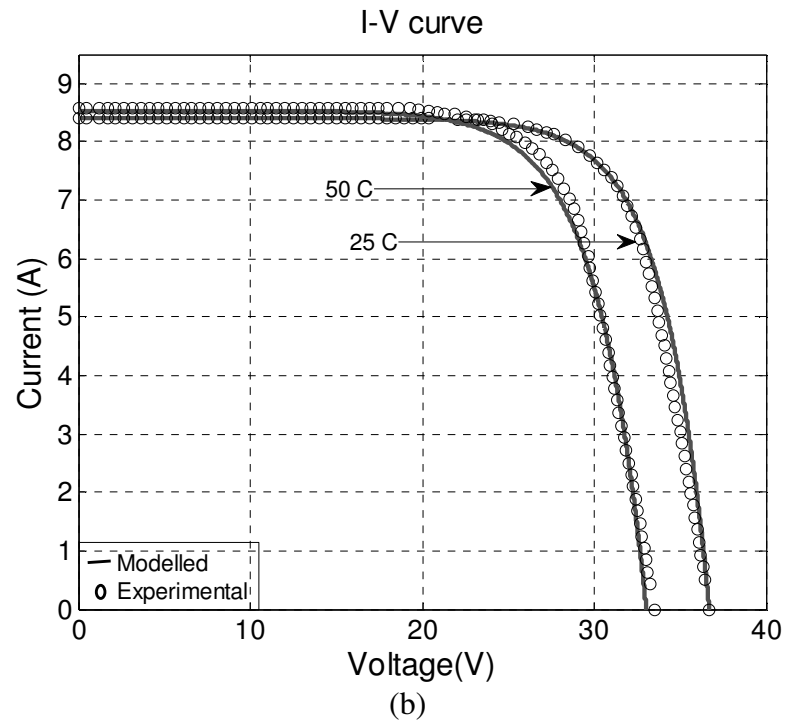
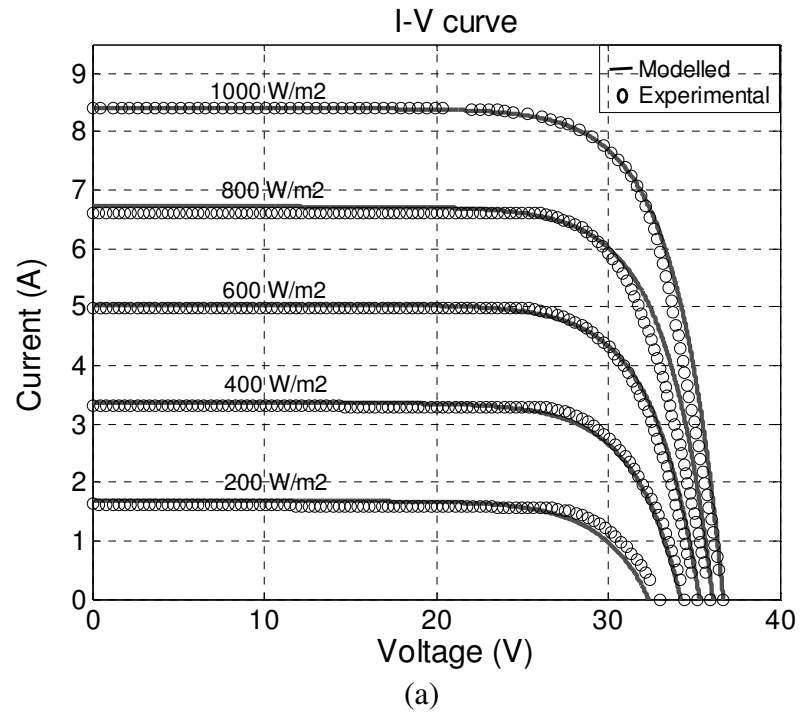


Figure 3.11: I-V characteristics for poly-crystalline technology (BP Solar 3230N) (a) different irradiation level and (b) different temperature.

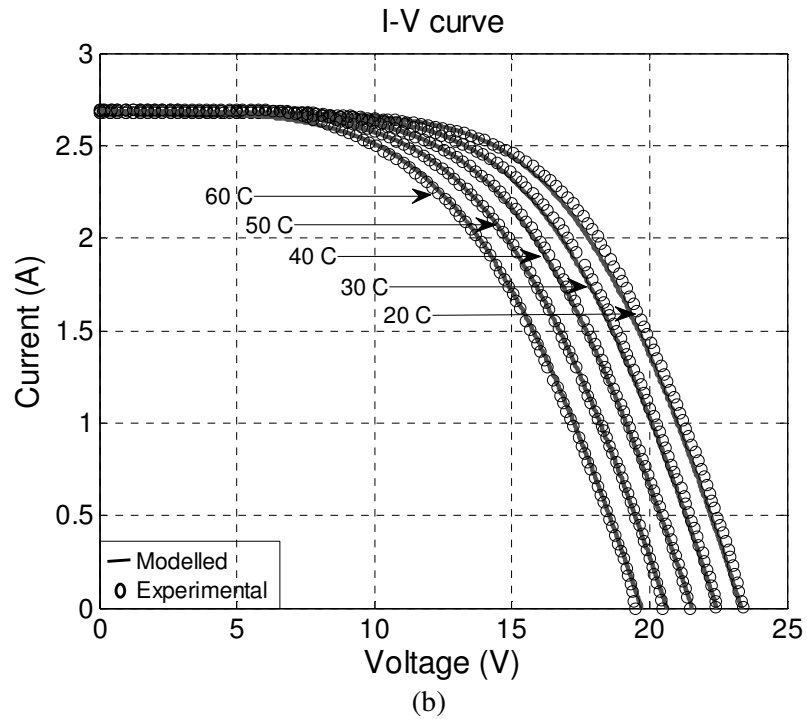
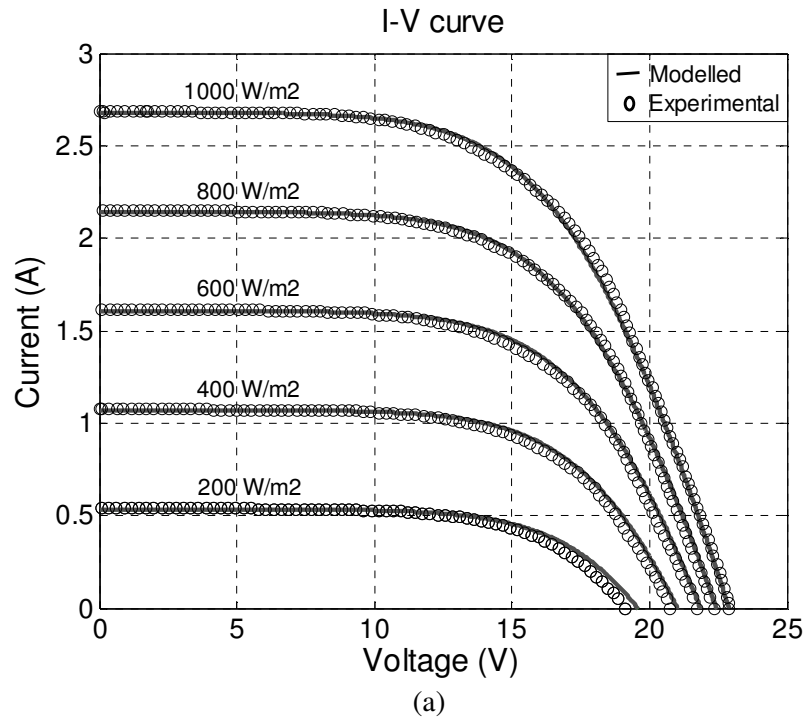


Figure 3.12: I-V characteristics for thin-film technology (Shell ST36) (a) different irradiation level and (b) different temperature.

Statistical Analysis

Three statistical errors are used for a comprehensive analysis of the proposed approach. These errors are the root mean square error (RMSE), the mean bias error (MBE) and the mean absolute error (MAE). They are given by the following equations;

$$RMSE = \frac{\sqrt{\frac{1}{n} \sum_{i=1}^n (y_i - x_i)^2}}{\frac{1}{n} \sum_{i=1}^n x_i} \quad (3.25)$$

$$MBE = \frac{\frac{1}{n} \sum_{i=1}^n (y_i - x_i)}{\frac{1}{n} \sum_{i=1}^n x_i} \quad (3.26)$$

$$MAE = \frac{\frac{1}{n} \sum_{i=1}^n |y_i - x_i|}{\frac{1}{n} \sum_{i=1}^n x_i} \quad (3.27)$$

Where; y and x represent the measured and experimental value, respectively and n is the number of data point taken (five in our case). The precision of the proposed method is analyzed by RMSE and MAE while MBE is used to show whether the approach is over-predicting or under-predicting the experimental value.

These errors are calculated for current and power at five key points for curves available in the datasheet. Figure 3.13 illustrates the values of current errors for irradiation and temperature variation. It can be observed that the error at STC is negligible and within the acceptable range for other conditions. Its value is increasing with the decrease in irradiation and increase in temperature and that is consistent with [8][13]. This behavior of increase in error is expected because the five parameters are optimized at STC and their values at other operating conditions are measured using

model translational equations Eq. (3.9)-(3.13). That explains why the error is increased in these conditions.

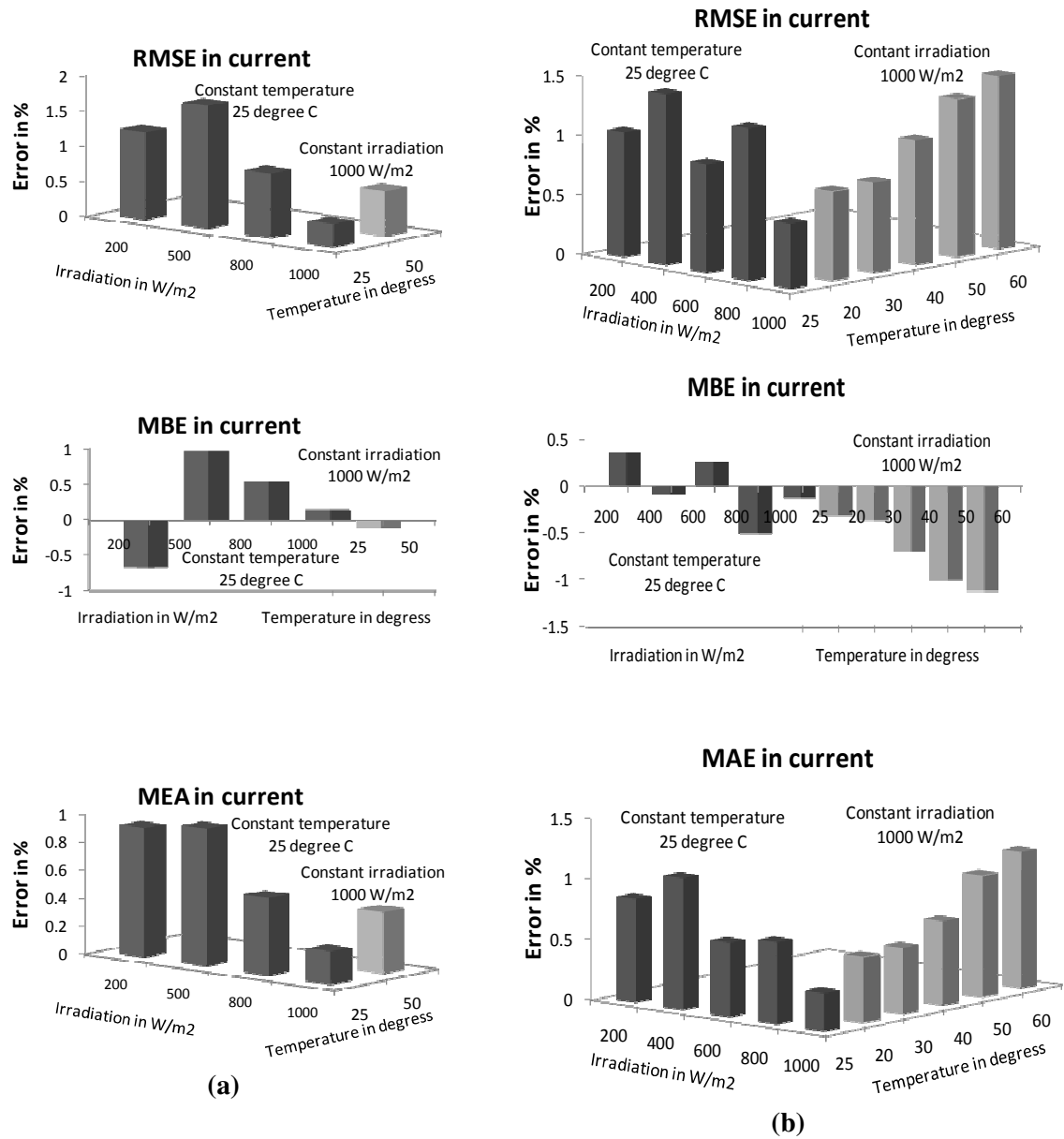


Figure 3.13: RMSE, MBE, MAE for different irradiation and temperature (a) mono-crystalline (m-Si) and (b) thin film (CIS)

Results obtained are then used to measure the cumulative error at all the available operating conditions. Figure 3.14 shows the cumulative error values of RMSE, MBE and MAE for the power and current of the mono-crystalline silicon technology PV panels (Sunpower and SunForte). It can be seen that the values are very small for all the three errors. Similarly, Figure 3.15 and Figure 3.16 show RMSE, MBE and MAE for polycrystalline silicon and thin-film technologies. Small values of these errors validate the effectiveness of the proposed parameter estimation method.

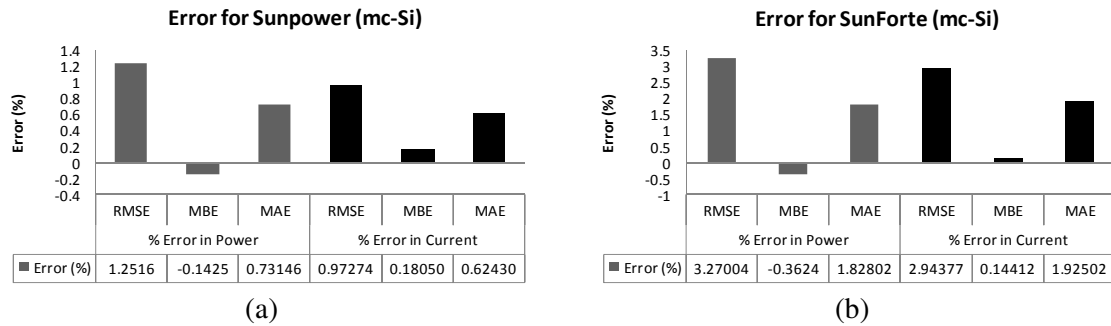


Figure 3.14: Cumulative error for power and current of mono-crystalline silicon technology (a) Sunpower 230W (b) SunForte PM318B00.

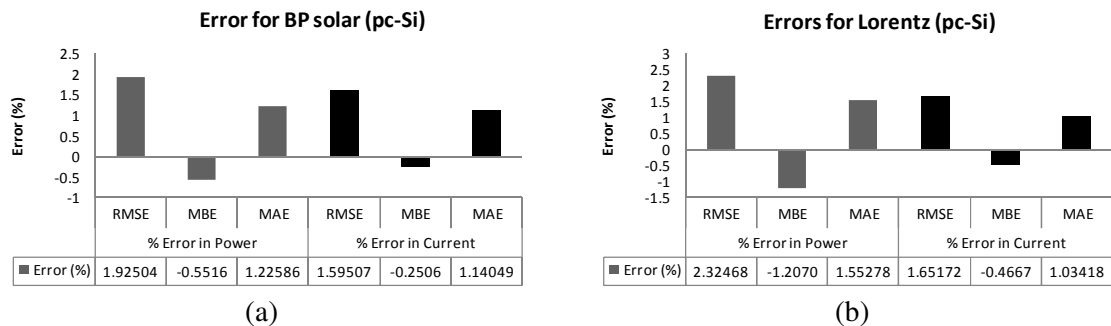


Figure 3.15: Cumulative error for power and current of polycrystalline silicon technology (a) BP Solar 3230N (b) Lorentz120W LC120-12P

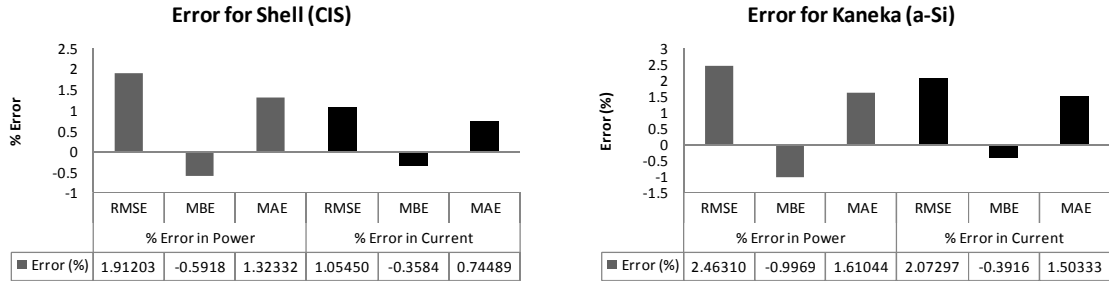


Figure 3.16: Cumulative error for power and current of thin-film technology (a) Shell ST36 (b) Kaneka U-EA110W.

In this test, the comprehensive analysis has been carried out to examine the effectiveness of the proposed parameter estimation method. Its efficiency has been tested for six PV panels of three different technologies by comparing the determined curves with the experimental curves. Three statistical errors have been used to measure its correctness at five key points. Cumulative error of each panel has been calculated. Results and analysis show that the estimated parameters can simulate the output characteristics of panels efficiently under all operating conditions.

3.6.2 Test 2: Performance as a large PV array

In this test performance of the proposed PV simulator as a large PV array is examined under different operating conditions. PV array is composed of 50 series and 20 parallel connected panels of mono-crystalline (mc-Si) [115] and electrical data of a PV panel is given in Table 3.2. Figure 3.17 shows the I-V curves of the selected PV array at different irradiation levels with constant temperature of 25⁰C. PV array has 20 panels in parallel as a result its short circuit current (I_{SC}) at STC become 20*5.99= 119.8 (20 is the short circuit of a PV a panel) and it has 50 panels in series thus its open circuit voltage (V_{OC}) at

STC become $48.7 \times 50 = 2435$ (48.7 is the open circuit voltage of a panel) and it is evident from Figure 3.17. It is also obvious from the graphs that the value of short circuit current (I_{SH}) is highly decreased and a value of open circuit voltage (V_{OC}) is slightly reduced by decreasing the irradiation level.

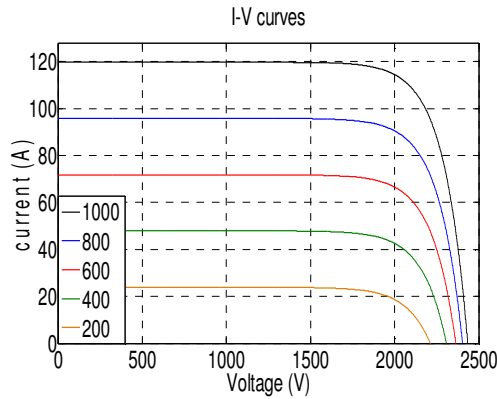


Figure 3.17: I-V characteristics of PV array at different irradiation (W/m^2) and constant temperature of 25°C .

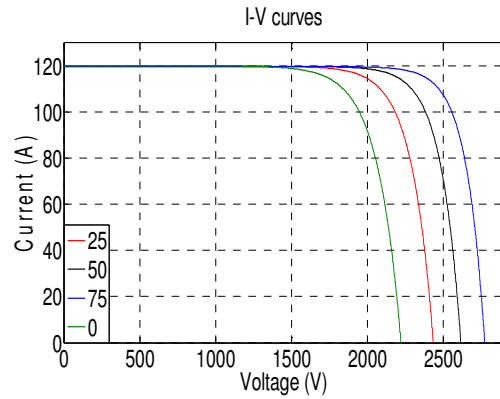


Figure 3.18: I-V characteristics of PV array at different temperatures ($^\circ\text{C}$) and constant irradiation of 1000W/m^2 .

Figure 3.18 shows the I-V curves of selected PV array at different temperatures and constant irradiation level of 1000W/m^2 . It is clear from the graphs that the I-V curve of the PV device are highly non-linear and short circuit current (I_{SH}) increased slightly and open circuit voltage (V_{OC}) decreased by increasing the cell temperature.

This test demonstrates that the proposed PV simulator can operate as a large PV array (PV power station) and can generate its I-V curves at different irradiation and temperatures. As these operating conditions cannot be constant and continuously varying with time, the proposed simulator can be a valuable tool to analyze the impacts of these changing condition on the overall power system performance and response.

3.6.3 Test 3: PV performance under partial shaded condition

In order to test the designed simulator under partial shaded condition, PV array configuration of Figure 3.8 is adopted. It consists of three series connected PV panels and each panel has dissimilar shading pattern hence representing a partially shaded PV array. Panel 1 is operating at 1000W/m^2 25°C , panel 2 at 800 W/m^2 25°C , and panel 3 at 300 W/m^2 25°C . Figure 3.19 and Figure 3.20 show the I-V and P-V curve of array. I-V curve shows the multiple steps and P-V curve shows multiple peaks.

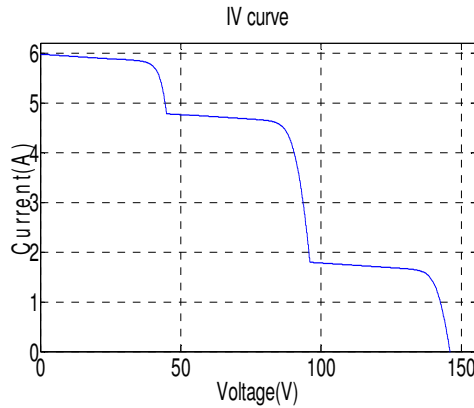


Figure 3.19: I-V curve for partial shaded PV array of Fig. 3.8.

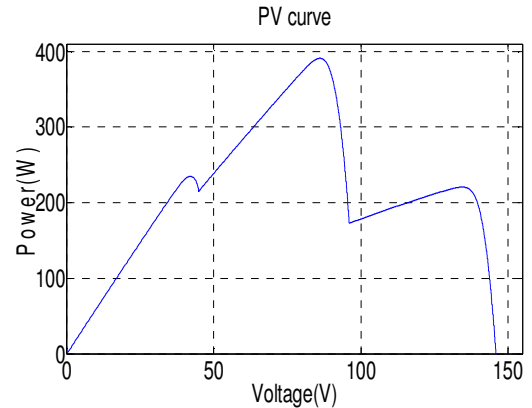


Figure 3.20: P-V curve for partial shaded PV array of Fig. 3.8.

The number of these steps/peaks depends upon the number of shaded pattern used. At lower voltage level (from 0-49V) only panel 1 is functioning and other two panels are by passed through the bypass diodes and they do not take part in the overall output voltage as the irradiation level of panel 1 is higher than other two panels. In the intermediate voltage level (from 49V-98V) panel 1 and panel 2 are operating and panel 3 is bypassed. From Figure 3.19 it can be noticed that when panel 2 start working PV array current trim down abruptly to reduced value of 4.8A. The reason for this drastic change is that the panel 2 is illuminated with lesser irradiation and it cannot produce higher current than

this value. Similarly, at high voltage level (greater than 98) all the three panels are functioning and current is limited by panel 3 because it has the lowest irradiation level. This test verifies the robustness of the designed simulator under the harsh condition of partial shading.

3.6.4 Test 4: Interfacing with converter and MPPT controller

This test shows the capability of a designed simulator to interface with the power electronics devices and maximum power point tracking controller. Figure 3.21 shows a complete PV system consisting of PV array simulator, DC-DC boost converter, MPPT controller and load. The PV simulator will generate the voltage and current depending upon the ambient conditions (irradiation and temperature). The current and voltage are varying due to changing atmospheric condition therefore DC-DC boost converter is used to maintain the output constant and available for the load where MPPT works as a controller for the DC-DC converter.

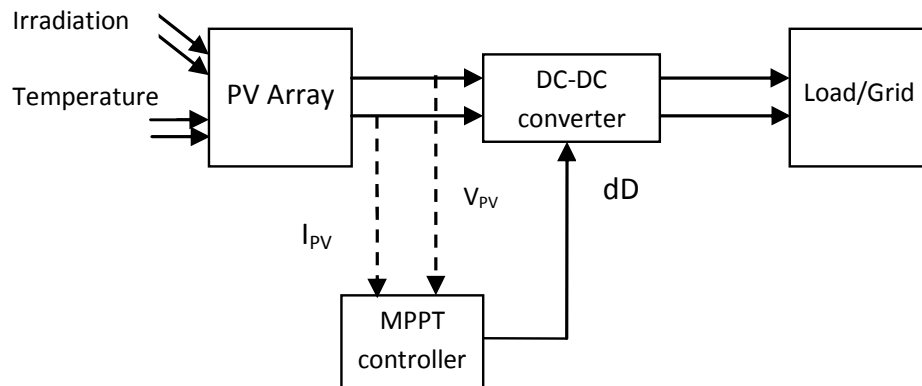


Figure 3.21: PV system used in test 4

A single PV panel is used in this test and its electrical data is given in the Table 3.2. A non-linear time domain simulation is carried out and a change in solar radiation is applied to assess the robustness of the proposed simulator in conjunction with converter and MPPT controller. Irradiation pattern is shown in Figure 3.22.

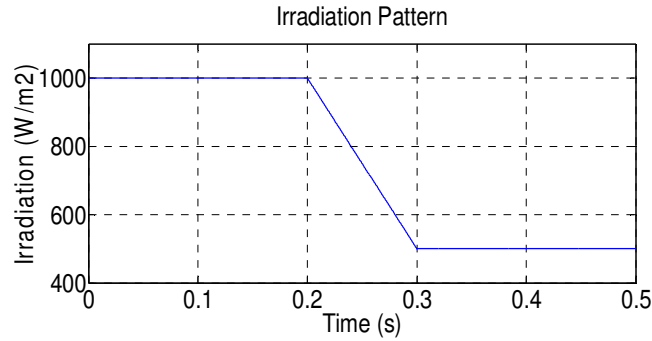


Figure 3.22: Irradiation pattern used in test

The solar radiation is decreased from 1000 (W/m^2) to 500 (W/m^2) from 0.2 sec to 0.3 sec. Figure 3.23 demonstrates that the MPPT controller is tracking the maximum power from the PV panel under both conditions. Result illustrates the dynamic performance of the overall system with the proposed simulator.

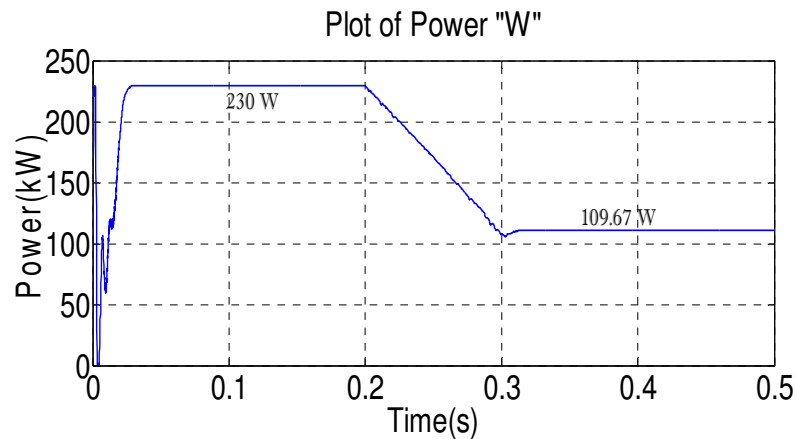


Figure 3.23: Plot of PV panel power (P_{PV}) vs time.

This test validates that the proposed PV simulator can function in conjunction with power electronics converters and their respective controllers. It allows the user to study the behavior of the whole system under different operating condition. Moreover, it can also be used to verify the effectiveness of MPPT controllers designed for normal and shaded conditions.

3.7 CONCLUSION

In this thesis a precise PV simulator has been developed based on the five parameters electric circuit model of PV device. Model parameters have been estimated by employing the efficient intelligent technique, Differential Evolution (DE), using only the data provided in the catalogue. PV simulator developed using these estimated parameters have been verified by comparing the curves of two different PV technologies at various operating conditions.

It has shown that the developed simulator can operate in harsh conditions of partial shading and rapidly changing irradiation condition. Further, the designed simulator can also be utilized in a complete PV system interfaced with different power electronic devices and MPPT controllers. Four different tests have been conducted and they verified the effectiveness of the proposed simulator. It is envisaged that the developed PV array simulator can be very helpful for the power system design engineers in the simulation study of the power systems before any experimental verification.

CHAPTER 4 PROPOSED MPPT CONTROLLER DESIGN

4.1 INTRODUCTION

PV devices have a non-linear I-V and P-V characteristics and have one optimum point called Maximum Power Point (MPP) as discussed in previous chapters. This maximum power point is highly vulnerable to the ambient conditions, that are irradiation and cell temperature, and these conditions are always changing with time which keeps varying the MPP. Therefore the maximum power point tracking (MPPT) controller is of great importance and is coupled with the PV arrays to track the MPP and extract the maximum possible power from the array. Many MPPT methods have been proposed in literature [49][50] from simple linear approximation methods to complex intelligent techniques [116]. Maximum power point tracker works with the DC-DC converter which is operated as an interface between the PV panel/array and load/inverter. DC-DC converter performs two major tasks, one is to track the maximum power point and to regulate and step up or step down the output voltage. Stepping up and stepping down of the output voltage depends entirely on the system requirements and boost or buck converter is used accordingly. Voltage from the PV panel, which is varying depending on ambient conditions, is given as input to the DC-DC converter and its output is constant voltage across the capacitor where load/inverter can be connected. MPPT works as a controller for the DC-DC converter and controls the duty ratio of the switch such that it

tracks the MPP under the changing ambient conditions. In short, maximum power point tracker (MPPT) is indispensable for all kinds of PV systems. Without MPPT controller PV array cannot not be able to operate at full efficiency and will work at a point on I-V curve that equivalent with the I-V characteristics of the connected load.

In this chapter, the conventional Incremental conductance (InCond) method and its shortcomings in tracking the MPP will be discussed. Then the new intelligent MPPT controller based on the Artificial Neuro-Fuzzy Inference System (ANFIS) is proposed and developed.

4.2 CONVENTIONAL INCREMENTAL CONDUCTANCE METHOD

The Incremental Conductance (InCond) method is basically based upon the Hill Climbing (HC) Method also known as Perturbation & Observation (P&O). A slight modification in HC and P&O results in a InCond with more robust tracking. First we will discuss the P&O method then InCond for better understanding.

P&O technique is based on the principle of moving the operating point of the PV array in the direction of power increases. The algorithm constantly adjusts the electrical operating point by measuring the operating voltage and current of the PV panel to observe the change in power transfer. The perturbation is applied by slightly changing the voltage in a certain direction, and the power change is observed. If the change is positive, it is obvious that the MPPT has moved the operating point of the PV panel closer to the MPP. Thus the voltage is perturbed in the same direction. If the change on the other hand

is negative, the operating point has become less optimal and the direction of perturbation must be changed. This algorithm can be described by the following statements:

If $dP/dV > 0$: The PV panel has achieved an operating point closer to the MPP

If $dP/dV < 0$: The PV panel has achieved an operation point further away from the MPP.

Algorithm of InCond is assumed as an improvement of the P&O method, as previously mentioned. As the name implies, the algorithm uses the incremental conductance as background of operation, which is the current divided by the voltage (inverted resistance). The MPPT finds the point where the gradient of the power over voltage equals zero and given by;

$$\frac{dP}{dV} = 0 \quad (4.1)$$

Using the product rule, the below relation can be found;

$$\frac{dP}{dV} = \frac{d(IV)}{dV} = \frac{dI}{dV} + I \frac{dV}{dV} = \frac{dI}{dV} V + I \quad (4.2)$$

$$\frac{dI}{dV} = -\frac{I}{V} \quad (4.3)$$

Flow chart for the InCond is shown in Figure 4.1

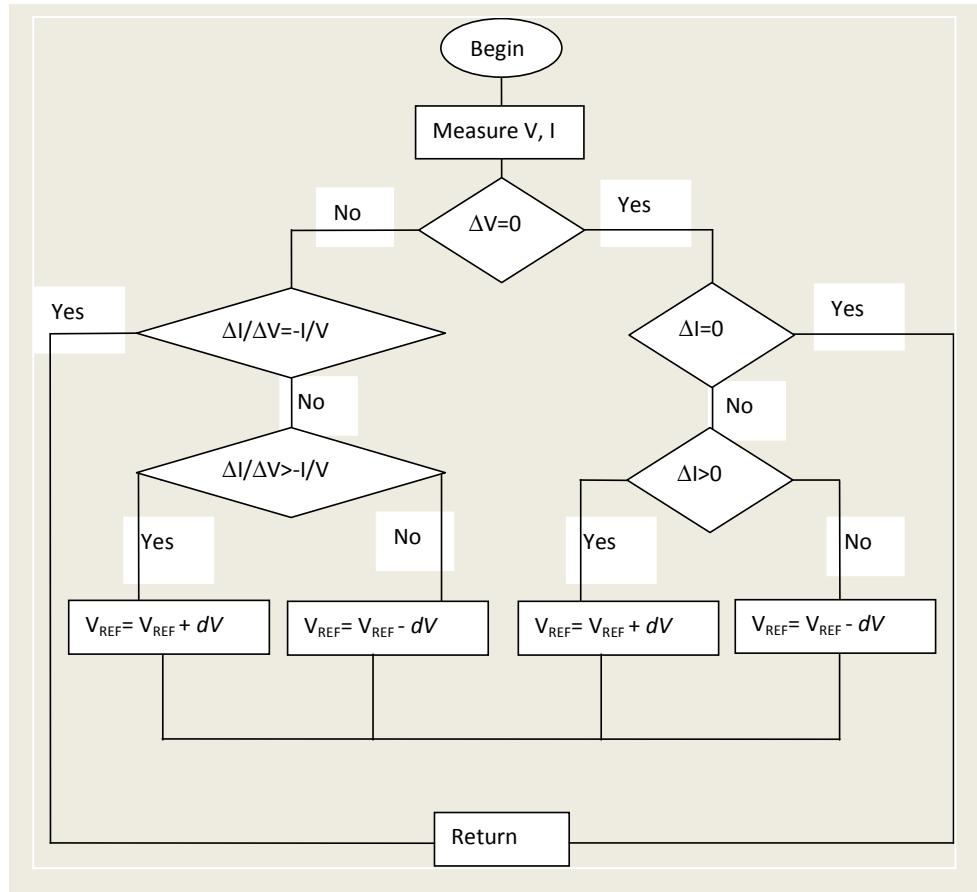


Figure 4.1: Flowchart for incremental conductance method.

Drawbacks of the conventional MPPT techniques are thoroughly discussed in [79] and are given below;

- Slow converging to the optimum operating point.
- At steady-state condition, the amplitude of the PV power oscillates around the maximum point that causes system power losses.
- During cloudy days when the irradiance varies quickly the operating point moves away from the maximum optimum point.

4.3 PROPOSED ANFIS-BASED MPPT

4.3.1 Adaptive Network-Based fuzzy Inference System (ANFIS)

Like neural network ANFIS also has network type structure and maps the input-output data set using the parameters of fuzzy membership functions. Figure 4.2 demonstrates a simple ANFIS architecture based on the two rule Sugeno system with two inputs (X and Y) and single output (F). Here A1, A2 and B1, B2 are fuzzy input memberships for input X and Y, respectively and are used to fuzzify the inputs [102].

A Two Rule Sugeno ANFIS has rules of the form:

$$\text{If } X \text{ is } A_1 \text{ and } y \text{ is } B_1 \text{ THEN } f_1 = p_1x + q_1y + r_1 \quad (4.4)$$

$$\text{If } X \text{ is } A_2 \text{ and } y \text{ is } B_2 \text{ THEN } f_2 = p_2x + q_2y + r_2 \quad (4.5)$$

Overall ANFIS architecture has 5 layers as shown in Figure 4.2 and now we discuss each layer in turn.

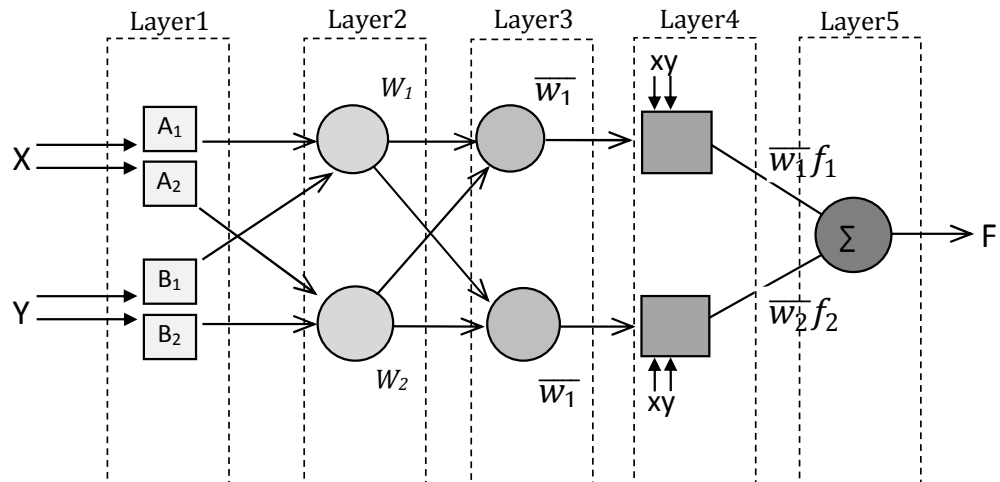


Figure 4.2: ANFIS architecture.

Layer 1:

In layer 1 every node is adaptive node and their number depends upon the number of input membership functions. Their output is given by:

$$O_{1,i} = \mu_{A_i}(x) \quad \text{for } i = 1,2 \quad (4.6)$$

$$O_{1,i} = \mu_{B_{i-2}}(y) \quad \text{for } i = 3,4 \quad (4.7)$$

Where, μ is the membership function and $O_{1,i}$ is the membership value for the crisp inputs X and Y . The subscripted 1 and i represent the layer number and node number, respectively.

Membership functions “ μ ” can be any shaped function like trapezoidal, triangle, gaussian. The most commonly used membership function is generalized bell and is given by:

$$\mu_A(x) = \frac{1}{1 + \left| \frac{x - c_i}{a_i} \right|^{2b_i}} \quad (4.8)$$

Where; a_i , b_i , c_i are parameters of the membership function (called **premise** parameter) and need to be optimize in the training process.

Layer2:

Every node in this layer is fixed node and accepts the output (membership values) from the layer 1 where t-norm is utilized to “AND” these values, given by;

$$O_{2,i} = w_i = \mu_{A_i}(x)\mu_B(y) \quad i = 1,2 \quad (4.9)$$

Output of each node corresponds to the firing strength of a rule.

Layer 3:

Every node in this layer is fixed node and used to normalize the firing strength by dividing the rule's firing strength by the sum of all rules firing strengths, given by;

$$O_{3,i} = \bar{w}_i = \frac{w_i}{w_1 + w_2} \quad (4.10)$$

Output of each node represents the normalized firing strength of a rule.

Layer 4:

Every node in this layer is adaptive node and given by the function;

$$O_{4,i} = \bar{w}_i f_i = \bar{w}_i (p_i x + q_i y + r_i) \quad (4.11)$$

Where; p_i , q_i , r_i is the consequent parameters and need to optimize in the training process.

Layer 5:

It has only one fixed node and sum up all the input signals to get the final output and is given by;

$$O_{5,i} = \sum_i \bar{w}_i f_i = \frac{\sum_i w_i f_i}{\sum_i w_i} \quad (4.12)$$

Learning Process:

In the learning algorithm ANFIS optimize and adapt its parameters using the training data sets to predict the output data with high accuracy. The Sugeno-type model has two types of parameters [103].

- Nonlinear parameters or membership functions parameters (premise parameters).
- Linear parameters or rules parameters (consequent parameters).

Various learning methods have been proposed by the researchers. Method used in this paper is based on the hybrid learning algorithm that employ the combination of back propagation (BP) and least square estimation (LSE) to optimize the premise and consequent parameters [102].

In this method two pass learning algorithms (forward pass and backward pass) are used:

- In forward pass consequent (linear) parameters are calculated using a LSE algorithm while premise (nonlinear) parameters are unmodified.
- In backward pass premise (nonlinear) parameters are calculated using a back propagation algorithm while consequent (linear) parameters are unmodified.

LSE learning algorithm calculates the square error between training data output and predicted output that is obtained from the Sugeno-type model. This error is utilized to adapt the consequence parameters of the Sugeno parameters. The back propagation gradient descent method uses the error between output training data and predicted output in backward pass to calculate the error in different nodes.

4.3.2 Application of ANFIS for MPPT

As the output characteristics of PV system are highly nonlinear, AI techniques are widely used to improve the efficiency of the MPPT controller [116]. Fuzzy logic can transform the linguistic and heuristic terms to numerical values and numerical values to linguistic terms using membership functions and fuzzy rules. Neural network can map the input output nonlinear functions but it does not have heuristic nature. Researchers combine the FIS with the ANN to build a hybrid system named as Adaptive Network-Based Fuzzy Inference System (ANFIS) to balance the shortcomings of one system with the advantages of another system [102].

To design a MPPT controller using ANFIS, first task is to gather the input-output data set for training purpose. This training data is generated using the developed PV model in chapter 3. A step by step process of data generation is illustrated in the flowchart shown in Figure 4.3. As a first step, values of the five unknown parameters for a considered PV panel and PV array are estimated using an efficient algorithm proposed in chapter 3. The training parameters are;

N_{MAX} : Number of training data points.

T_{MIN} : Minimum temperature

T_{MAX} : Maximum temperature

S_{MIN} : Minimum Irradiation

S_{MAX} : Maximum Irradiation

Where; T_{MIN} , T_{MAX} and S_{MIN} , S_{MAX} represent the range of temperature and irradiation and can be specified depending upon the geographical location where PV array is installed.

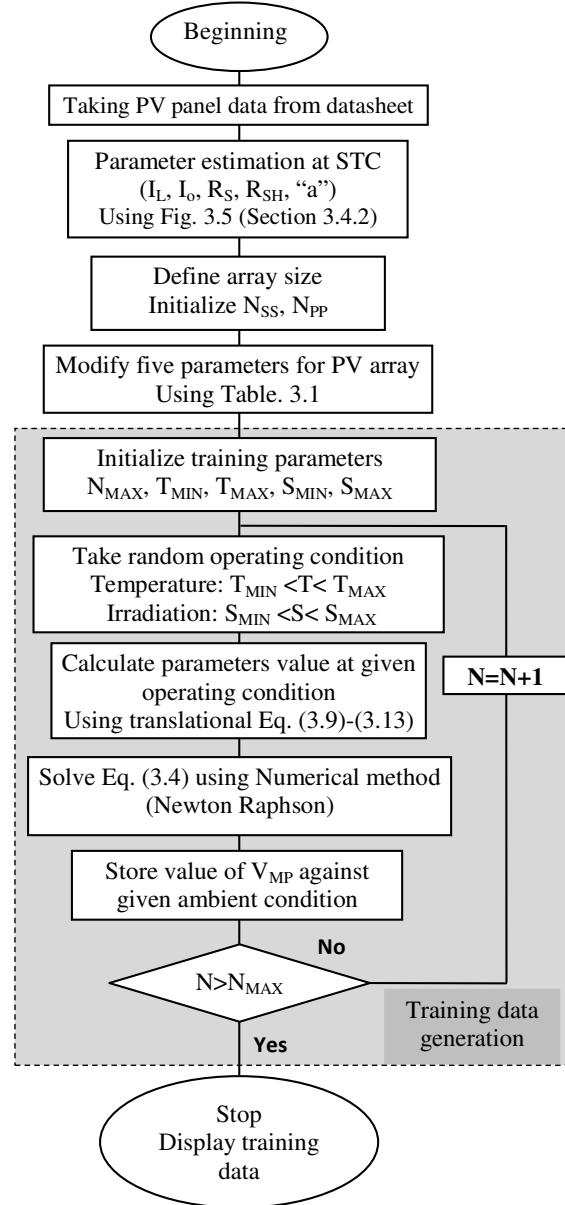


Figure 4.3: Proposed method to generate input output data set for ANFIS training

It is followed by the generation of random operating condition within the specified range and modification of five parameters at this operating condition using Eq. (3.9) to (3.13). Advantage of using the random operating condition is that it includes the uncertainties of the weather conditions within the training process. Then the transcendental non-linear equation Eq. (3.4) is solved for current calculation using proficient numerical technique (Newton-Raphson in our case) and value of voltage corresponding to maximum power point is stored against the specified operating condition. This process is executed for N_{MAX} times to generate the training data set of length N_{MAX} . After getting the input-output data set, next step is to design the ANFIS-based MPPT by hybrid learning algorithm. In the learning algorithm parameters of the membership functions are adapted such that they track the input output data finely.

The arrangement of the developed ANFIS-based MPPT controller is shown in Figure 4.4. Input of the proposed ANFIS-based MPPT controller is the ambient conditions, i.e irradiation and temperature and its output is the reference voltage (V_{REF}) which is normalized using DC link voltage (V_{DC}). The normalized reference voltage ($V_{REF, norm}$) is fed back to the voltage control loop where PI controller is used to maintain the output voltage of PV array (V_{PV}) to the reference optimal voltage by adjusting the duty ratio of DC-DC converter, which results in maximum power extraction.

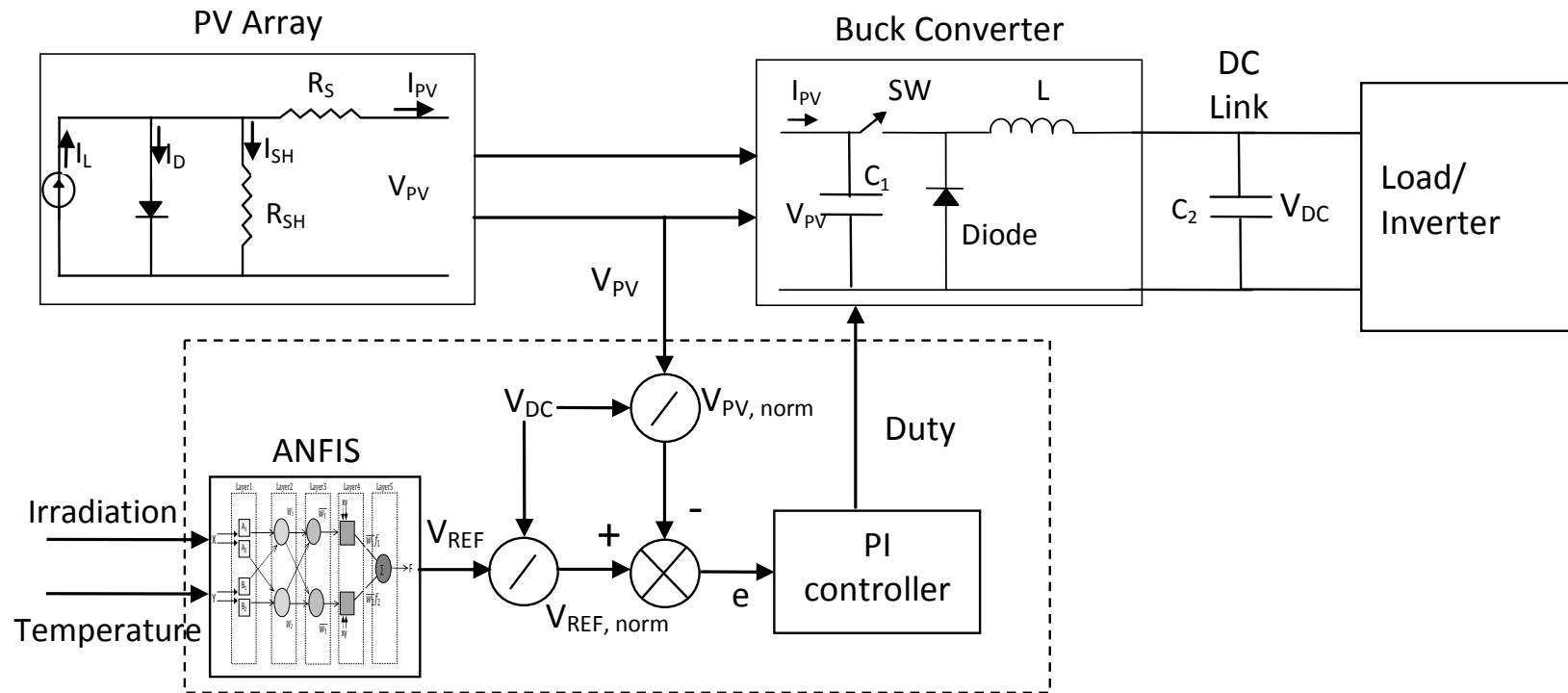


Figure 4.4: PV system.

4.3.3 Testing of ANFIS

A PV system used to verify the competence of the proposed ANFIS-based MPPT controller is shown in Figure 4.4. It consists of PV array, DC-DC buck converter, MPPT controller, DC link capacitor and inverter. PV array will generate a varying DC voltage (V_{PV}) and current (I_{PV}) depending upon the weather conditions. Buck converter and DC link capacitor are utilized to smooth these varying quantities and make accessible for the inverter. MPPT is employed as a controller for buck converter that adjusts the duty ratio of switch to extract maximum possible power from the PV array under all operating conditions.

Specifications of a PV panel used are shown in Table 4.1. An array of 50x20 panels is used to show the operation of the proposed ANFIS-based MPPT controller with a large PV power station.

Table 4.1: Specification of PV panel at STC.

Panel parameters from data sheet	Value	Estimated model parameters	Values
V_{OC}	21.7	I_L	3.35
I_{SC}	3.35	I_0	1.7053e-05
V_{MP}	17.4	R_S	0.00477
I_{MP}	3.05	R_{SH}	3.9601e+04
N_c	36	a	1.78044

Buck converter is designed to work in a continuous conduction mode (CCM) and have the specifications of; $C_1=100 \mu\text{F}$, $L=5 \text{ mH}$, switching frequency of 5 kHz and DC link capacitor $C_2=500 \mu\text{F}$. Training parameters used to generate the set of input-output

data set are; $N_{MAX}=1000$, $T_{MAX}=80^{\circ}\text{C}$, $T_{MIN}=0^{\circ}\text{C}$, $S_{MAX}=2000\text{W/m}^2$, $S_{MIN}=0\text{W/m}^2$. These parameters show the wide and dynamic range for temperature and irradiation that allows the designed MPPT to work efficiently under uncertain operating conditions.

The ANFIS-based MPPT is developed in MATALB/Simulink using three generalized bell (g-bell) membership functions. Hybrid learning algorithm is utilized that use the LSE to adapt the consequent parameters and back propagation method to optimize the premise parameters of the membership functions. The epochs selected for training purpose is 300 that reduced the training root mean square error (RMSE) to the lower value of 0.8 as shown in Figure 4.5.

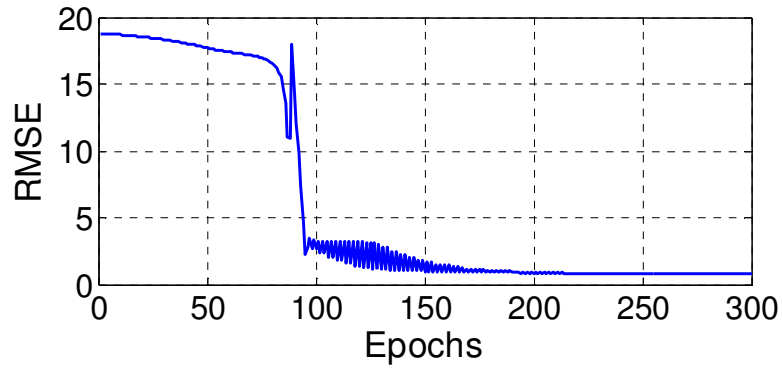


Figure 4.5: Training error versus epochs for the ANFIS

4.4 RESULT AND DISCUSSION

To validate the effectiveness of the proposed ANFIS-based MPPT a comparison with conventional incremental conductance (InCond) method is carried out. Four different tests are conducted to verify the effectiveness of the proposed controller. These tests are

step-up change in irradiation, step-down change in irradiation, step-up change in temperature and step-down change in temperature and are explained below.

4.4.1 Test 1: Step-up change in irradiation

This test is conducted under the step-up change in irradiation level and its pattern is shown in the Figure 4.6. It shows that the solar radiation is constant with a value of 500 W/m^2 up to 0.25 seconds and then increases drastically to 1000 W/m^2 . The P-V curves for selected PV array under low (500 W/m^2 and 25°C) and normal (1000 W/m^2 and 25°C) irradiation level are shown in Figure 4.7. It can be seen that the maximum power that can be generated by PV array at low irradiation level is 24.669 kW and labeled as point X on the graph. After a step-up change in irradiation, the operating point shifts to point Y having the maximum possible power of 53.07 kW ($V_{MP} \cdot I_{MP} \cdot N_{SS} \cdot N_{PP} = 53.07 \text{ kW}$).

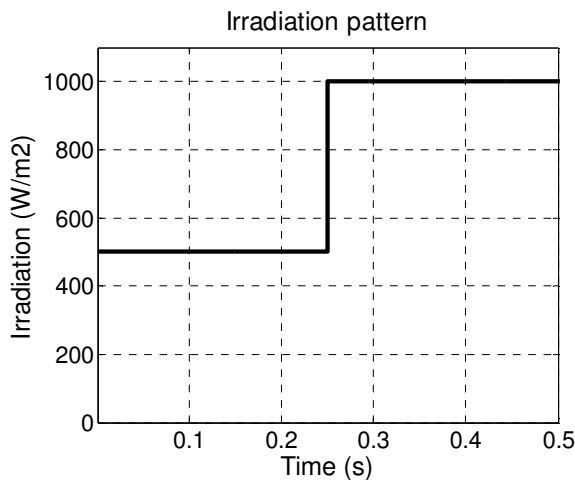


Figure 4.6: Setup-up irradiation pattern.

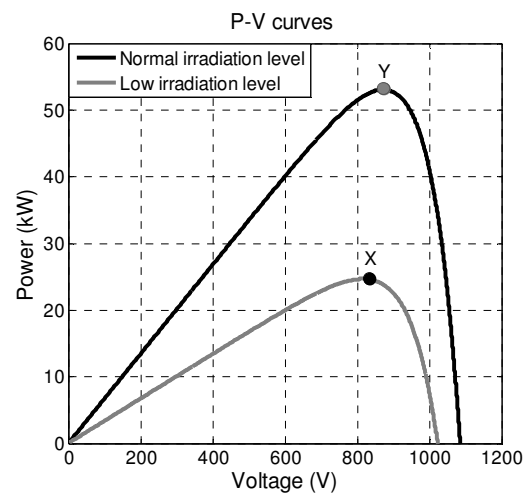


Figure 4.7: PV curve under normal and low irradiation conditions.

A non-linear time domain simulation is carried out with the proposed ANFIS-based and InCond-based MPPT controllers. For InCond method fixed value of perturbation step

size is chosen based on a tradeoff between fluctuations in the steady state and tracking speed. Figure 4.8 shows a comparison of PV array power output (P_{PV}) for both the controllers. It can be seen from the graph that the MPP reached by the proposed ANFIS-based MPPT controller is much faster than the conventional InCond in both the tracking regions, i.e start of the algorithm and step-up change in irradiation. For example it can track the MPP in 0.04 sec while the InCond take 0.1 sec in the start of the algorithm. When a step-up change in irradiation occur, the MPPT controller shifts the operating point from point X to Y and it can be noticed from the plot that the response of InCond is much slower than the proposed ANFIS-based MPPT.

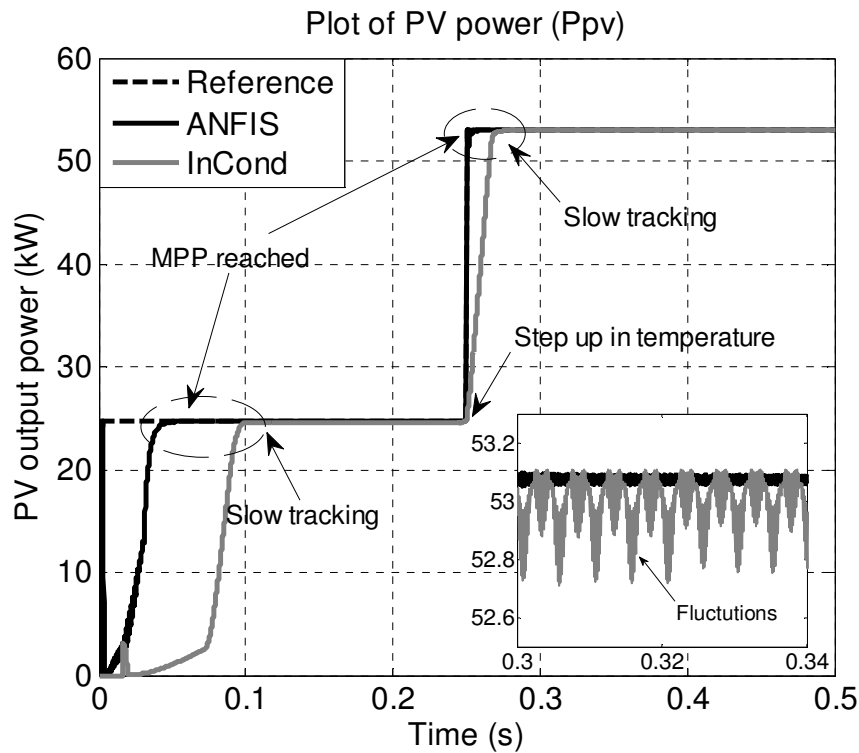


Figure 4.8: Characteristics of PV power output under step-up irradiation change

To demonstrate the efficiency of a proposed controller in the steady state region, portion of a graph from 0.3sec to 0.34sec is enlarged where irradiation level is maintained at 1000W/m^2 . It can be noticed from the enlarged graph that the proposed ANFIS-based MPPT has smoother response as compare to InCond which shows a considerable amount of fluctuation in the steady state and its power varies from 53.07 kW to 52.78 kW that shows oscillation of 294W. Although, it is possible to diminish these fluctuations by reducing the perturbation step size but that results in even more slow tracking of MPP.

The simulation results for duty cycle, PV array voltage (V_{PV}) and current (I_{PV}) are shown in Figure 4.9, Figure 4.10, Figure 4.11, respectively, and verify the effectiveness of the proposed MPPT under the rapidly changing irradiation condition.

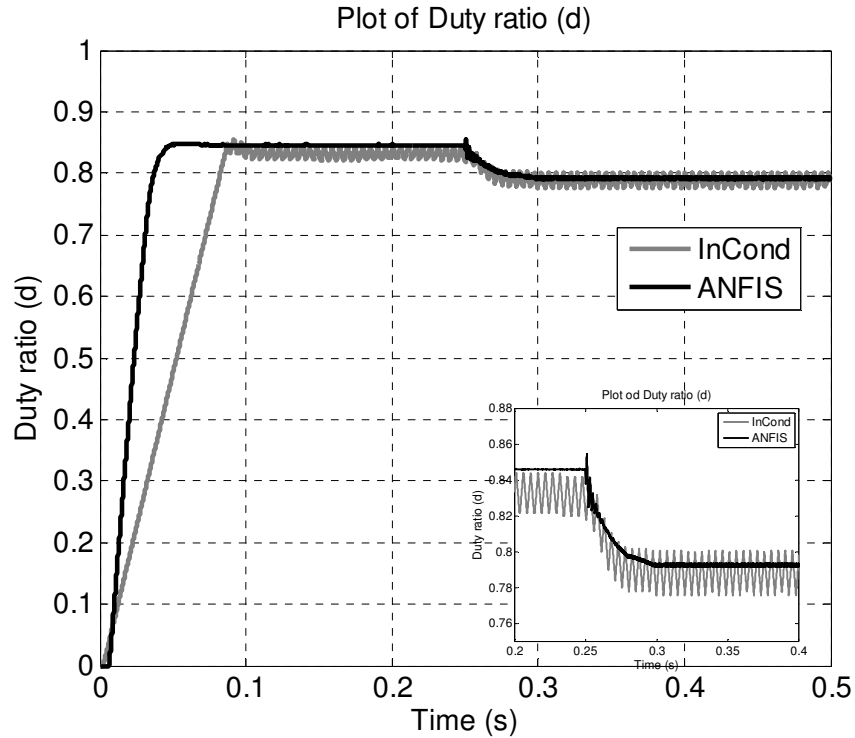


Figure 4.9: Plot of duty ratio under step-up change in irradiation.

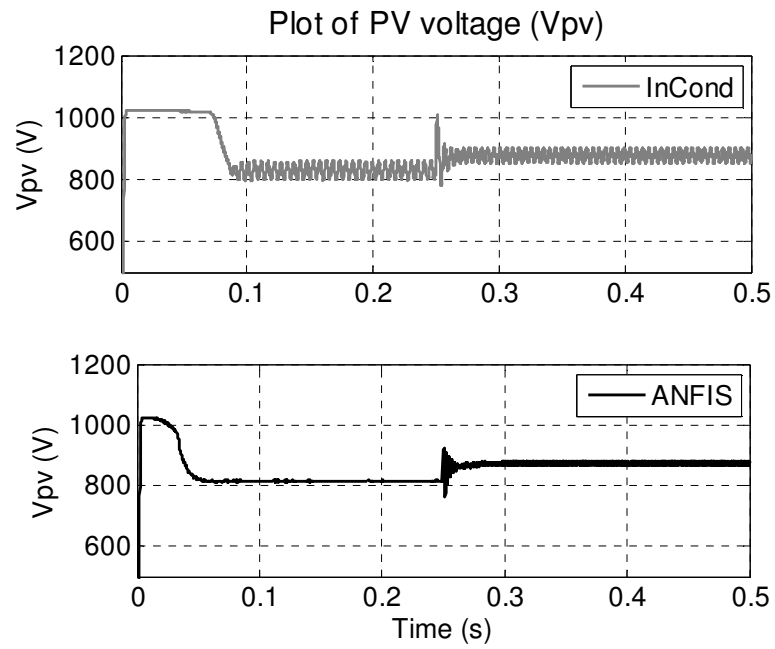


Figure 4.10: Characteristics of PV voltage under step-up irradiation change.

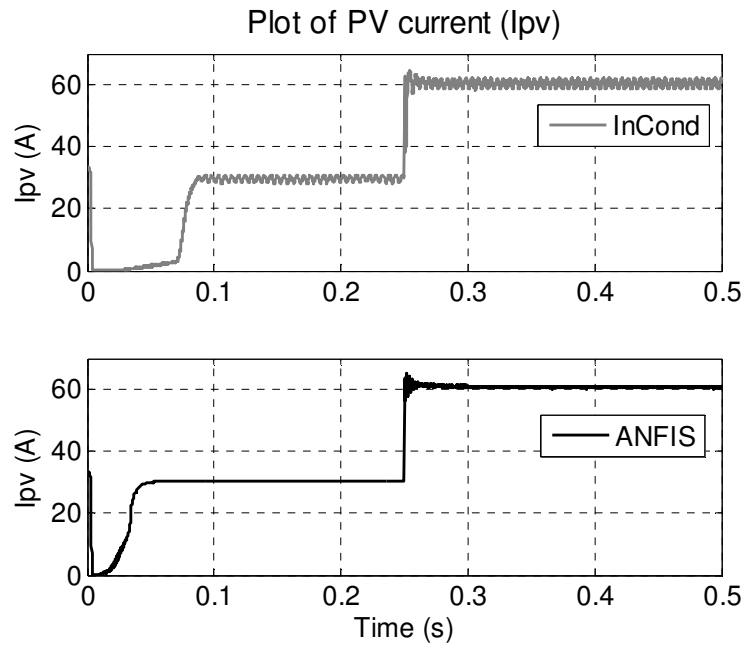


Figure 4.11: Characteristics of PV current under step-up irradiation change.

4.4.2 Test 2: Step-down change in irradiation

This test is conducted under the step-down change in irradiation level and its pattern is shown in the Figure 4.12. It shows that the solar radiation is constant with a value of 1000 W/m^2 up to 0.25 seconds and then decrease drastically to 500 W/m^2 . The P-V curves for selected PV array under normal (1000 W/m^2 and 25°C) and low (500 W/m^2 and 25°C) irradiation level are shown in Figure 4.13. It can be seen that the maximum power that can be generated by PV array at normal irradiation level is 53.07kW ($V_{MP} \cdot I_{MP} \cdot N_{SS} \cdot N_{PP} = 53.07\text{kW}$) and labeled as point X on the graph. After a step-down change in irradiation, the operating point shifts to point Y having the maximum possible power of 24.669kW as shown in Figure 4.13.

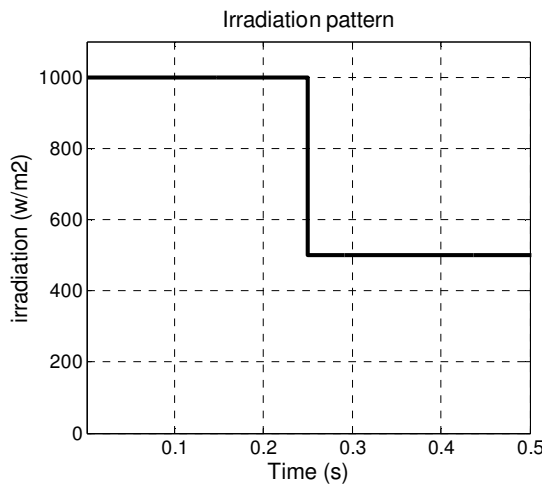


Figure 4.12: Setup-down irradiation pattern.

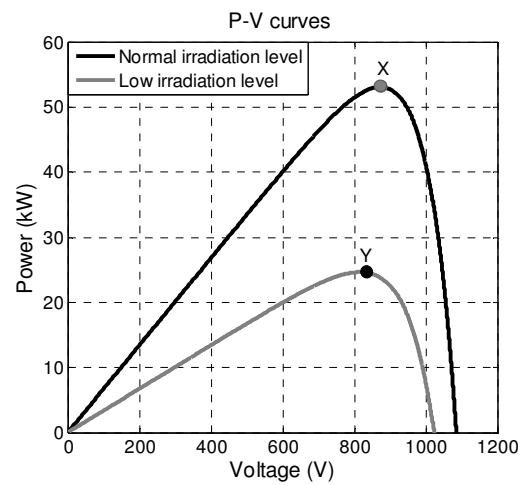


Figure 4.13: PV curve under normal and low irradiation conditions.

A non-linear time domain simulation is carried out with the proposed ANFIS-based and InCond MPPT controllers. For InCond method fixed value of perturbation step size is chosen based on a tradeoff between fluctuations in the steady state and tracking speed. Figure 4.14 shows a comparison of PV array power output (P_{PV}) for both the controllers.

It can be seen from the graph that the MPP reached by the proposed ANFIS-based controller is much faster than the conventional InCond in both the tracking regions, i.e start of the algorithm and step-up change in irradiation. For example it can track the MPP in 0.04 sec while the InCond take more than 0.1 sec in the start of the algorithm. When a step-down change in irradiation occur, the MPPT controller shifts the operating point from point X to Y and it can be noticed from the plot that the response of InCond is much slower than the proposed ANFIS-based MPPT.

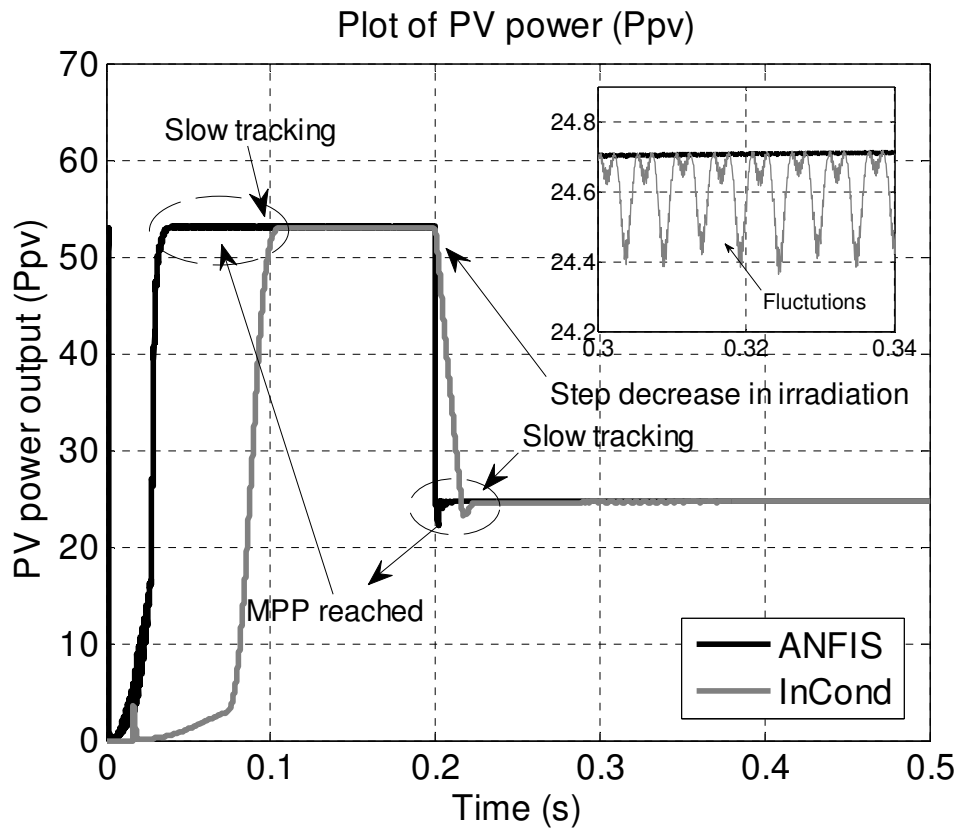


Figure 4.14: Characteristics of PV power output under step-down irradiation change.

To demonstrate the efficiency of a proposed controller in the steady state region, portion of a graph from 0.3 sec to 0.34 sec is enlarged where irradiation level is

maintained at 500 W/m^2 . It can be noticed from the enlarged graph that the proposed ANFIS-based MPPT has smoother response as compare to InCond which shows a considerable amount of fluctuation in the steady state and its power varies from 24.67 kW to 24.39 kW that shows oscillation of 280 W. Although, it is possible to diminish these fluctuations by reducing the perturbation step size but that results in even more slow tracking of MPP.

The simulation results for duty cycle, PV array voltage (V_{PV}) and current (I_{PV}) are shown in Figure 4.15, Figure 4.16, Figure 4.17, respectively, and verify the effectiveness of the proposed MPPT under the rapidly changing irradiation condition.

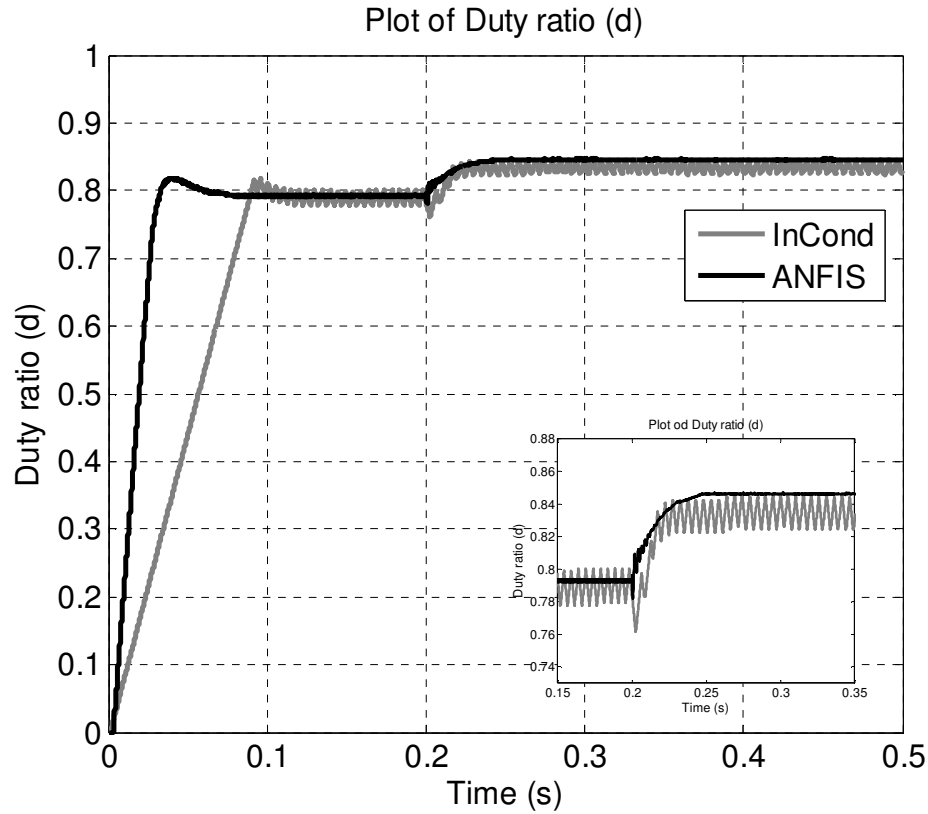


Figure 4.15: Plot of duty ratio under step-down irradiation change.

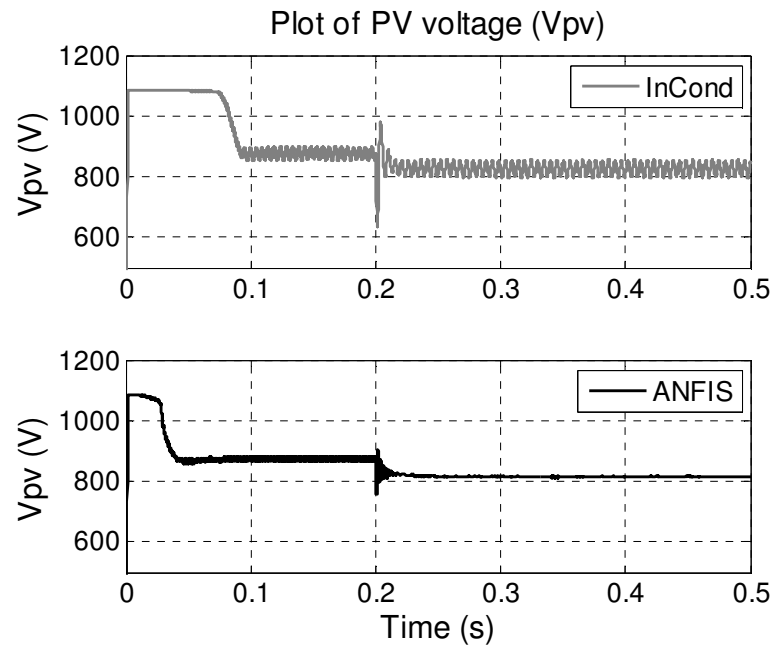


Figure 4.16: Characteristics of PV voltage under step-up irradiation change.

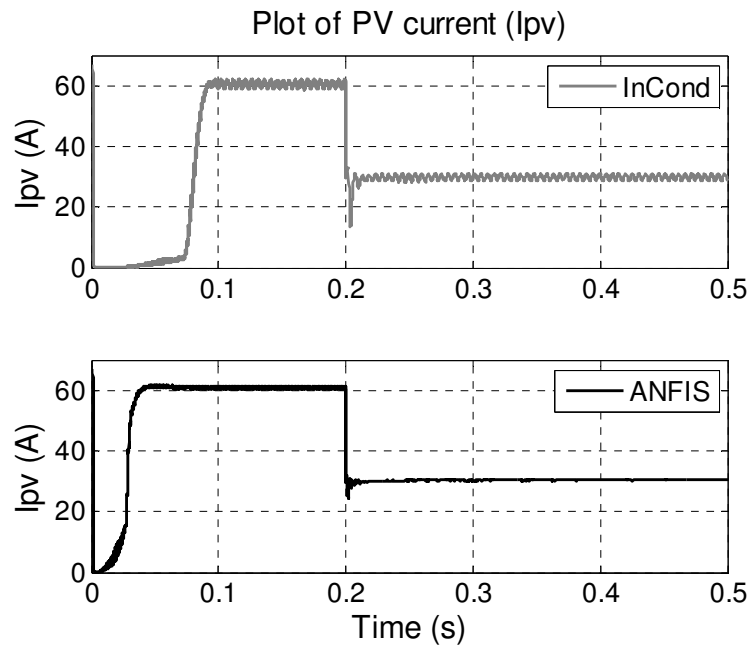


Figure 4.17: Characteristics of PV current under step-up irradiation change.

4.4.3 Test 3: Step-up change in temperature

This test is conducted under the step-up change in temperature and its pattern is shown in the Figure 4.18. It shows that the temperature is constant with a value of 0°C up to 0.25 seconds and then increases drastically to 25°C . The P-V curves for selected PV array at low temperature (0°C and 1000 W/m^2) and normal (1000 W/m^2 and 25°C) temperature are shown in Figure 4.19. It can be seen that the maximum power that can be generated by PV array at low temperature is 59.53 kW and labeled as point X on the graph. After a step-up change in temperature, the operating point shifts down to point Y having the maximum possible power of 53.07 kW ($V_{MP} \cdot I_{MP} \cdot N_{SS} \cdot N_{PP} = 53.07 \text{ kW}$) as shown in Figure 4.19.

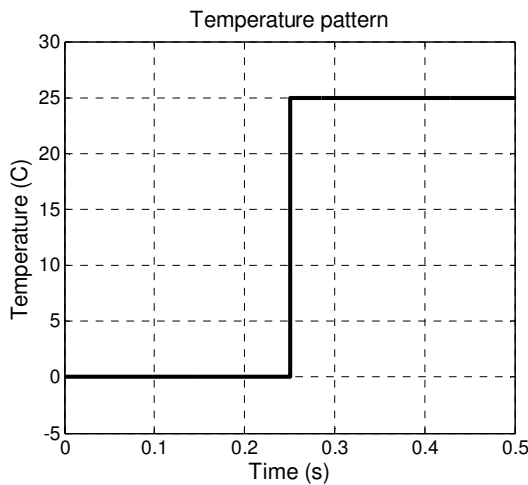


Figure 4.18: Step-up temperature pattern.

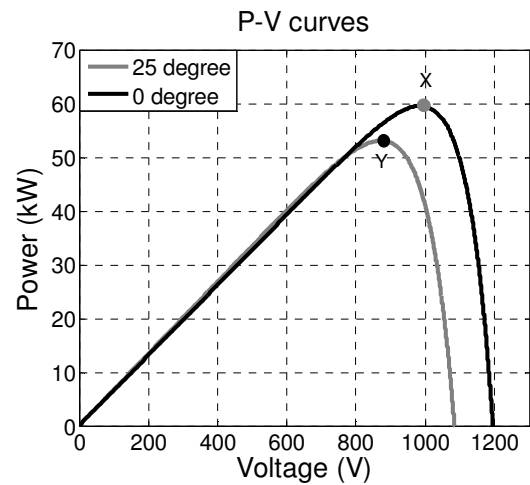


Figure 4.19: PV curve under normal and low temperature conditions.

A non-linear time domain simulation is carried out with the proposed ANFIS-based and InCond MPPT controllers. For InCond method fixed value of perturbation step size is chosen based on a tradeoff between fluctuations in the steady state and tracking speed. Figure 4.20 shows a comparison of PV array power output (P_{PV}) for both the controllers.

It can be seen from the graph that the MPP reached by the proposed ANFIS-based controller is much faster than the conventional InCond in both the tracking regions, i.e start of the algorithm and step-up change in temperature. For example it can track the MPP in 0.04 sec while the InCond take more than 0.1 sec in the start of the algorithm. When a step-up change in temperature occur, the MPPT controller shifts the operating point from point X to Y and it can be noticed from the plot that the response of InCond is much slower than the proposed ANFIS-based MPPT.

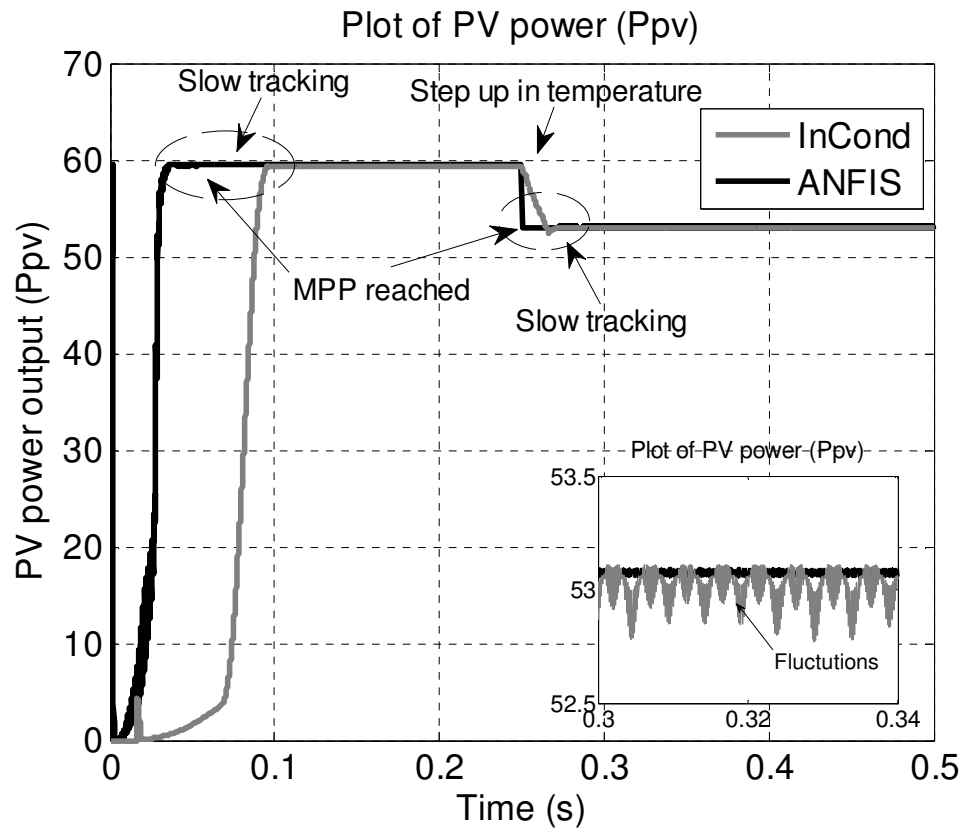


Figure 4.20: Characteristics of PV power output under step-up temperature change.

To demonstrate the efficiency of a proposed controller in the steady state region, portion of a graph from 0.3 sec to 0.34 sec is enlarged where temperature and irradiation

level are maintained at 25°C and 1000 W/m^2 . It can be noticed from the enlarged graph that the proposed ANFIS-based MPPT has smoother response as compare to InCond which shows a considerable amount of fluctuation in the steady. Although, it is possible to diminish these fluctuations by reducing the perturbation step size but that results in even more slow tracking of MPP. The simulation results for duty cycle, PV array voltage (V_{PV}) and current (I_{PV}) are shown in Figure 4.21, Figure 4.22, Figure 4.23 respectively, and verify the effectiveness of the proposed MPPT under the rapidly changing temperature condition.

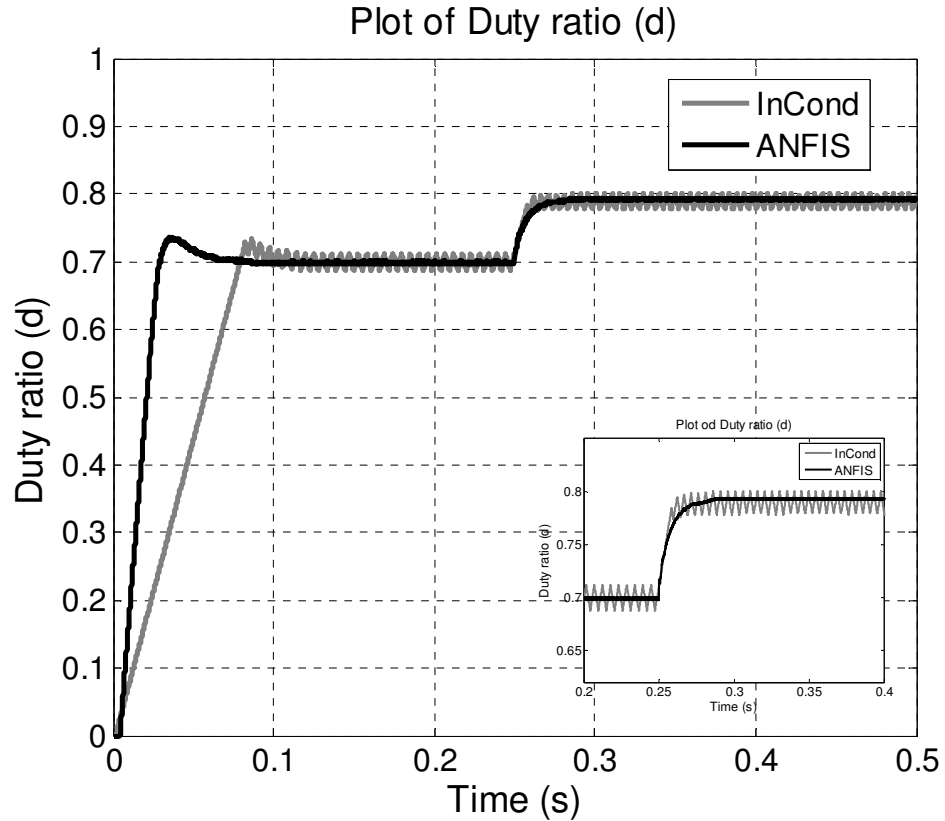


Figure 4.21: Plot of duty ratio under step-up temperature change.

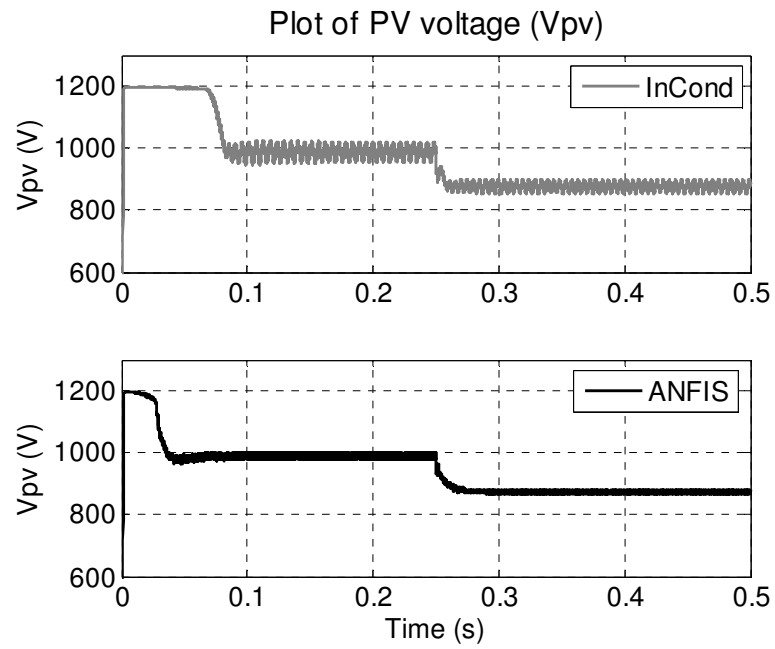


Figure 4.22: Characteristics of PV voltage under step-up temperature change.

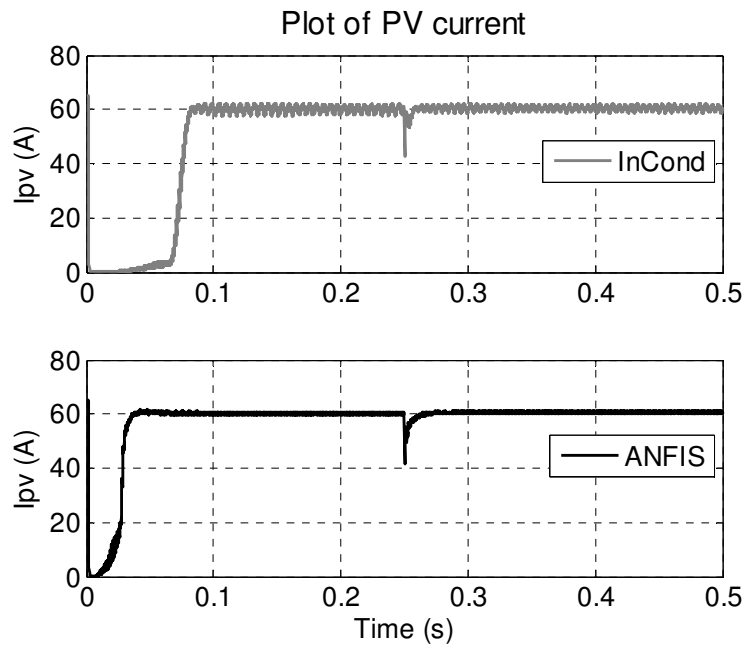


Figure 4.23: Characteristics of PV voltage under step-up temperature change.

4.4.4 Test 4: Step-down change in temperature

This test is conducted under the step-down change in temperature and its pattern is shown in the Figure 4.24. It shows that the temperature is constant with a value of 25°C up to 0.25 seconds and then decreases drastically to 0°C . The P-V curves for selected PV array under normal (25°C and 1000 W/m^2) and low temperature (0°C and 1000 W/m^2) irradiation level are shown in Figure 4.25. It can be seen that the maximum power that can be generated by PV array at normal irradiation level is 53.07kW ($V_{\text{MP}}*I_{\text{MP}}*N_{\text{SS}}*N_{\text{PP}}=53.07\text{kW}$) and labeled as point X on the graph. After a step-down change in temperature, the operating point shifts up to point Y having the maximum possible power of 59.53kW as shown in Figure 4.25.

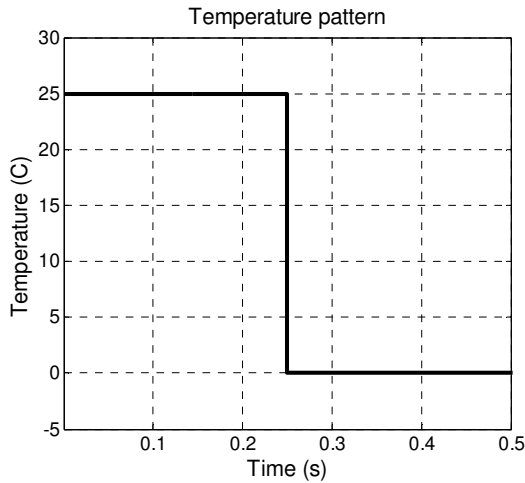


Figure 4.24: Step-down temperature pattern.

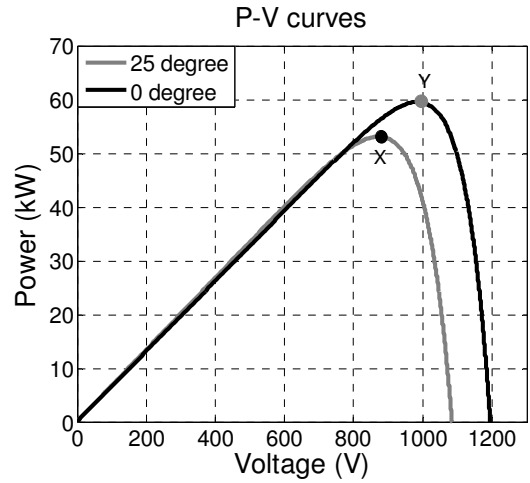


Figure 4.25: PV curve under normal and low temperature conditions.

A non-linear time domain simulation is carried out with the proposed ANFIS-based and InCond MPPT controllers. For InCond method fixed value of perturbation step size is chosen based on a tradeoff between fluctuations in the steady state and tracking speed. Figure 4.26 shows a comparison of PV array power output (P_{PV}) for both the controllers.

It can be seen from the graph that the MPP reached by the proposed ANFIS-based controller is much faster than the conventional InCond in both the tracking regions, i.e start of the algorithm and step-up change in irradiation. For example it can track the MPP in 0.04 sec while the InCond take more than 0.1 sec in the start of the algorithm. When a step-down change in temperature occur, the MPPT controller shifts the operating point from point X to Y and it can be noticed from the plot that the response of InCond is much slower than the proposed ANFIS-based MPPT.

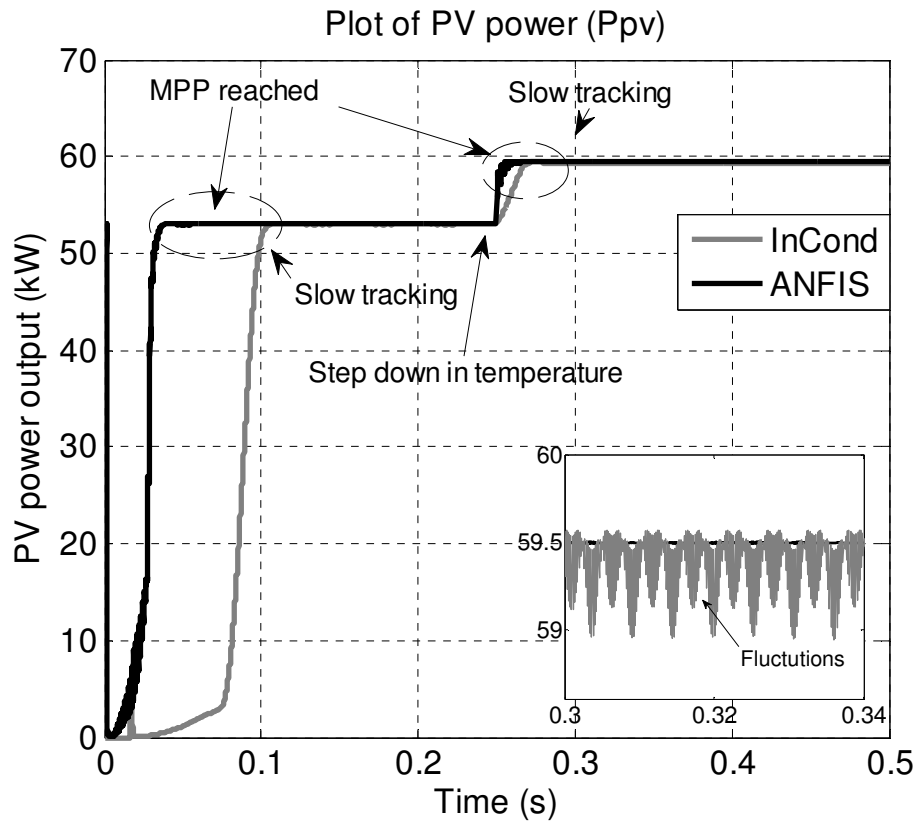


Figure 4.26: Characteristics of PV power output under step-down temperature change.

To demonstrate the efficiency of a proposed controller in the steady state region, portion of a graph from 0.3 sec to 0.34 sec is enlarged where temperature and irradiation

level is maintained at 0°C and 1000 W/m^2 . It can be noticed from the enlarged graph that the proposed ANFIS-based MPPT has smoother response as compare to InCond which shows a considerable amount of fluctuation in the steady state. Although, it is possible to diminish these fluctuations by reducing the perturbation step size but that results in even more slow tracking of MPP.

The simulation results for duty cycle, PV array voltage (V_{PV}) and current (I_{PV}) are shown in Figure 4.27, Figure 4.28, Figure 4.29, respectively, and verify the effectiveness of the proposed MPPT under the rapidly changing irradiation condition.

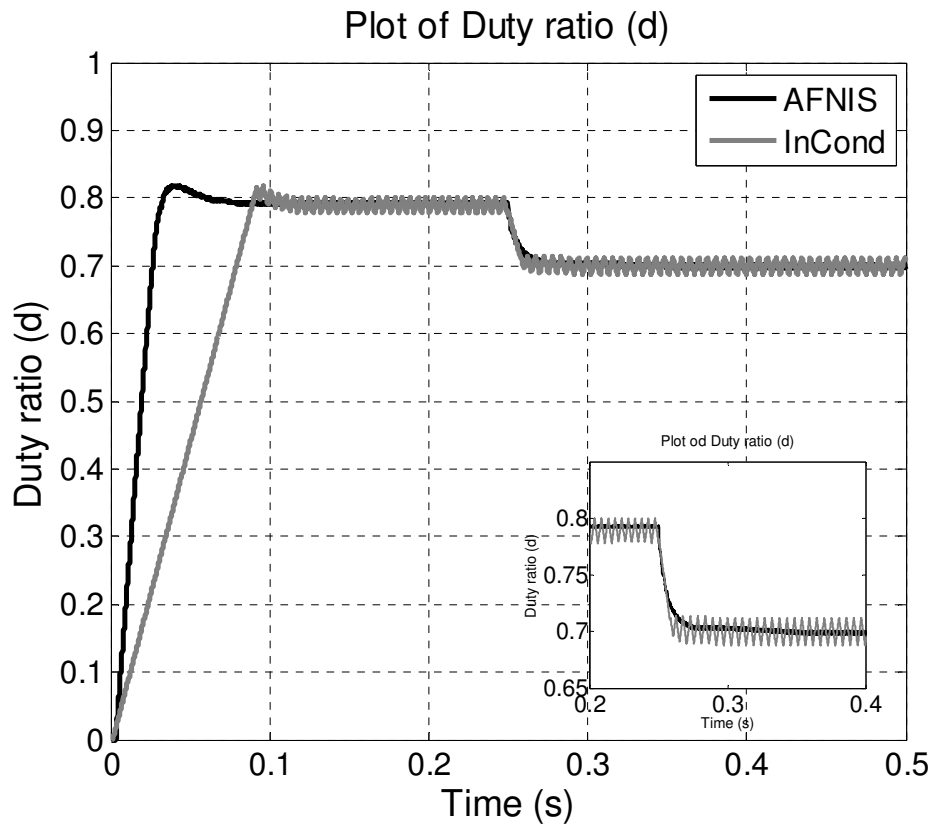


Figure 4.27: Plot of duty ratio under step-down temperature change.

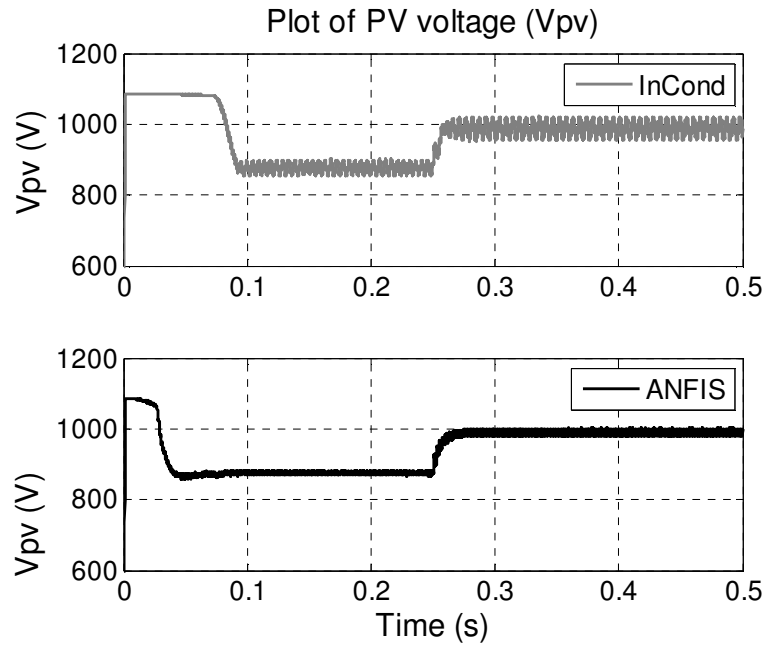


Figure 4.28: Characteristics of PV voltage under step-down temperature change

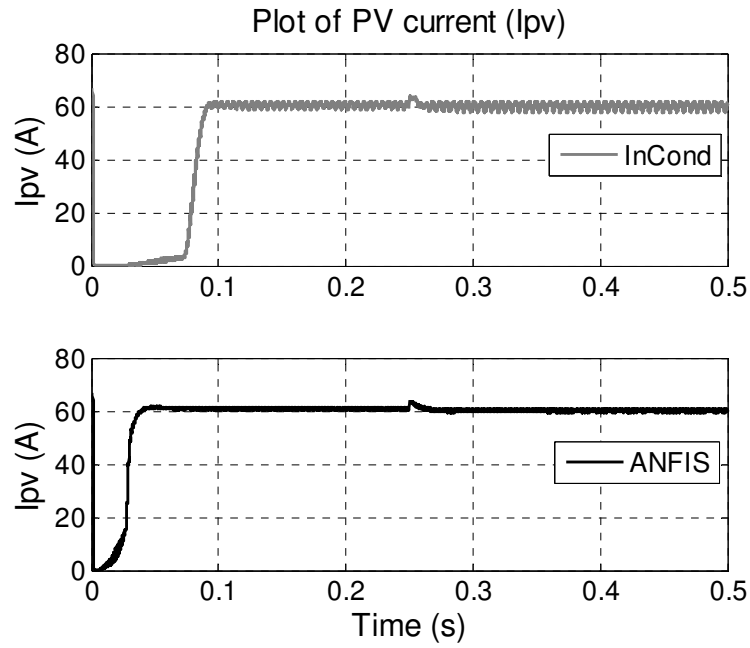


Figure 4.29: Characteristics of PV current under step-down temperature change.

4.4.5 Test 5: Linear change in irradiation

This test is conducted under the linear change in irradiation level and its pattern is shown in the Figure 4.30. It shows that the solar radiation is constant with a value of 500 W/m² up to 0.2 seconds and then increases linearly to 1000 W/m² at 0.4 seconds. The P-V curves for selected PV array under low (500 W/m² and 25⁰C) and normal (1000 W/m² and 25⁰C) irradiation level are shown in Figure 4.31. It can be seen that the maximum power that can be generated by PV array at low irradiation level is 24.669 kW and labelled as point X on the graph. After a linear change in irradiation, the operating point shifts to point Y having the maximum possible power of 53.07 kW ($V_{MP} \cdot I_{MP} \cdot N_{SS} \cdot N_{PP} = 53.07 \text{ kW}$).

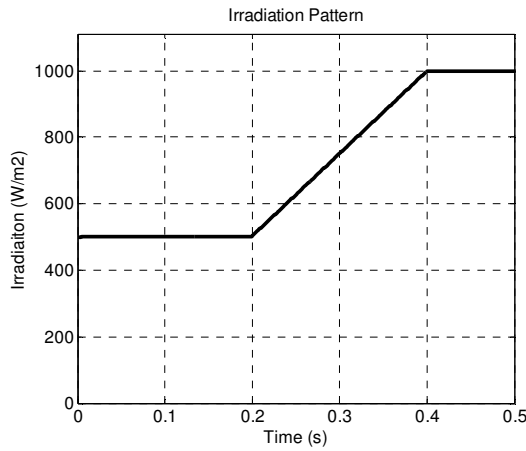


Figure 4.30: linear change in irradiation.

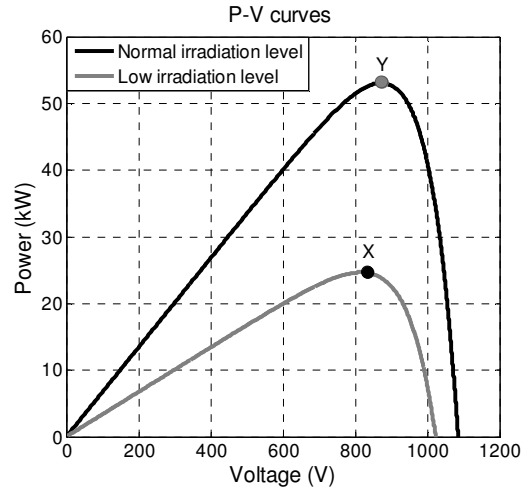


Figure 4.31: PV curve under normal and low irradiation conditions.

A non-linear time domain simulation is carried out with the proposed ANFIS-based and InCond-based MPPT controllers. For InCond method fixed value of perturbation step

size is chosen based on a trade-off between fluctuations in the steady state and tracking speed. Figure 4.32 shows a comparison of PV array power output (P_{PV}) for both the controllers. It can be seen from the graph that the MPP reached by the proposed ANFIS-based MPPT controller is much faster than the conventional InCond. For example it can track the MPP in 0.04 sec while the InCond take 0.1 sec in the start of the algorithm. During changing irradiation, the MPPT controller tracks the MPP point and shift the operating point from point X to Y and it can be noticed from the plot that the response of InCond is much slower than the proposed ANFIS-based MPPT.

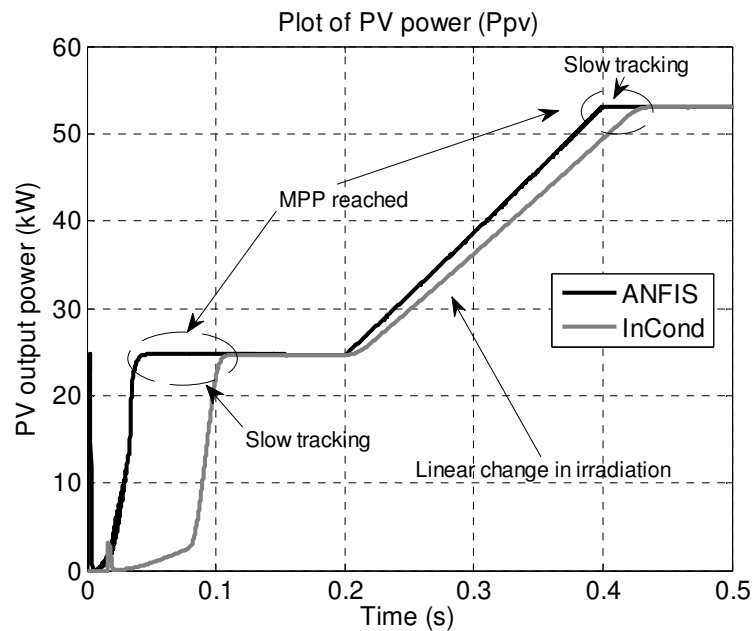


Figure 4.32: Characteristics of PV power output under linear irradiation change

The simulation results for duty cycle, PV array voltage (V_{PV}) and current (I_{PV}) are shown in Figure 4.33, Figure 4.34, Figure 4.35, respectively, and verify the effectiveness of the proposed MPPT under the linear changing irradiation condition.

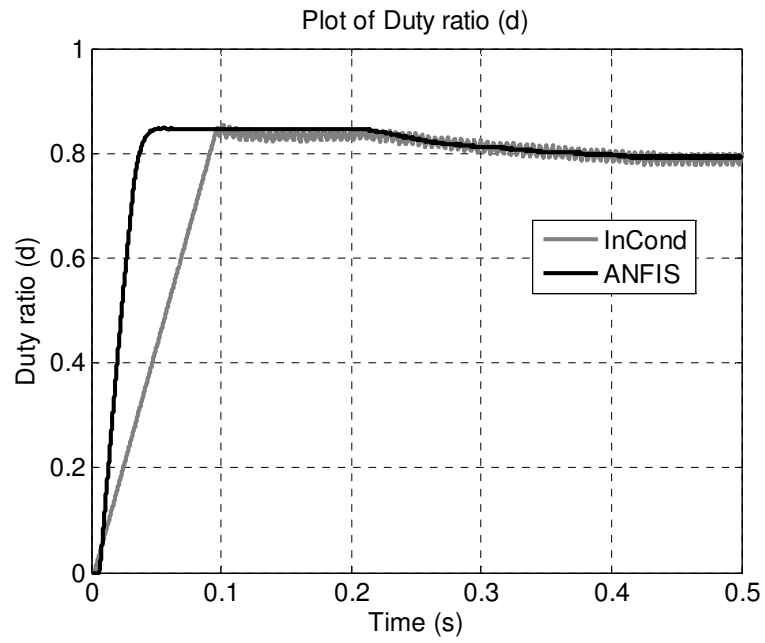


Figure 4.33: Plot of duty ratio under linear irradiation change

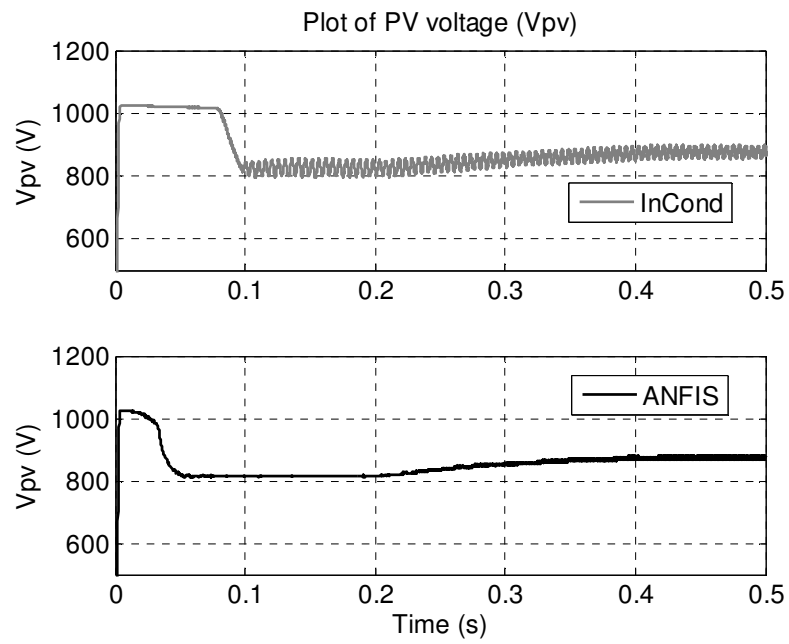


Figure 4.34: Characteristics of PV voltage under linear irradiation change

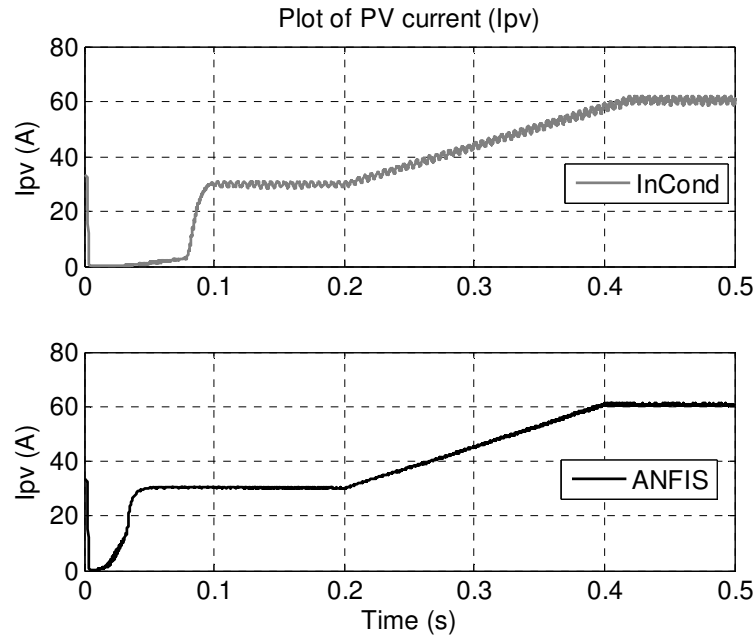


Figure 4.35: Characteristics of PV current under linear irradiation change.

4.4.6 Test 6: Comparison of ANFIS and FUZZY based MPPT controllers

In this test a comparison is made between the proposed ANFIS-based and Fuzzy Logic based MPPT controller (FLC) under the step-down change in irradiation level and its pattern is shown in the Figure 4.36. It shows that the solar radiation is constant with a value of 1000 W/m^2 up to 0.25 seconds and then decrease drastically to 500 W/m^2 . The P-V curves for selected PV array under normal (1000 W/m^2 and 25°C) and low (500 W/m^2 and 25°C) irradiation level are shown in Figure 4.37. It can be seen that the maximum power that can be generated by PV array at normal irradiation level is 53.07kW ($V_{MP} \cdot I_{MP} \cdot N_{SS} \cdot N_{PP} = 53.07\text{kW}$) and labeled as point X on the graph. After a step-down change in irradiation, the operating point shifts to point Y having the maximum possible power of 24.669kW as shown in Figure 4.37.

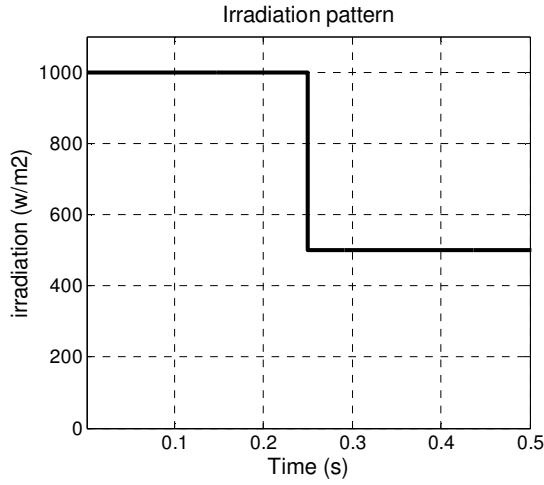


Figure 4.36: Step-down change in irradiation.

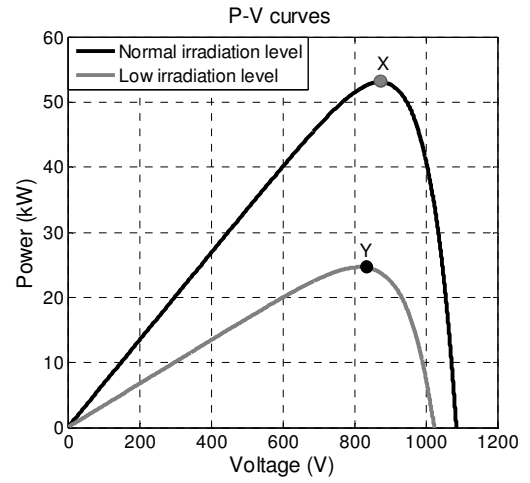


Figure 4.37: PV curve under normal and low irradiation conditions.

A non-linear time domain simulation is carried out with the proposed ANFIS-based and Fuzzy-based MPPT controllers. FLC MPPT developed in [2] (list of publication) is used. Figure 4.38 shows a comparison of PV array power output (P_{PV}) for both the controllers. It can be seen from the graph that the MPP reached by the proposed ANFIS-based controller is faster than the FLC MPPT in both the tracking regions, i.e start of the algorithm and step-up change in irradiation. When a step-down change in irradiation occur, the MPPT controller shifts the operating point from point X to Y and it can be noticed from the plot that the response of FLC MPPT is slower than the proposed ANFIS-based MPPT. The simulation results for duty cycle, PV array voltage (V_{PV}) and current (I_{PV}) are shown in Figure 4.39, Figure 4.40, Figure 4.41, respectively, and verify the effectiveness of the proposed ANFIS-based MPPT over the FLC MPPT controller.

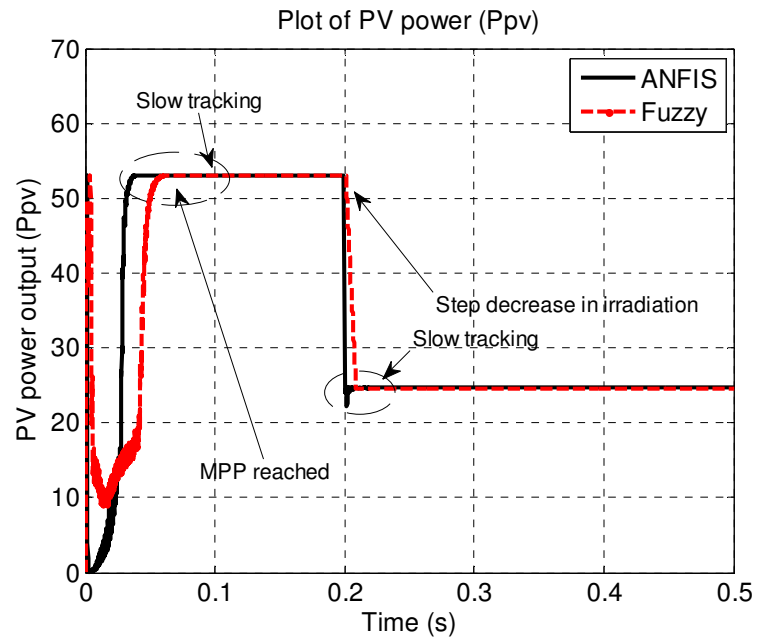


Figure 4.38: Characteristics of PV power output under step-down irradiation change.

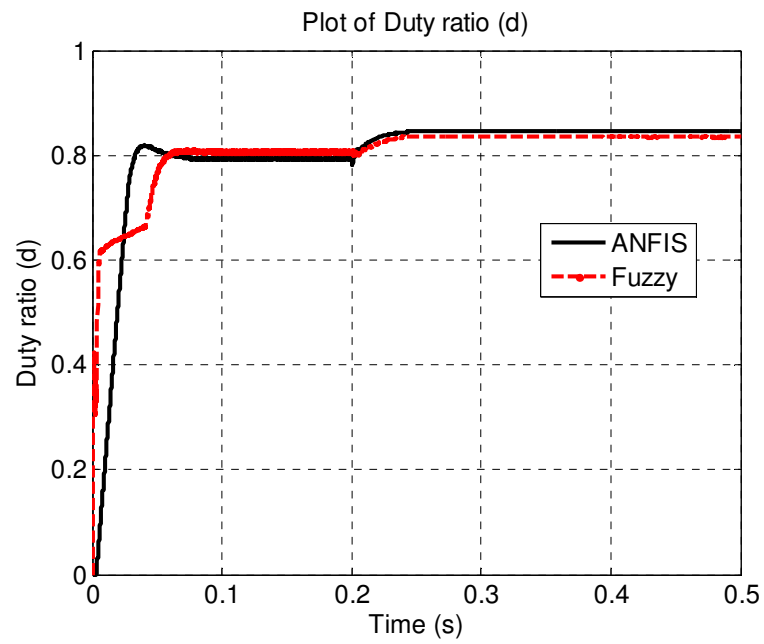


Figure 4.39: Plot of duty ratio under step-down irradiation change

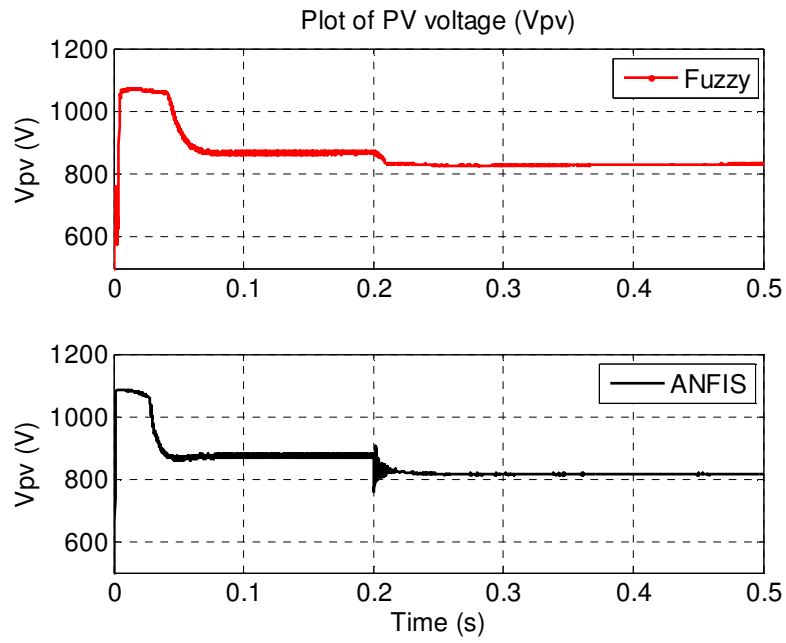


Figure 4.40: Characteristics of PV voltage under step-up irradiation change

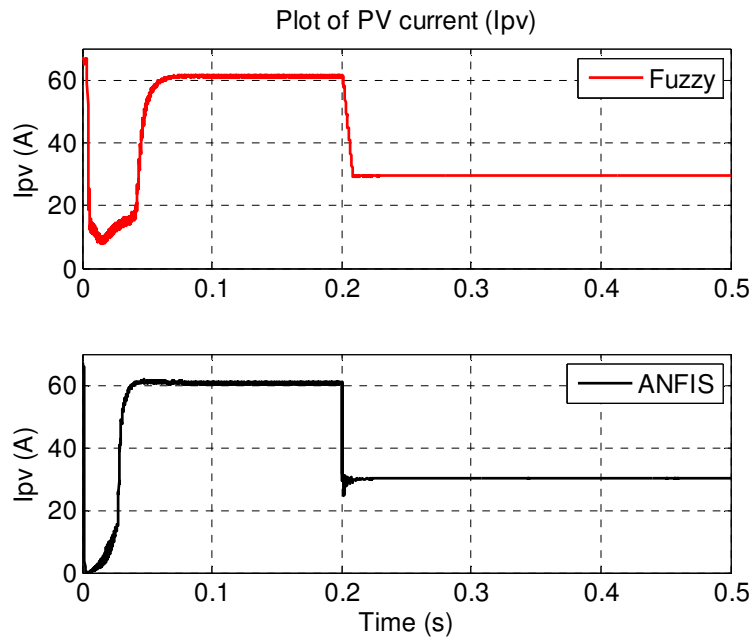


Figure 4.41: Characteristics of PV current under step-up irradiation change

4.4.7: Robustness of the Proposed Controller

The competence of proposed ANFIS-based MPPT at different operating condition is illustrated by comparing the maximum power extracted by ANFIS-based MPPT with the conventional InCond method. Percentage error is calculated using the reference power calculated from the efficiently developed PV model described in chapter 3 and is shown in Figure 4.42 and Figure 4.43.

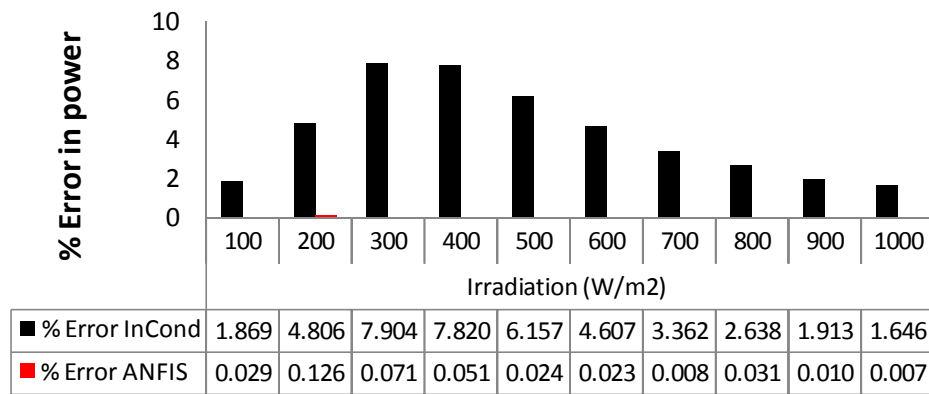


Figure 4.42: Percentage error in P_{MP} at different irradiation level and constant temperature

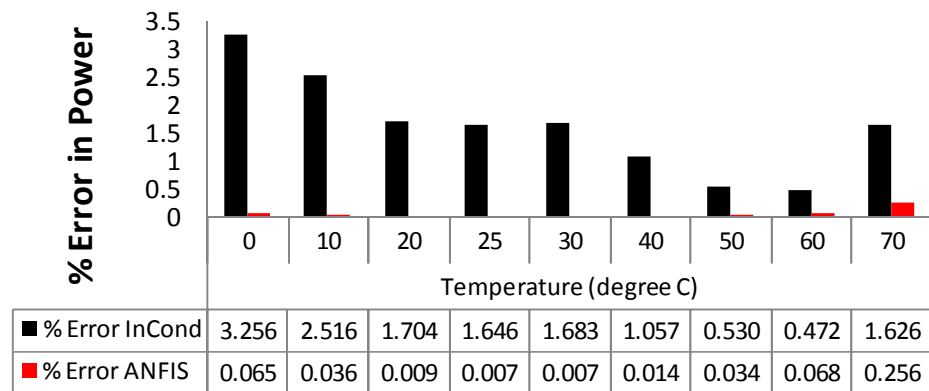


Figure 4.43: Percentage error in P_{MP} at different temperature and constant irradiation

Figure 4.42 shows the percentage error at different irradiation levels with constant temperature of 25°C. It can be seen that the value of error is negligible for the ANFIS-based MPPT for a wide range of operating conditions. Lower value of error depicts that the proposed controller is able to extract maximum possible from the PV array at all weather condition. Its proficiency at varying temperature is shown Figure 4.43. From the simulation results, it can be inferred that the proposed ANFIS-based controller is faster than InCond controller in transitional state, and has fewer oscillations in steady state. All these factors will cause less power loss and results in more power output from PV array.

4.5 CONCLUSION

Maximum Power Point Tracking (MPPT) controllers are used to extract maximum possible power from the PV system and all operation condition. The conventional MPPT controllers have some drawbacks associated with them that causes significant amount of power loss. In this chapter, a novel MPPT controller has been proposed and developed based on the ANFIS. The proposed controller hybridizes the principles of two efficient intelligent techniques; Fuzzy Inference systems (FIS) and Artificial Neural Network (ANN). A nonlinear time domain simulation has been carried out to assess the effectiveness of the proposed controllers under different disturbances. Results and comparison showed that the proposed ANFIS-based MPPT controller can fulfill the shortcomings of the conventional method and can track the MPP in shorter time with fewer fluctuations. The obtained results demonstrate that the proposed ANFIS-based controller has better dynamic and steady state performance than the conventional method.

CHAPTER 5 EXPERIMENTAL SETUP

5.1 INTRODUCTION

The effectiveness of the proposed ANFIS-based MPPT controller is experimentally verified using the Real Time Digital Simulator (RTDS) and dSPACE controller. A complete PV system is developed in RTDS and the proposed ANFIS-based MPPT is designed in dSPACE controller. This chapter explains the design and implementation of the PV system and proposed the ANFIS-based MPPT controller and integration of RTDS with dSPACE controller. All the experimental setup is developed in the Department of Electrical Engineering, King Fahd University of Petroleum and Minerals (KFUPM) under the supervision of Prof. M. A. Abido.

5.2 EXPERIMENTAL SETUP COMPONENTS

5.2.1 Real Time Digital Simulator (RTDS)

Digital techniques are the most important techniques that simulate the modern power systems since later 1960s, especially for power system simulation. In the past, modern technology has gone through tremendous development in the area of power system and digital simulation. The microprocessor progresses, communication and transducer

technologies have provided new means for the development in power system protection and relay testing.

In this thesis, Real Time Digital Simulator (RTDS) is used to simulate a complete PV system. It is a fully digital electromagnetic transient power system simulator. It can be used to conduct close-loop testing of physical devices such as protection equipment and control equipment; to perform analytical system studies and to educate operators, engineers and students [117]. It is a cost-effective replacement for transient network analyzers and analogue/hybrid simulators. RTDS allows the user to investigate the effects of disturbances on power system equipment and networks to prevent outages or complete failure. Moreover, RTDS added the capability to improve the simulation accuracy and better capture the switching events [118].

RTDS is generally designed to simulate power systems in real time with time step-sizes on the order of $50\mu\text{s}$. The system uses a number of digital signal processors (DSPs) which operated in parallel. It provides a number of digital and analog I/O ports for interfacing hardware to the simulation. It features a more powerful processor combined with FPGAs which allow the simulation of a limited number of power electronics devices with time step as small as $1.4 - 2.5\mu\text{s}$ embedded in the $50\mu\text{s}$ time-step environment. Therefore, it allows the simulation of power electronics converter operating at higher switching frequency with sufficient accuracy. In addition, its real time capability allows the user to incorporate real devices into the simulation in a closed loop environment.

Its advantage is that it can solve the power system equations continuously and computes the outputs fast enough such that the simulation realistically represents the situation of the real systems. As it replicates the situation of real time systems it can be interfaced directly to the protective relays and power system control equipments to analyze their performance [117].

RTDS is a combination of advanced computer hardware and comprehensive software called RSCAD. The custom parallel processing hardware architecture was assembled in modular units called racks. Each rack contains slot and rail-mounted cards. The specific composition of an RTDS depends on the processing and I/O requirements of the intended application. A common communications backplane links all rack mounted cards facilitating information exchange. RTDS cubicle rack is shown in Figure 5.1.



Figure 5.1: Real Time Digital Simulator (RTDS) rack.

The RTDS™ employs an advanced and easy to use graphical user interface - the RSCAD Software Suite. All loading, running and controlling of the simulations are done entirely from the host workstation through the RSCAD/Runtime module. The Power and Control System Software is an integral part of RSCAD for RTDS™. The software is comprised of several modules designed to allow the user to perform the simulation and result analysis. Any power system network can be created on the computer screen of the RTDS. This can be done by selecting the components from a number of customized component model libraries then arranging them to build the network. Once the system has been drafted and with all parameter settings, the appropriate compiler automatically generates the low-level code necessary to perform the simulation using the RTDS Simulator. The Software is used to interface with the RTDS hardware. It is designed to allow the user to perform all the steps necessary to prepare and run the simulation then analyze its output. It has now become one of the most important product test and development tools throughout the world [119].

RTDS works in real-time to provide solutions to power system equations quickly enough to accurately represent conditions in the real world. RTDS offers superior accuracy over analogue systems. It allows for comprehensive product and/or configuration tests. RTDS provides a variety of transient study possibilities.

5.2.2 dSPACE Controller

The dSPACE controller offers an inclusive solution for electronic control unit (ECU) software development. It is powerful development tools for dedicated services in the field

of function prototyping, target implementation, and ECU testing. Real time control systems can be built using dSPACE and the control logic can be implemented [120].

In this study dSPACE DS1104 R&D Controller Board is used. It is a standard board that can be plugged into a PCI (Peripheral Component Interconnect) slot of a PC. The DS1104 is specifically designed for the development of high-speed multivariable digital controllers and real-time simulations in various fields. It is a complete real-time control system based on a 603 PowerPC floating-point processor running at 250MHz. For advanced I/O purposes, the board includes a slave-DSP subsystem based on the TMS320F240 DSP microcontroller. The dSPACE DS1104 Controller Card is shown in Figure 5.2.

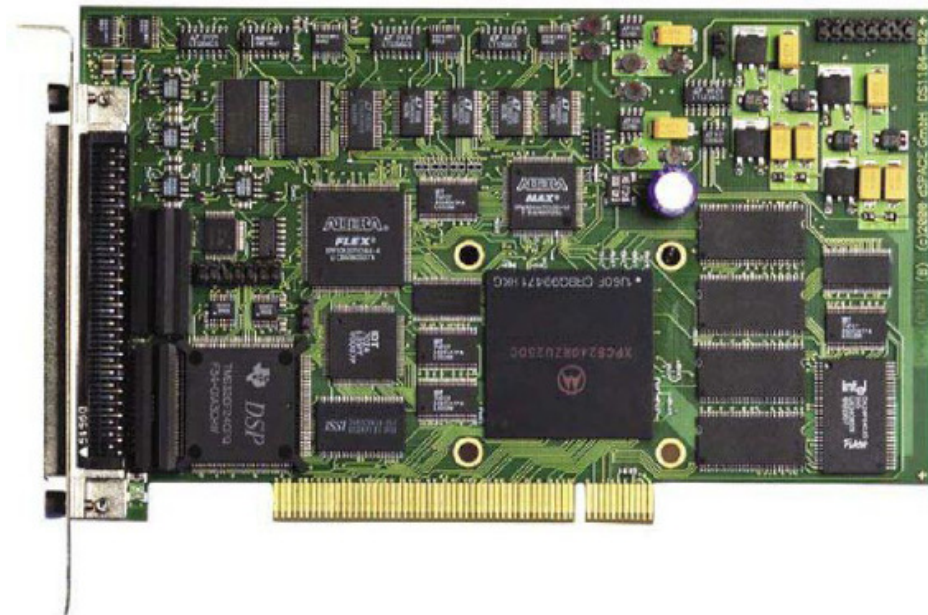


Figure 5.2: dSPACE controller card.

Using an adapter cable one can link the external signals from the 100-pin I/O connector on the board to Sub-D (D-sub miniature) connectors. So, one can make a high-density connection between the board and the devices of your application through Sub-D connectors. Specific interface connector panels provide easy access to all the input and output signals of the DS1104 Controller Board. The Connector Panel (CP1104) provides easy-to-use connections between the DS1104 Controller Board and devices to be connected to it. Devices can be individually connected, disconnected or interchanged without soldering via BNC (Bayonet Neill–Concelman) connectors and Sub-D connectors. This simplifies system construction, testing and troubleshooting. In addition to the CP1104, the Connector/LED Combi Panel (CLP1104) provides an array of LEDs indicating the states of the digital signals [121].

For purposes of rapid control prototyping (RCP), specific interface connectors and connector panels, discussed above, provide easy access to all input and output signals of the board. Thus, the dSPACE DS1104 Controller Board is the ideal hardware for cost-sensitive RCP applications. The dSPACE works on Matlab/Simulink platform which is a common engineering software and easy to understand. Another feature of the dSPACE is the Control desk which allows the graphical user interface. Through the control desk the user can observe the response of the system also he can give command to the system through this interface. Real time interface is needed for the dSPACE to work. Real-time Interface (RTI) is the link between dSPACE's real-time systems and the MATLAB/Simulink. RTI is an easy graphical I/O configuration and automatic code generation system it executes the C code for Real Time Workshop so that the Simulink

models can easily be implemented on dSPACE real-time hardware. Once the I/O has been configured and the controller has been programmed in a Simulink block diagram, model code can be generated using Real-Time Workshop. The real-time model is compiled and downloaded to the dSPACE hardware. The compilation of the .mdl file in Simulink using RTI also generates a file with extension .sdf. This file can be accessed in ControlDesk – software that helps in managing real-time and Simulink experiments. The dSPACE connector panel (PCI) controller board is shown in Figure 5.3.

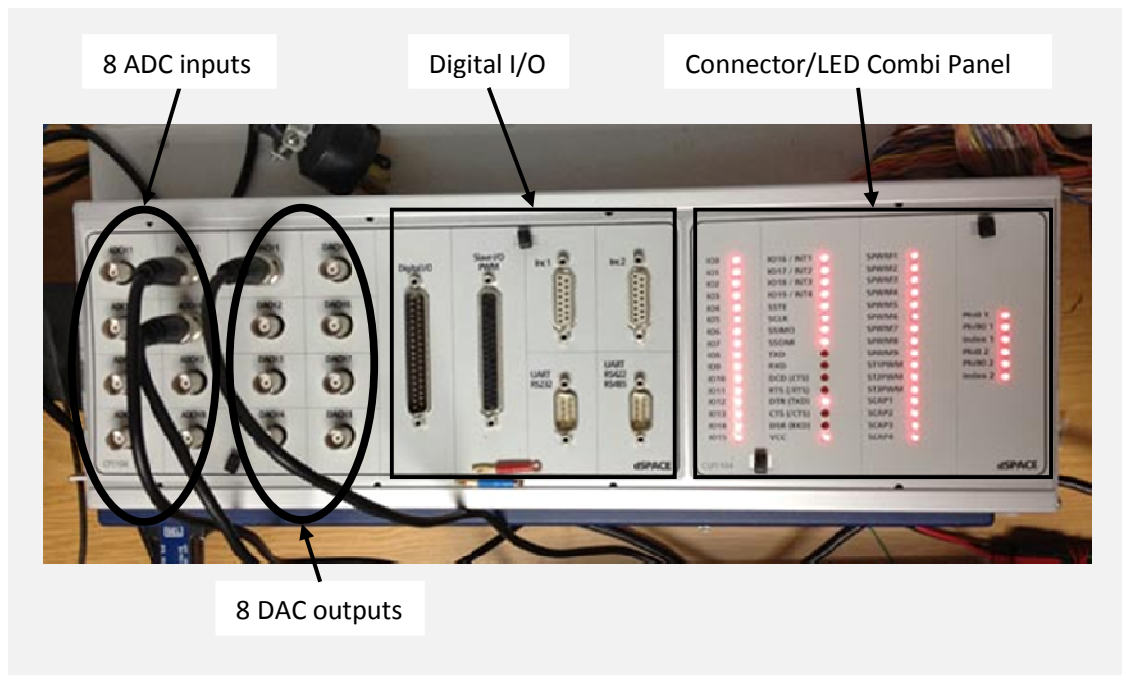


Figure 5.3: dSPACE panel connector board.

5.3 BUILDING PV MODEL USING RTDS

A complete PV system is developed on RSCAD software which is then compiled and sent for real-time simulations on RTDS. Real-time digital simulator (RTDS) is a

combination of specialized computer hardware and software designed specifically for electromagnetic transient simulations in real-time. Its response is much nearer to the existing practical systems. RTDS is used for high speed simulations, closed-loop testing of protecting and control equipment and hardware in the loop (HIL) applications.

5.3.1 PV array

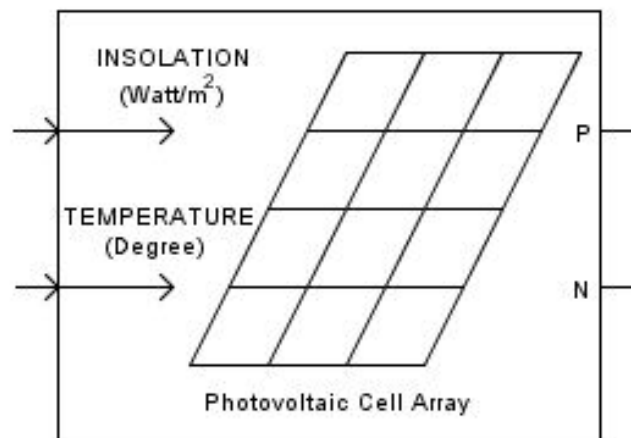


Figure 5.4: PV array model in RTDS.

Figure 5.4 shows the PV array model in RTDS. It has two power system nodes which allows it to be interfaced with the RTDS Network Solution; nodes P and N represent the positive and negative terminals respectively. The connections labeled “INSOLATION” and “TEMPERATURE” are the PV array input signals. Model can simulate PV panels with different specifications and able to work with any number of series and parallel connected PV panels depending upon the output power requirement.

5.3.2 Buck Converter

In RTDS buck converter is designed with the help of IGBT switch, diode and inductor, available in the component library. Switching of the IGBT is controlled by PWM signal generated by comparing the duty cycle with the triangle wave. The value of the duty cycle is adjusted by the MPPT controller to track maximum power from PV array. Figure 5.5 shows the designed buck converter.

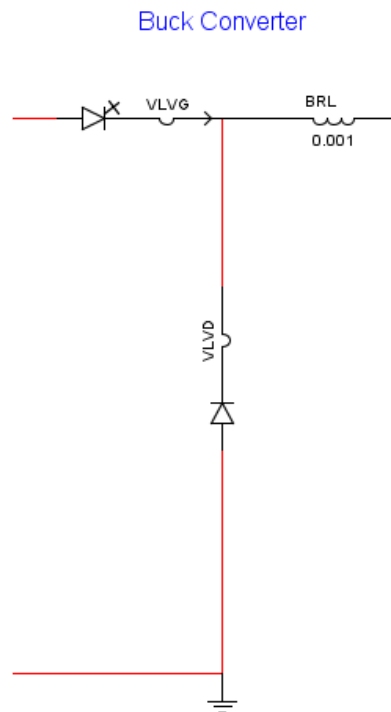


Figure 5.5: Buck converter in RTDS.

5.3.3 Gigabit Transceiver Analogue Output (GTAO)

The Gigabit Transceiver Analogue Output Card (GTAO) is used to convert the digital signals from RTDS to analogue signals and interface RTDS to external devices shown in

Figure 5.6. The GTAO card includes twelve, 16 bit analogue output channels with an output range of ± 10 volts. The 16 bit DACs provide a wide dynamic range. It is mounted in the rear of the RTDS cubicle rack and connects to a GPC processor card via an optical cable. A single +24 volt power supply signal is required to power the card. Analogue output signals connect to terminal blocks available on the GTAO card.

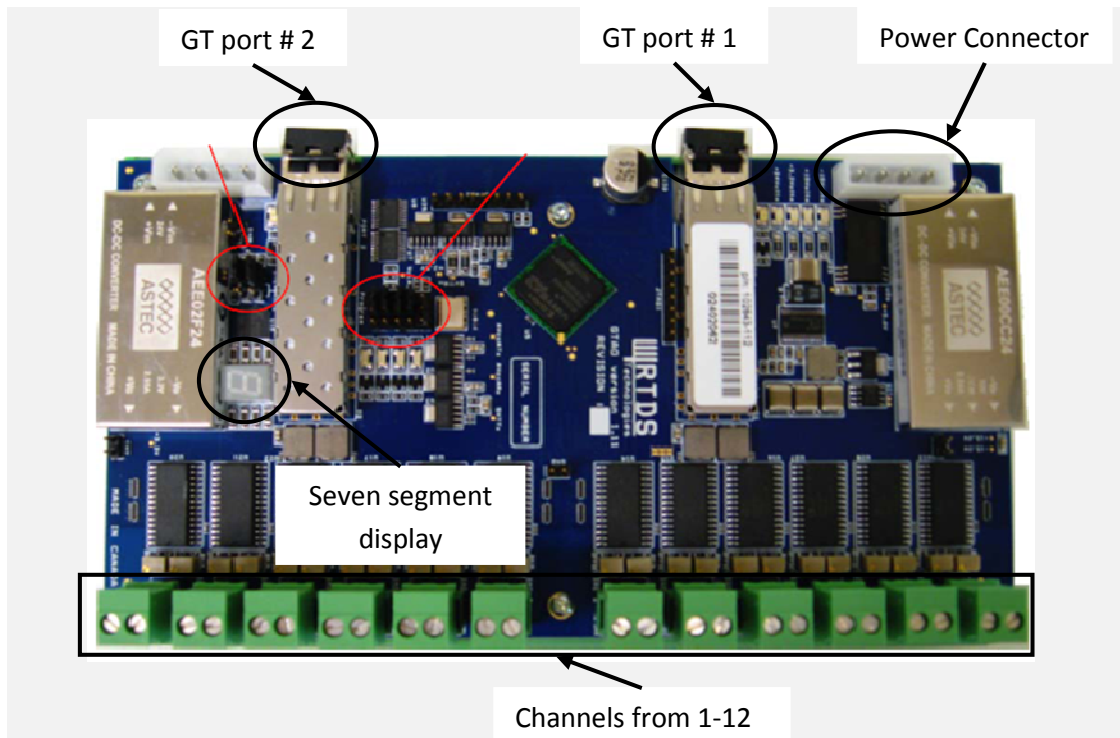


Figure 5.6: Gigabit Transceiver Analogue Output (GTAO) card.

To write the signals on the GTAO card a GTAO component is available in RSCAD/Draft named as “rtds_risc_ctl_GTAO OUT” and is located in the I/O Components hierarchy box under the Controls tab in the Master Library. The user is able to individually enable the channels and set scale factors for each enabled channel. The GTAO component with its twelve channels is shown in Figure 5.7

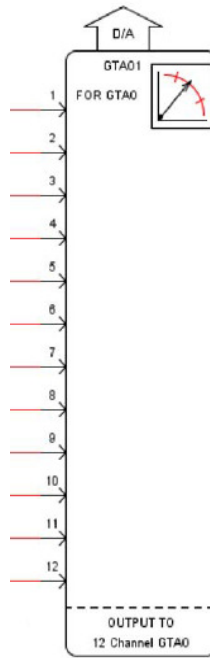


Figure 5.7: GTAO component in RSCAD.

Inputs to the GTAO model are IEEE–754 double precision floating point numbers. This model converts and scales input signals to 16–bit integers and writes them to the GTAO. The GTAO card’s output range is ± 10 volts. Inputs to the GTAO component must be scaled to produce a desired voltage on the output channels of the GTAO card. The scale values can be entered in the “D/A Output Scaling” menu item. For example, an input signal of magnitude 187.79 kV L–N peak is input to the GTAO component. Entering a scale value of 187.79 will result in a 5V peak signal output of the GTAO card.

5.3.4 Gigabit Transceiver Analogue Input (GTAI)

The Gigabit Transceiver Analogue Input Card (GTAI) is used to interface analogue signals from an external device to the RTDS and shown in Figure 5.8. The GTAI card

includes 12 analogue input channels with each channel configured as a differential input with an input range of ± 10 volts. Sixteen bit A/D converters are used on the GTAI card. The GTAI card is mounted on the rear of the RTDS cubicle and connects to a GPC processor card via an optical cable. A single +24 volt power supply signal is required to power the card. Analogue input signals connect to terminal blocks available on the GTAI card. The GTAI card uses two Analog Devices AD7656 ADCs. Each AD7656 chip includes six independent sixteen bit A/D converters.

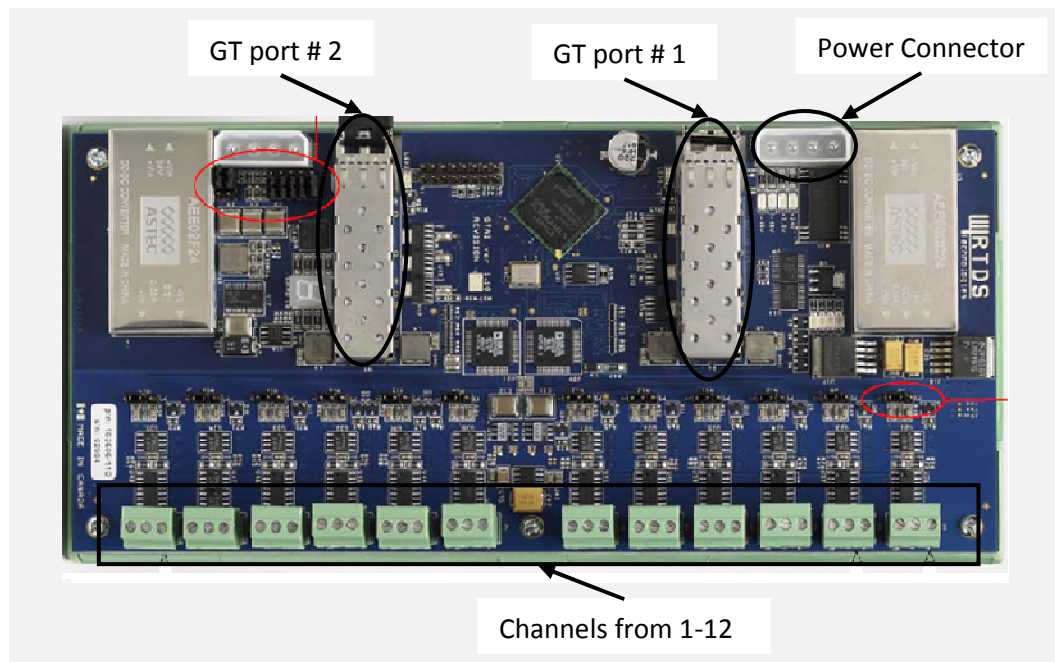


Figure 5.8: Gigabit Transceiver Analogue Input (GTAI) Card.

To read the signals from the GTAI card a GTAI component is available in RSCAD/Draft named as “rtds_risc_ctl_GTAI” and is located in the I/O Components hierarchy box under the Controls tab in the Master Library. The user is able to individually enable the channels and set scale factors for each enabled channel.

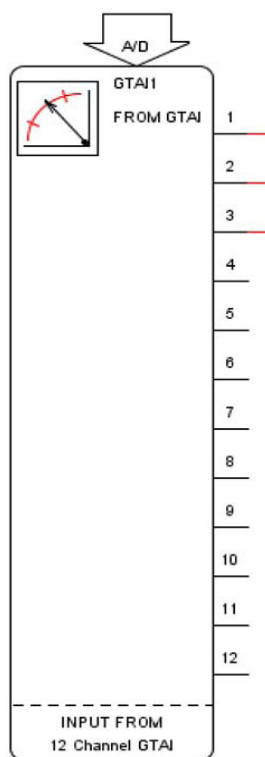


Figure 5.9: GTAI component in RSCAD.

The GTAI reads data from up to twelve analogue input channels and converts it to digital format for use by the RTDS. Each channel may be enabled or disabled using the toggle boxes provided in the 'ENABLE A/D INPUT CHANNELS' menu. A separate scale value is specified for each input signal. Scale values represent the analogue signal peak voltage (in volts) which will result in a value of 1.0 to be present on the corresponding output signal wire. For example, a scale value of $sc11=5.0$ means that a voltage of 1 volt on the analogue input channel #1 will result in a value of $1/5$ (0.2) on the output wire labeled '1'. The maximum input range of the GTAI is ± 10 volts peak. The GTAI component with its twelve channels is shown in Figure 5.9.

5.3.5 PV system in RSCAD

A complete PV system in RSCAD is shown in Figure 5.10. PV array takes irradiation and temperature as inputs and its outputs are DC voltage and DC current. It is then connected with Buck converter that is developed in bridge block (dotted border in Figure 5.10) and shown in Figure 5.11. It consists of the designed buck converter, triangular wave generator and comparator block. Switching of the buck converter is controlled by PWM signal generated by comparing the duty cycle with the triangle wave. The value of the duty cycle is adjusted by the MPPT controller to track maximum power from the PV array. Black box in Figure 5.10 shows the measurement and control unit and its inner logic is shown in Figure 5.12. It shows the control arrangement of the PV system. Figure 5.13 shows the arrangement of the GTAO and GTAI components to interface the RTDS with the external MPPT controller. GTAO sends the irradiation and temperature signals to the external MPPT controller and GTAI receives the control signal (V_{REF}) from it. The reference voltage (V_{REF}) is then normalized using DC link voltage (V_{DC}) and feedback to the voltage control loop. In voltage control loop PI controller is used to maintain the output voltage of PV array (V_{PV}) to the reference optimal voltage by adjusting the duty cycle of buck converter which results in maximum power extraction.

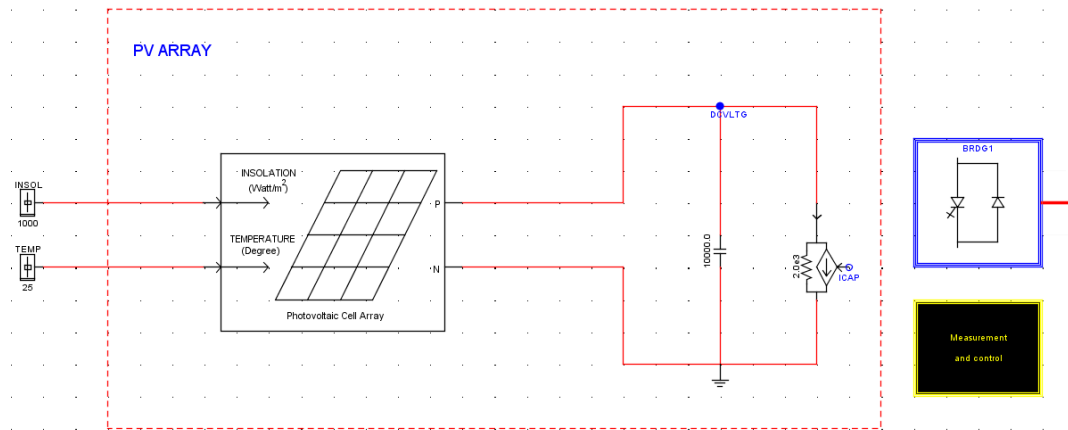


Figure 5.10: PV system in RSCAD.

Triangle wave data generator
for DC/DC Converter

Buck Converter

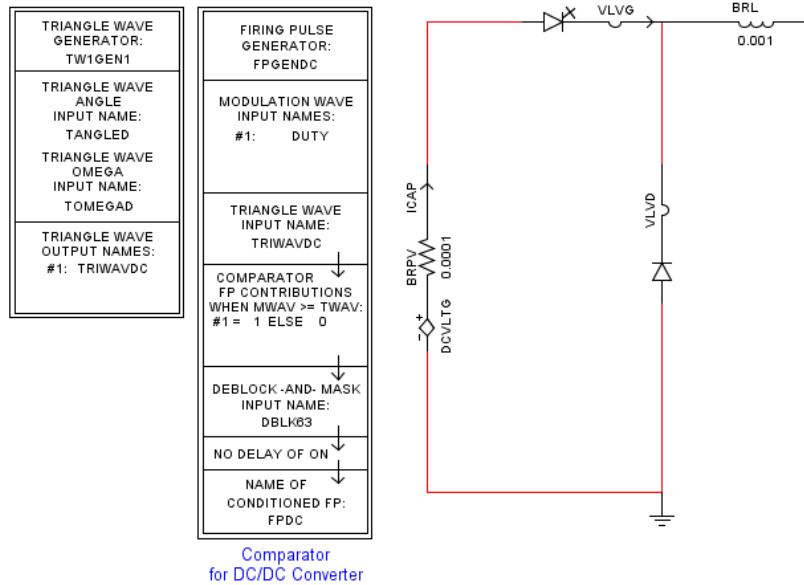


Figure 5.11: Buck converter, triangular wave generator and comparator block in

RSCAD.

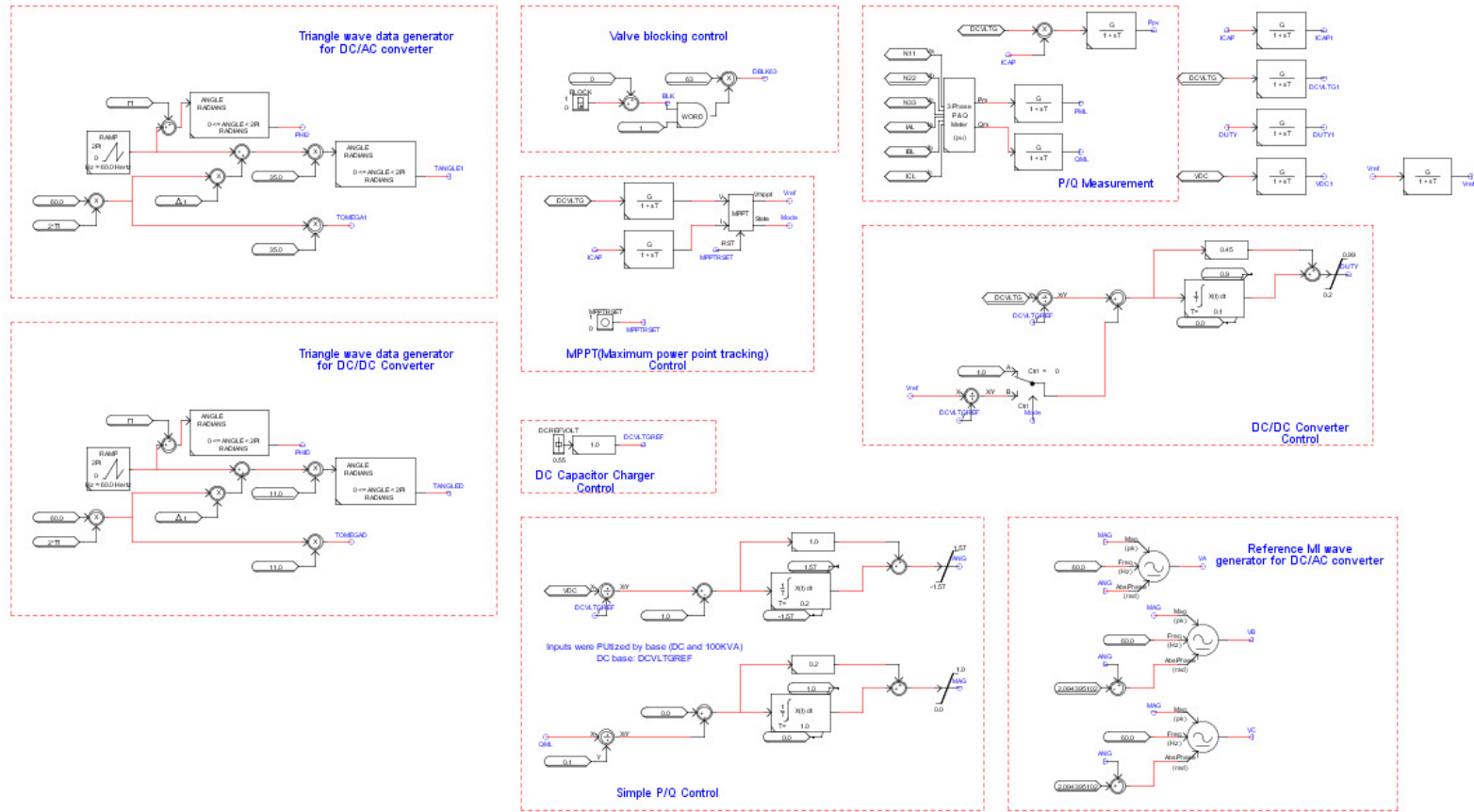


Figure 5.12: Measurement and control unit in RSCAD.

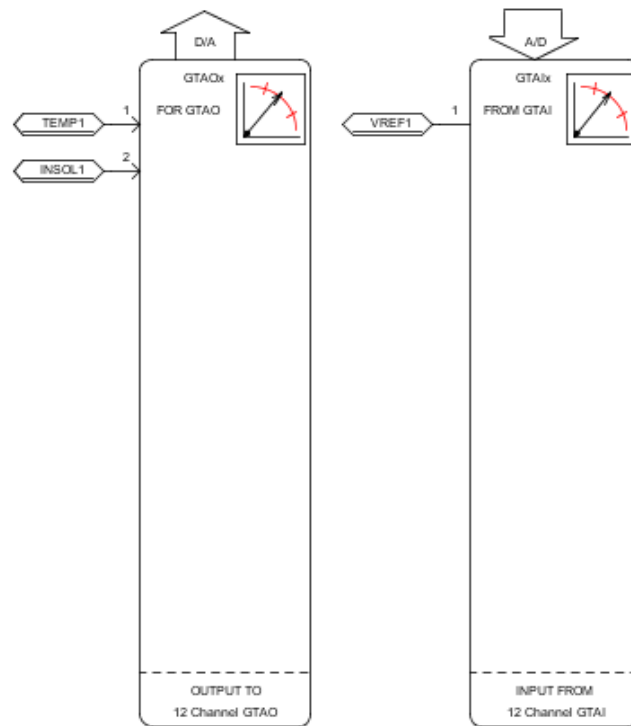
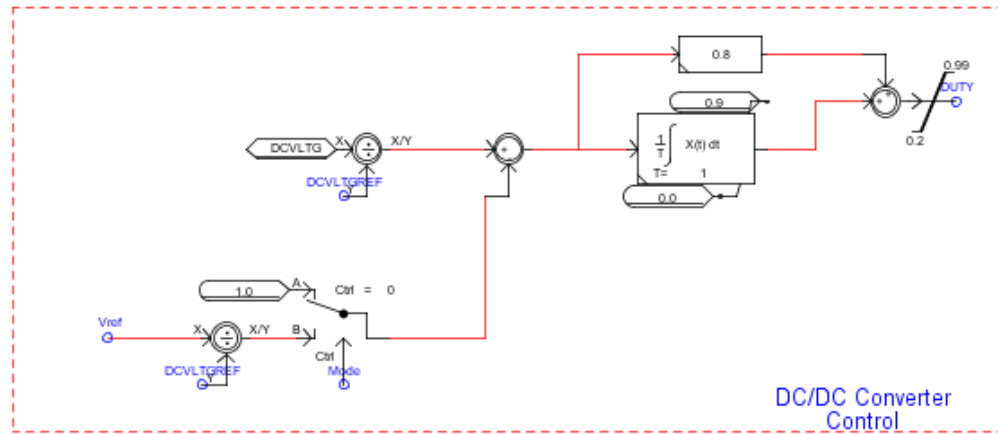


Figure 5.13: Arrangement of GTAO and GTAI in interfacing the RTDS with external controller.

5.4 BUILDING MPPT IN dSPACE

The proposed ANFIS--based MPPT controller designed in chapter 4 is implemented in real domain using dSPACE DS1104 shown in Figure 5.14. Inputs to the proposed controller are irradiation and temperature and these are represented by DS1104ADC_C5 and DS1104ADC_C6 blocks in real time simulink model, respectively. These blocks are obtained from a dSPACE library in SIMULINK and convert the analog signal to digital signal. Here ADC in the name of the blocks depicts the analog to digital conversion. Similarly the output of the proposed controller is V_{REF} and represented by DA1104DAC_C1 and converts the digital signal to analog (DAC). Basically these blocks are used to integrate the dSPACE controller with external analog signals and devices. In our case these blocks are linked to GTAO and GTAI of the RTDS. DS1104ADC_C5 and DS1104ADC_C6 blocks are linked with the GTAO and accept the analog signals of temperature and irradiation as input. In the same way, DA1104DAC_C1 is linked with GTAI of RTDS and send the control signal back to RTDS. A detailed interfacing of RTDS and dSPACE will be discussed in the next section. The gain blocks in Figure 5.14 are used to get the actual values of inputs.

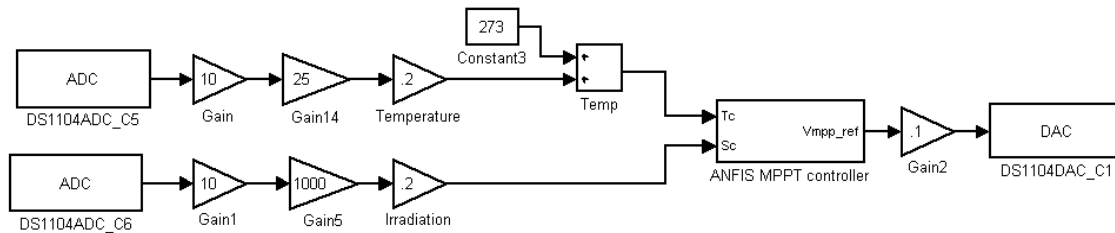


Figure 5.14: ANFIS-based MPPT controller in simulink to build in dSPACE.

After designing the controller in the Simulink next step is to set time-step of a model to 100μsec to synchronous with the time-step of dSPACE. In every time-step, the designed MPPT controller (DS1104) monitors the input quantities (irradiation and temperature) and after making the decision, based on the designed algorithm, generates the controlled output signal (V_{REF}). Real time implementation of a controller should run continuously for infinite time therefore set the stop time to infinite. Then the designed controller is converted into real time code and becomes ready to work in a real time domain.

5.5 INTEGRATING DSPACE WITH RTDS

A complete PV system build in RTDS and proposed ANFIS-based MPPT controller is designed in dSPACE DS1104 as explained previously. The dSPACE controller is integrated with RTDS to analyze the effectiveness of the proposed ANFIS-based MPPT experimentally. Interfacing of the equipments is carried out via analog link and two sets of analog to digital and digital to analog converters are utilized to achieve this job. GTAO and GTAI are associated with RTDS and ADC and DAC are associated with dSPACE as shown in Figure 5.15.

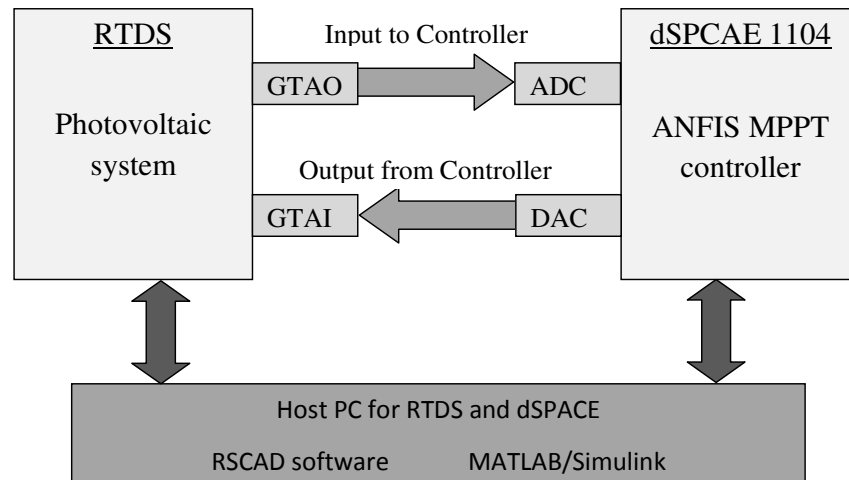


Figure 5.15: Closed loop control system.

Figure 5.15 shows complete closed loop control system. Outputs (irradiation and temperature) from the RTDS are converted to analog signal in the range of 0-10V and send to the dSPACE controller where ADC utilized to convert them back to digital signal and processed by the designed controller. After processing the inputs, control signal is given out from dSPACE controller which is then changed into analog signal within the same range of 0-10V and provided to the RTDS where GTAI accepts it and converts back to the digital domain and present it to the RTDS where PV system is developed. A complete experimental setup is shown in Figure 5.16. The experimental setup is developed in the Department of Electrical Engineering, King Fahd University of Petroleum and Minerals (KFUPM).

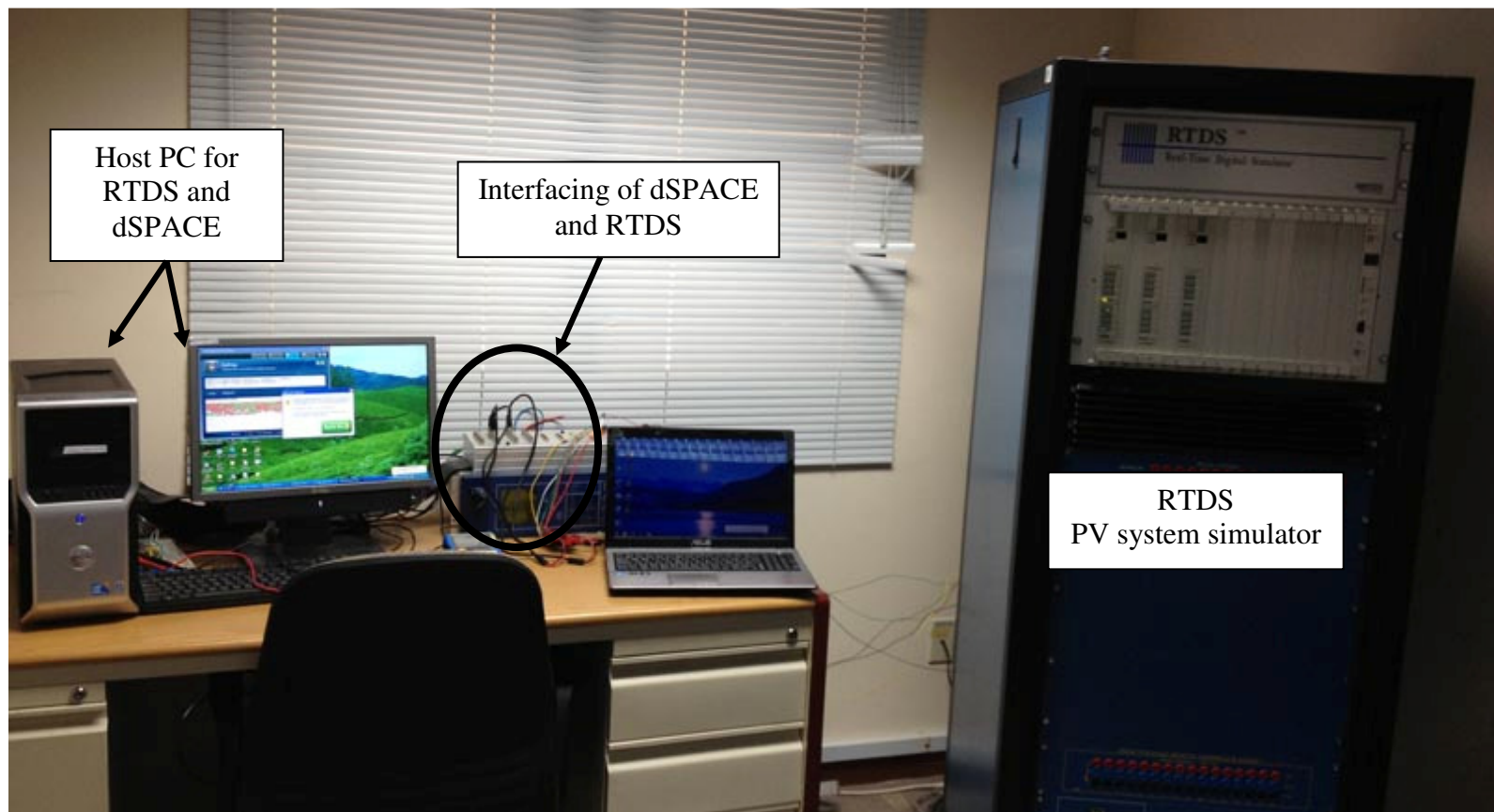


Figure 5.16: A complete experimental setup.

CHAPTER 6 EXPERIMENTAL VERIFICATION OF PROPOSED ANFIS-BASED MPPT

6.1 INTRODUCTION

Setup described in chapter 5 is utilized to verify the effectiveness of the proposed controller experimentally. PV system is developed in real time digital simulator (RTDS) and the proposed ANFIS-based MPPT is designed in dSPACE DS1104. In this chapter, experimental superiority of the proposed controller over conventional Incremental Conductance (InCond) controller will be investigated. Additionally, experimental results have been compared with the MATLAB simulation results to validate the accuracy of the proposed controller.

6.2 EXPERIMENTAL RESULTS

Experimentally, a series of tests are conducted in the RTDS and dSPACE DS1104 environment to examine the effectiveness of the proposed controller for different step changes in irradiation and temperature.

6.2.1 Test 1: Step-up change in irradiation level

In this test step-up change in irradiation level is applied which is same as that applied in simulation studies and its irradiation pattern shown in chapter 4 in Figure. 4.6. The

system response and performance under such disturbance are shown in Figure 6.1 -6.4 and depict the experimental comparison between the proposed and conventional controllers. The experimental comparison of PV power output (P_{PV}) is shown in Figure 6.1 and demonstrates that the proposed controller can track the MPP much faster than conventional controller and without significant oscillations in steady state. The characteristic of the duty ratio for buck converter switch is shown in Figure 6.2 and shows much better performance than the conventional InCond controller cannot follow the rapidly changing irradiation condition. The PV output voltage and current under the step-up change in irradiation are shown in Figure 6.3 and 6.4, respectively and confirm the effectiveness of the proposed controller. This verifies the competence of the proposed ANFIS-based MPPT over conventional method for the worst case of step-up change in irradiation condition, experimentally.

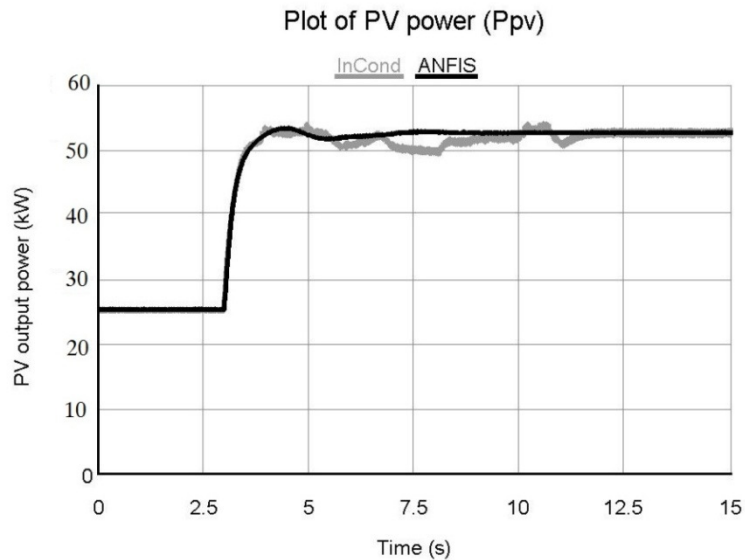


Figure 6.1: PV output power (P_{PV}) for step-up change in irradiation.

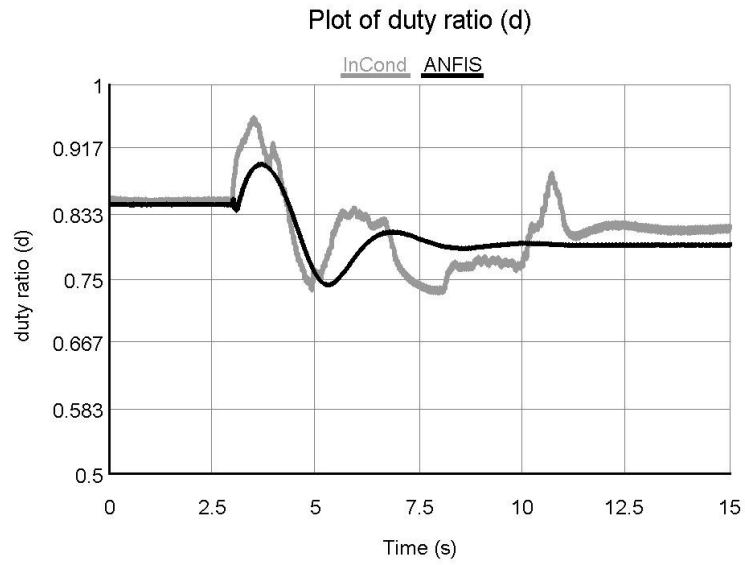


Figure 6.2: Plot of duty ratio for step-up change in irradiation.

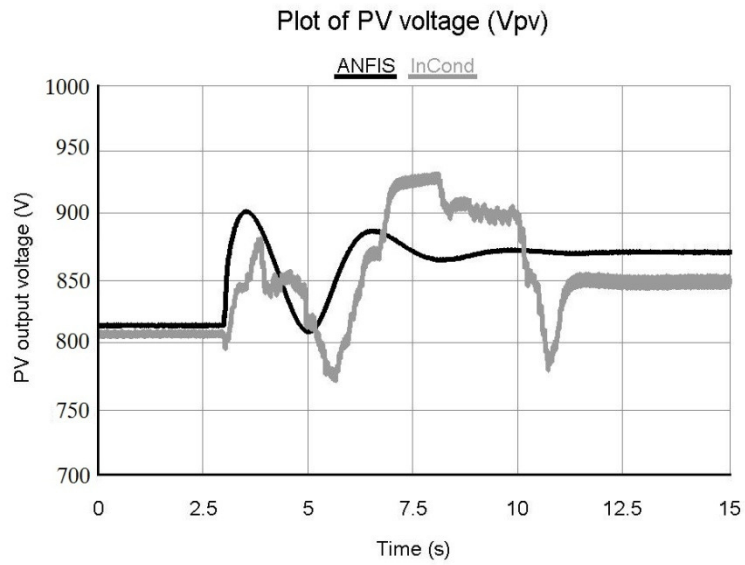


Figure 6.3: PV voltage (V_{PV}) for step-up change in irradiation.

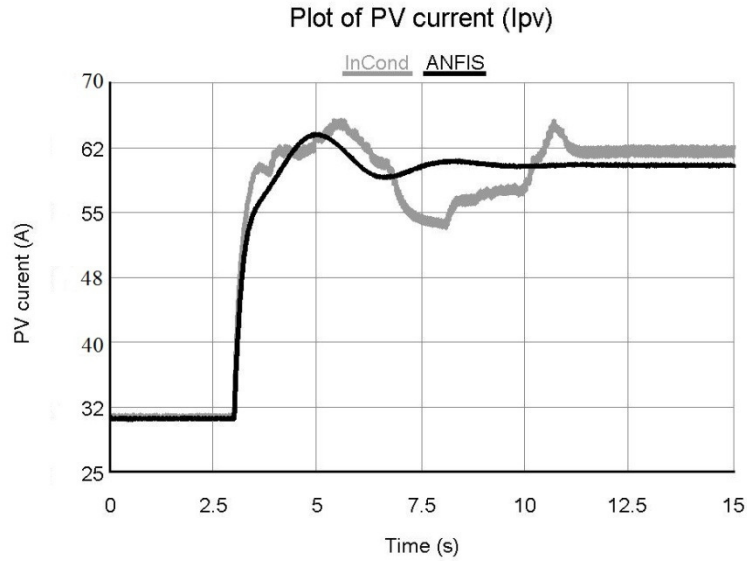


Figure 6.4: PV current (I_{PV}) for step-up change in irradiation.

6.2.2 Test 2: Step-down change in irradiation level

In this test a step-down change in irradiation level is applied that has the similar pattern of the simulation studies and shown in chapter 4 in Figure 4.12. The system response and performance under such disturbance are shown in Figure 6.5 - 6.8 that depict the experimental comparison between the proposed and conventional controllers. Experimental results for PV power (P_{PV}) is shown in Figure 6.5 which confirms that the proposed controller has less fluctuations and can reach the steady state faster and then the conventional InCond method. The behavior of the duty ratio for the buck converter switch is shown in Figure 6.6. The output characteristics of PV voltage (V_{PV}) and current (I_{PV}) are shown in Figure 6.7 and 6.8 respectively and verify the effectiveness of the proposed controller. This verifies experimentally the competence of the proposed

ANFIS-based MPPT over conventional method for the worst case of step-down change in irradiation condition.

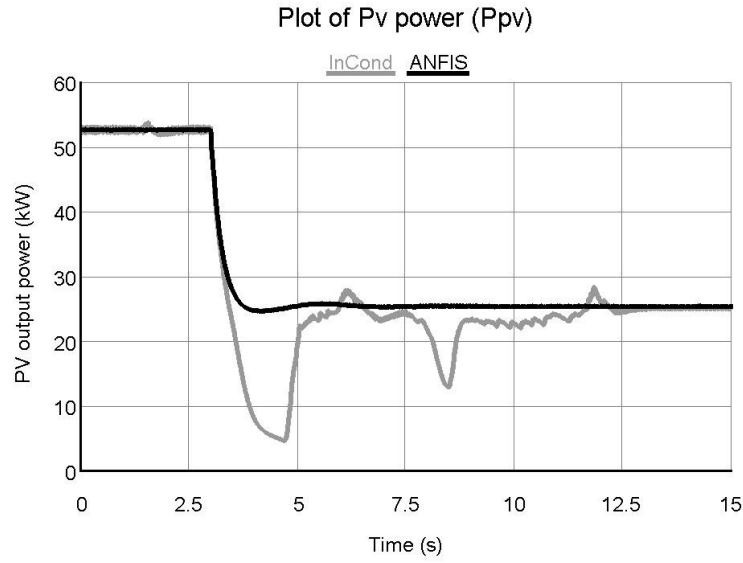


Figure 6.5: PV output power (P_{PV}) for step-down change in irradiation

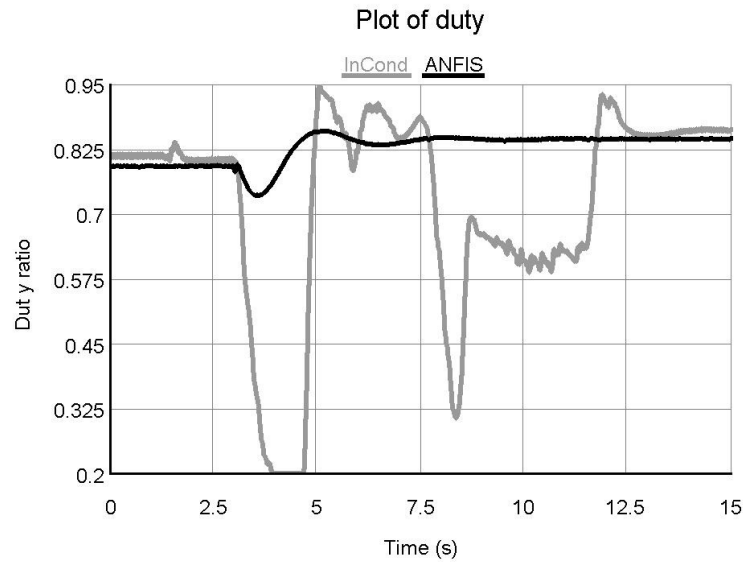


Figure 6.6: Plot of duty ratio for step-down change in irradiation.

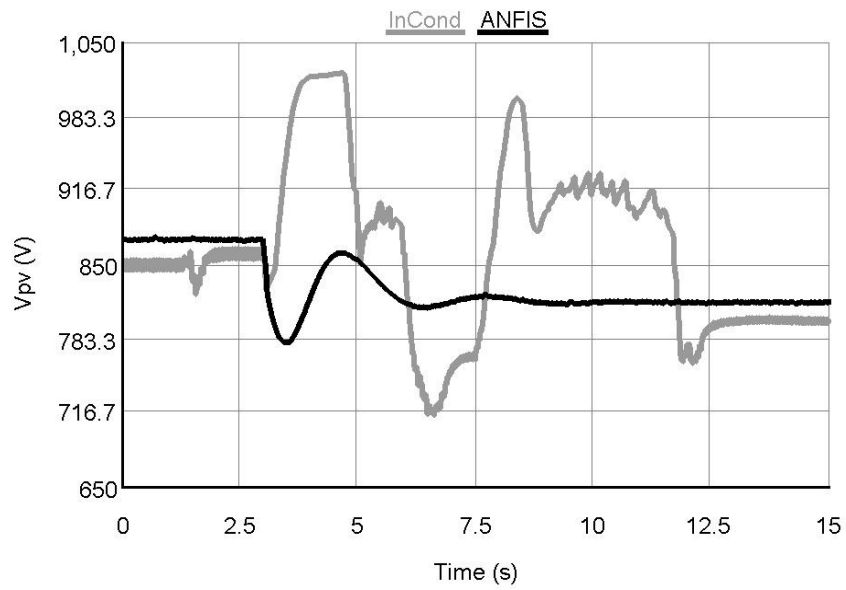


Figure 6.7: PV voltage (V_{PV}) for step-down change in irradiation.

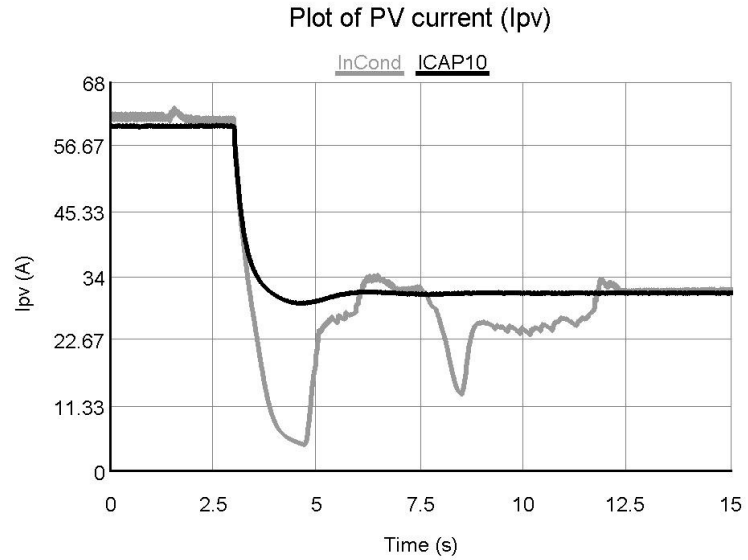


Figure 6.8: PV current (I_{PV}) for step-down change in irradiation.

6.2.3 Test 3: Step-up change in temperature level

In this test step-up change in temperature is applied which is the same as that applied in simulation studies and its temperature pattern shown in chapter 4 in Figure 4.18. The system's experimental response and performance under such disturbance are shown in Figure 6.9 - 6.12. Experimental result for PV power (P_{PV}) is shown in Figure 6.5 and depicts that the proposed controller can track the MPP point in reasonable time and without significant fluctuations in the steady state. The behavior of the duty ratio for the buck converter switch is shown in Figure 6.6. The output characteristics of PV voltage (V_{PV}) and current (I_{PV}) are shown in Figure 6.7 and 6.8 respectively and verify the effectiveness of the proposed controller. This verifies experimentally the competence of the proposed ANFIS-based MPPT for the worst case of step-up change in temperature.,.

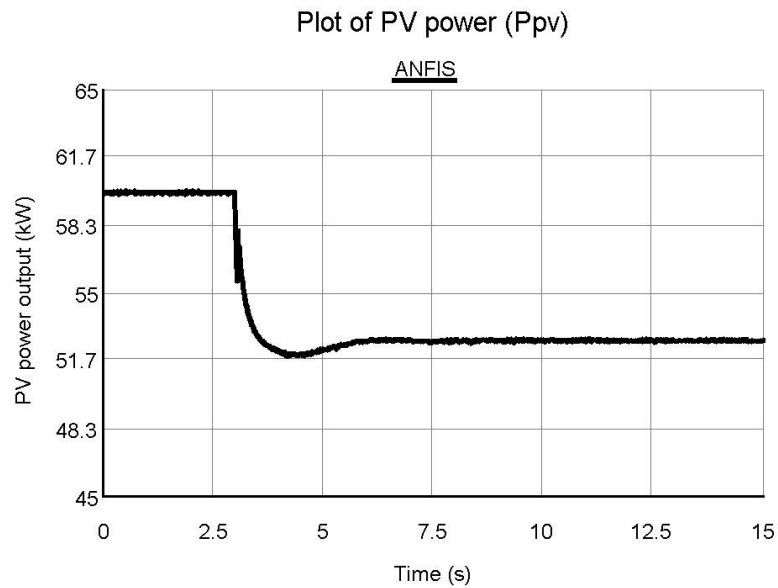


Figure 6.9: PV output power (P_{PV}) for step-up change in temperature.

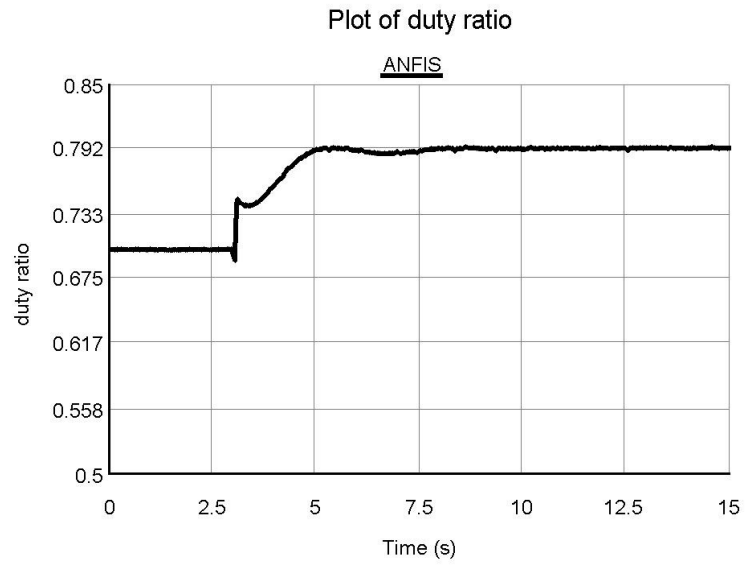


Figure 6.10: Plot of duty ratio for step-up change in temperature.

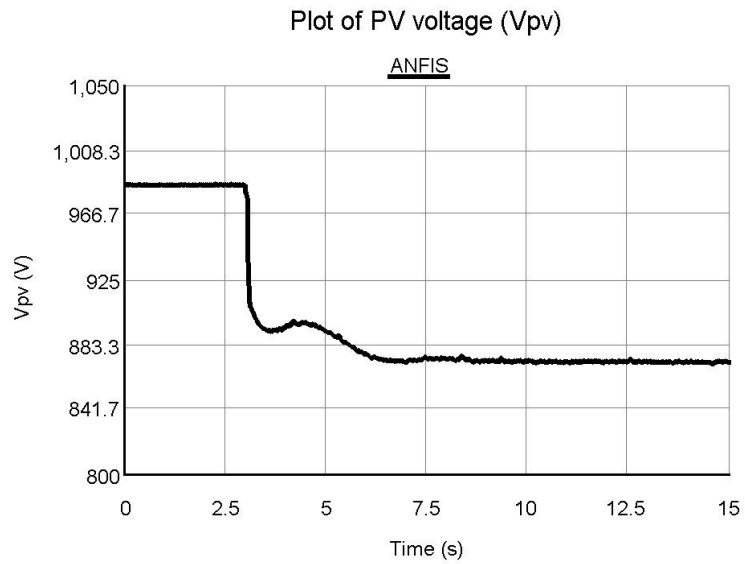


Figure 6.11: PV voltage (V_{PV}) for step-up change in temperature.

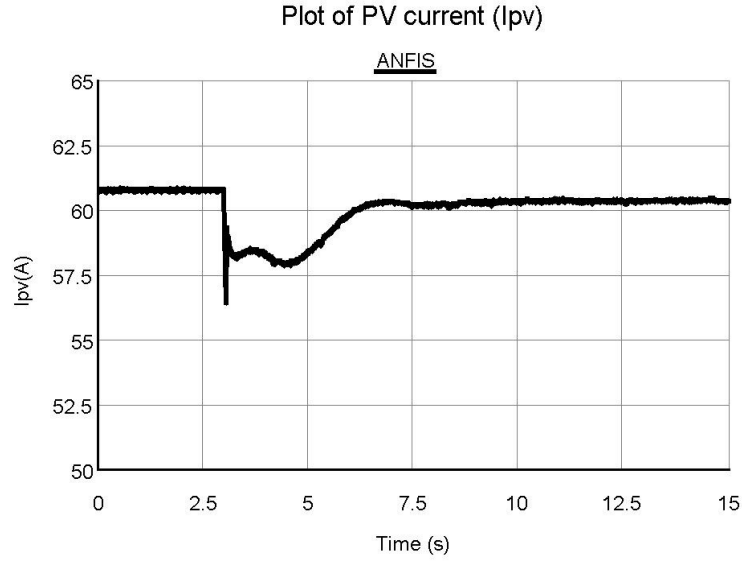


Figure 6.12: PV current (I_{PV}) for step-up change in temperature.

6.2.4 Test 4: Step-down change in temperature level

In this test step-down change in temperature is applied and have the same pattern is used in the simulation studies and shown in chapter 4 in Figure 4.24. The system's experimental response and performance under such disturbance are shown in Figure 6.13-6.16. Experimental result for PV power (P_{PV}) is shown in Figure 6.13 and depicts that the proposed controller can track the MPP point in reasonable time and without significant fluctuations in the steady state. The behavior of the duty ratio for the buck converter switch is shown in Figure 6.14. The output characteristics of PV voltage (V_{PV}) and current (I_{PV}) are shown in Figure 6.15 and 6.16 respectively and verify the effectiveness of the proposed controller. This verifies experimentally the competence of the proposed ANFIS-based MPPT for the worst case of step-down change in temperature.

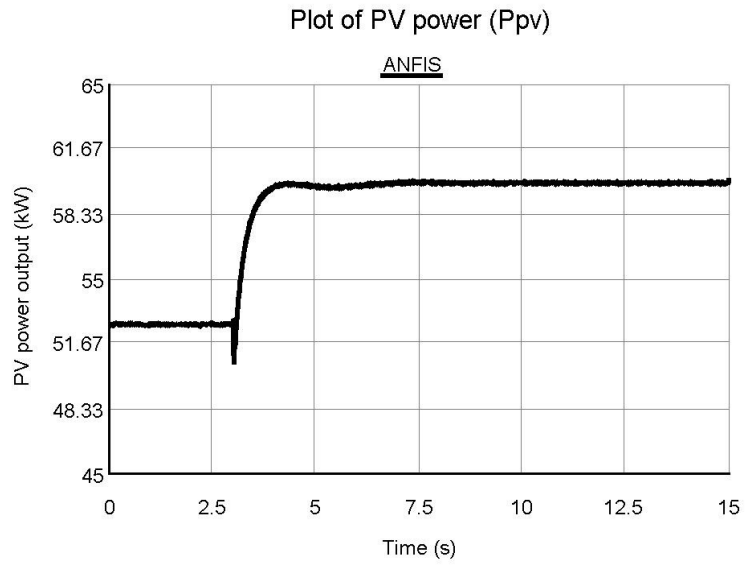


Figure 6.13: PV output power (P_{PV}) for step-down change in temperature.

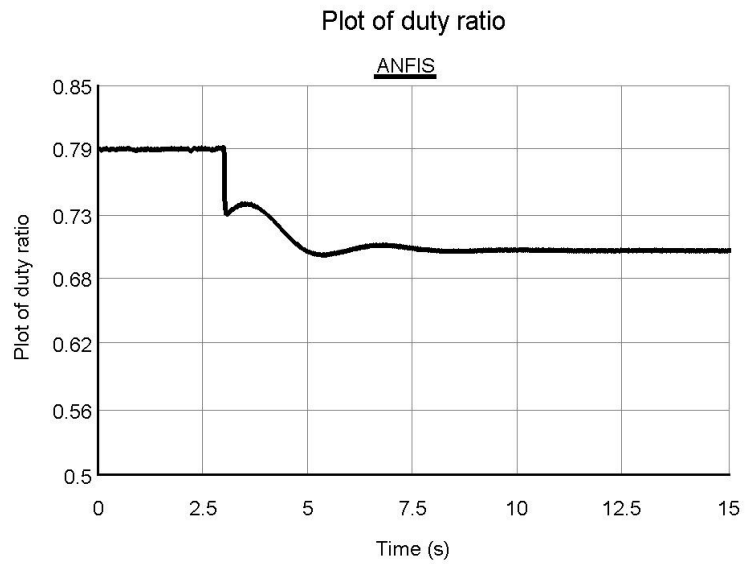


Figure 6.14: Plot of duty ratio for step-down change in temperature.

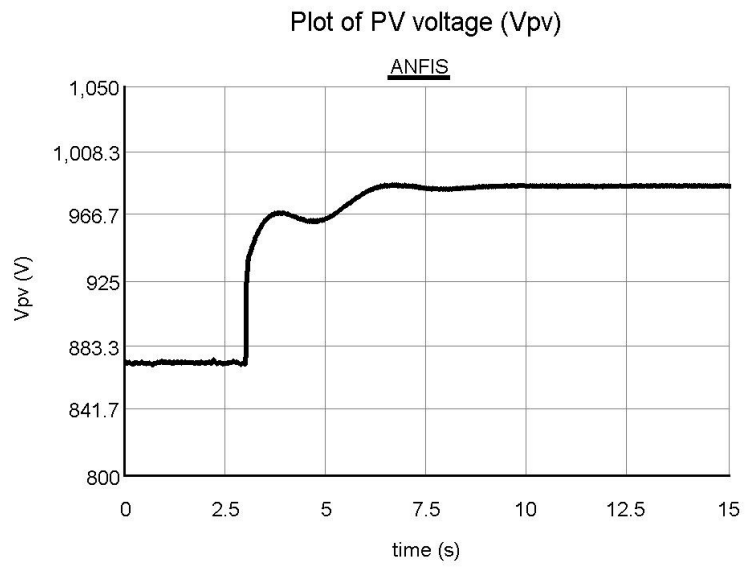


Figure 6.15: PV voltage (V_{PV}) for step- down change in temperature.

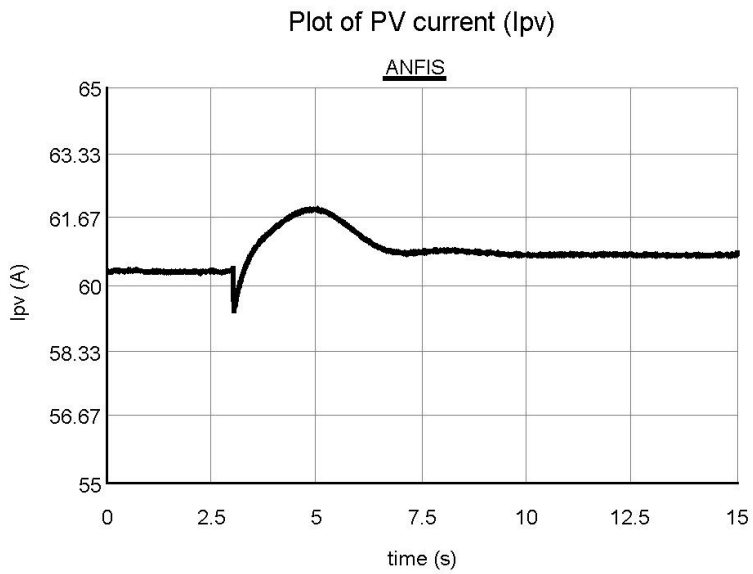


Figure 6.16: PV current (I_{PV}) for step- down change in temperature.

6.3 COMPARISON OF SIMULATION AND EXPERIMENTAL RESULTS

The results from the MATLAB/Simulink simulations, discussed in chapters 4, are compared with the experimental results to explore the validity of the proposed ANFIS-based MPPT controller. The results and comparison show that the proposed controller has noticeable improvement in tracking the MPP under varying environmental conditions. Experimental and MATLAB/Simulink simulations results have confirmed the effectiveness of the proposed ANFIS-based MPPT for all the tests considered.

6.3.1 Test 1: Step-up change in irradiation level

In test 1, comparison is made between the simulation and experimental results for the step-up change in irradiation level to verify the working of the proposed controller. A comparison of the system response and performance under this disturbance is shown in Figure 6.17 – 6.20. Figure 6.17 depicts the PV power output (P_{PV}) and how the proposed controller track the MPP in MATLAB/Simulink and experimental simulations under the step-up change in irradiation level. Comparison of duty ratio is shown in Figure 6.18 and PV output voltage (V_{PV}) and current (I_{PV}) are illustrated in Figure. 6.19 and 6.20 respectively. It can be seen that the experimental results are very much similar to the simulation results. A small difference can be noticed in the transient phase that is because RTDS has a detailed real time simulation and depicts in depth response. On the other hand, model developed for MATLAB simulations is simplified. Both the experimental and MATLAB/Simulink results validate the accuracy of the proposed controller model.

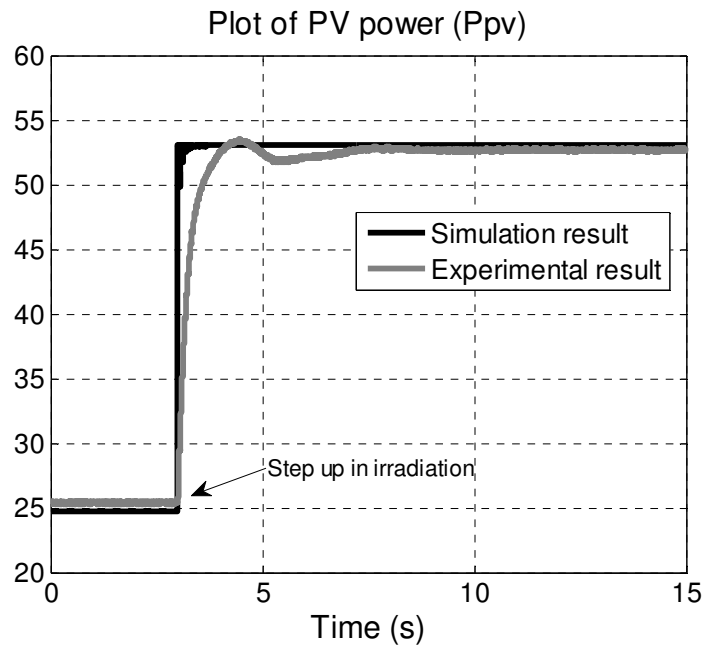


Figure 6.17: Comparison of PV power (P_{PV}) for step-up change in irradiation.

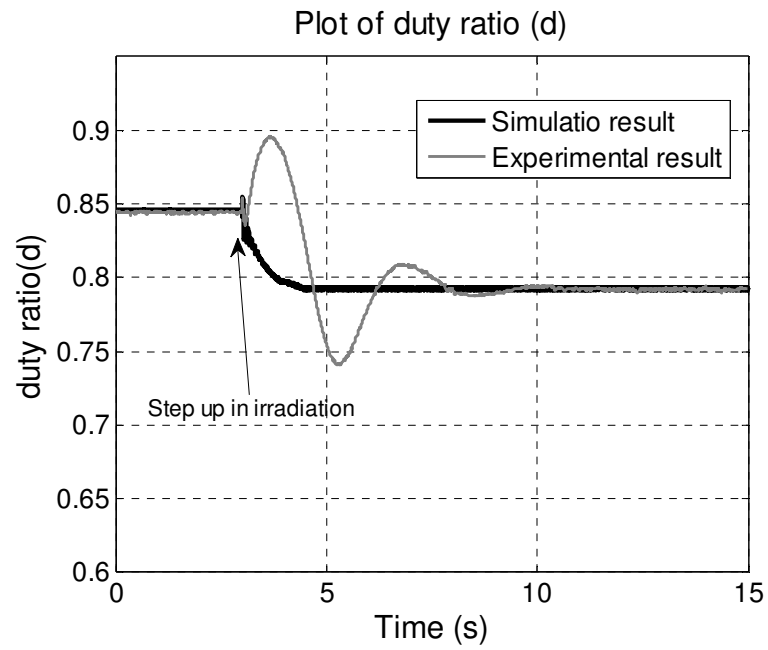


Figure 6.18: Comparison of duty ratio for step-up change in irradiation.

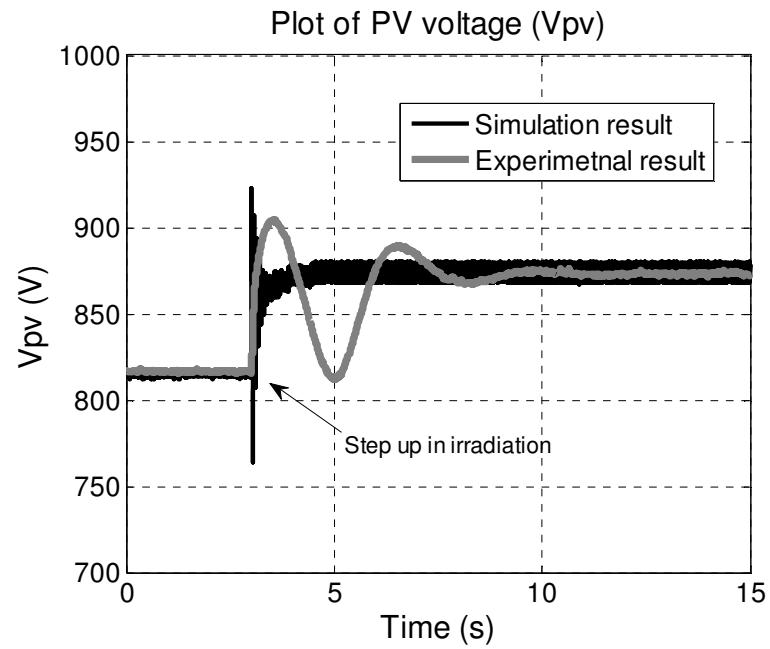


Figure 6.19: Comparison of PV voltage (V_{PV}) for step-up change in irradiation.

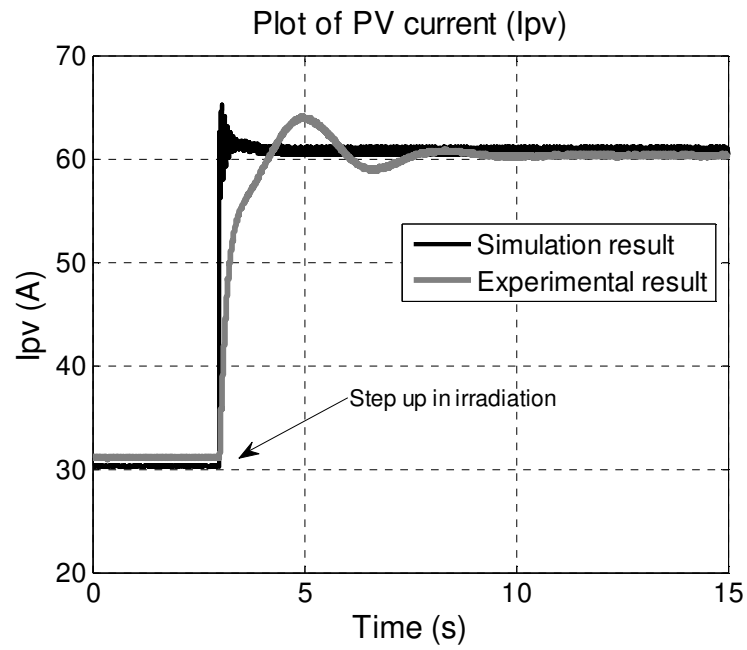


Figure 6.20: Comparison of PV current (I_{PV}) for step-up change in irradiation.

6.3.2 Test 2: Step-down change in irradiation level

In this test, simulation results are compared with the experimental results to verify the accuracy of the proposed controller under the step-down change in irradiation condition. A comparison of the system response and performance under this disturbance is shown in Figure 6.21 – 6.24. PV power output (P_{PV}) is shown in Figure 6.21 that confirms the similarity between the experimental and simulation results and show how the proposed controller track the MPP under the step-up change in irradiation level. Behavior of duty ratio is compared Figure 6.22 and comparison for PV output voltage (V_{PV}) and current (I_{PV}) are illustrated in Figure 6.23 and 6.24 respectively. It can be noticed that the simulation results are very much similar to the experimental results. This verifies the working of the proposed controller experimentally under the step-down change in irradiation condition.

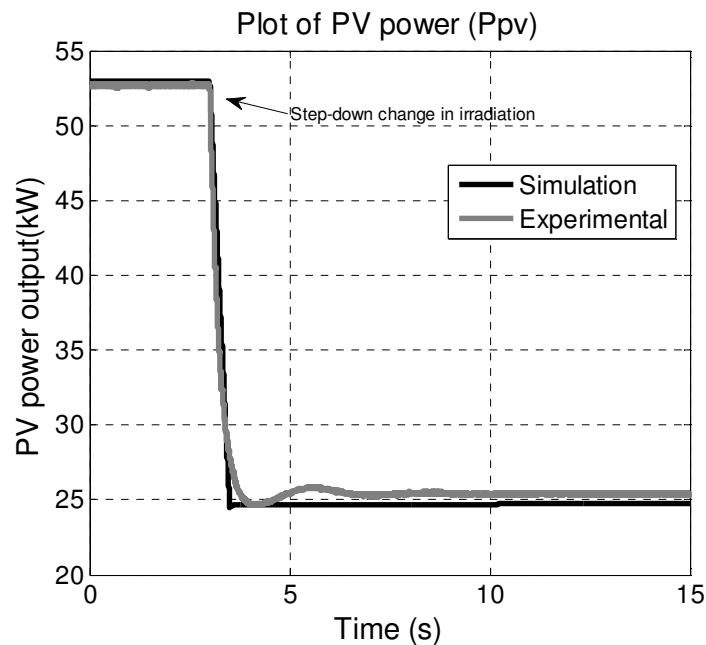


Figure 6.21: Comparison of PV power (P_{PV}) for step-down change in irradiation.

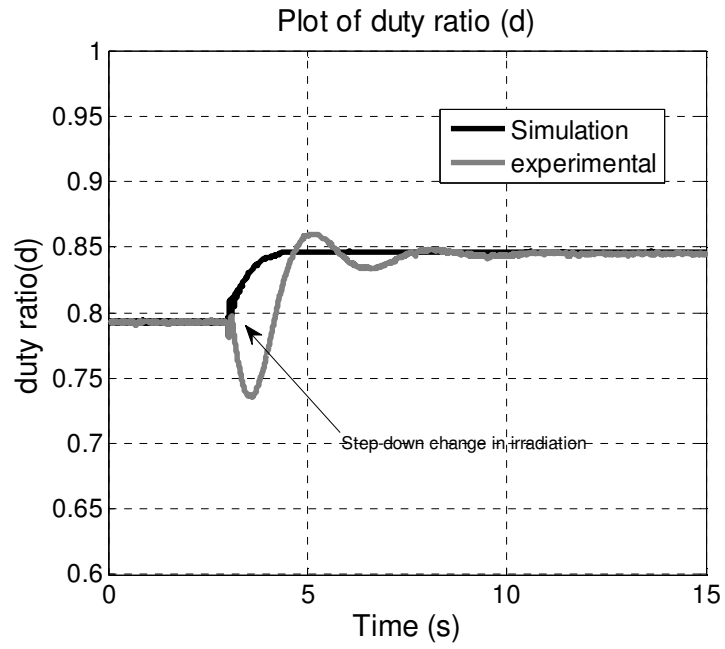


Figure 6.22: Comparison of duty ratio for step-down change in irradiation.

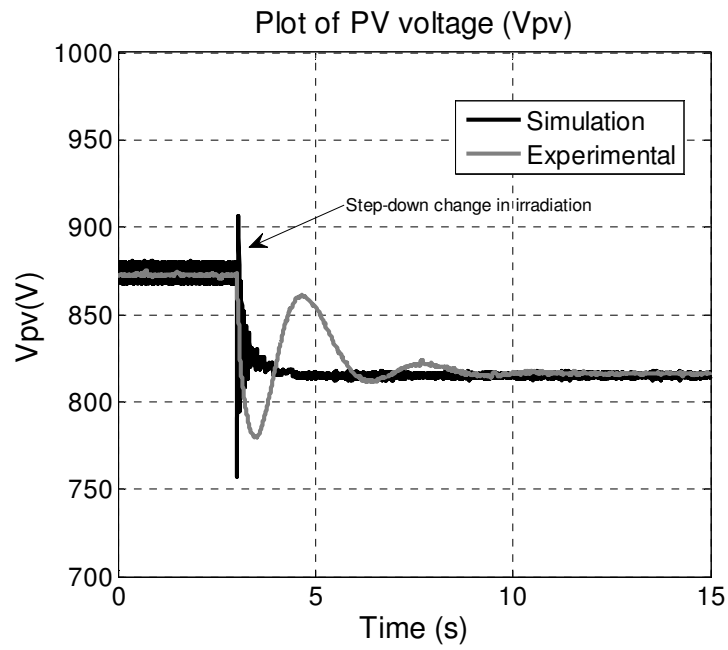


Figure 6.23: Comparison of PV voltage (V_{pv}) for step-down change in irradiation.

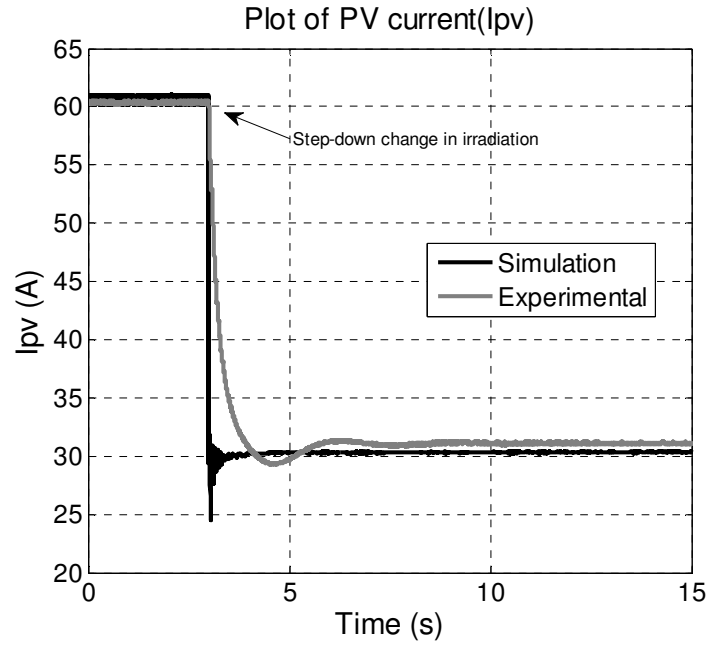


Figure 6.24: Comparison of PV current (I_{PV}) for step-down change in irradiation.

6.3.3 Test 3: Step-up change in temperature level

In this test, comparison is made between the simulation and experimental results for the step-up change in temperature to verify the effectiveness of the proposed controller. A comparison of the system response and performance under this disturbance is shown in Figure 6.25 – 6.28. Figure 6.25 depicts the PV power output (P_{PV}) and how the proposed controller track the MPP in MATLAB/Simulink and experimental simulations under the step-up change in temperature. Comparison of duty ratio is shown in Figure 6.26 and PV output voltage (V_{PV}) and current (I_{PV}) are illustrated in Figure 6.27 and 6.28 respectively. .It can be seen from all the graphs that the experimental curves are very close to the simulation curves. Both the experimental and MATLAB/Simulink results validate the accuracy and the effectiveness of the proposed controller model.

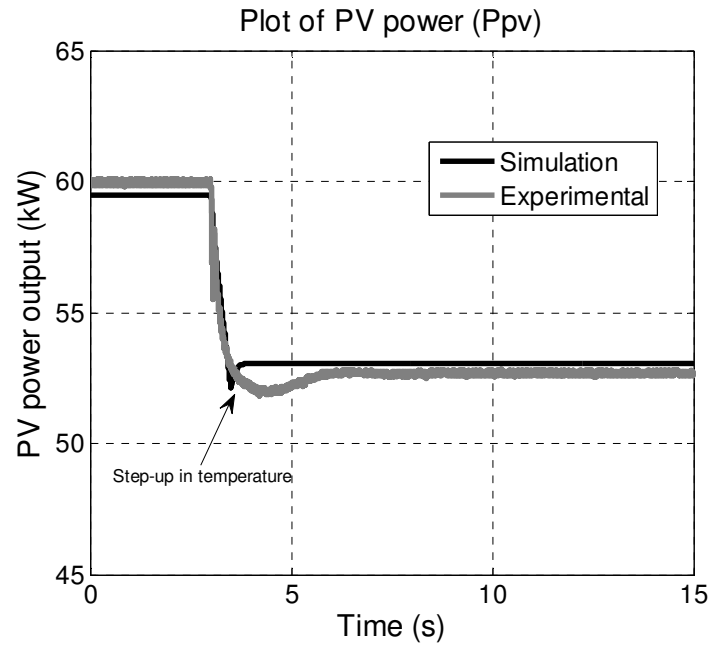


Figure 6.25: Comparison of PV power (P_{PV}) for step-up change in temperature.

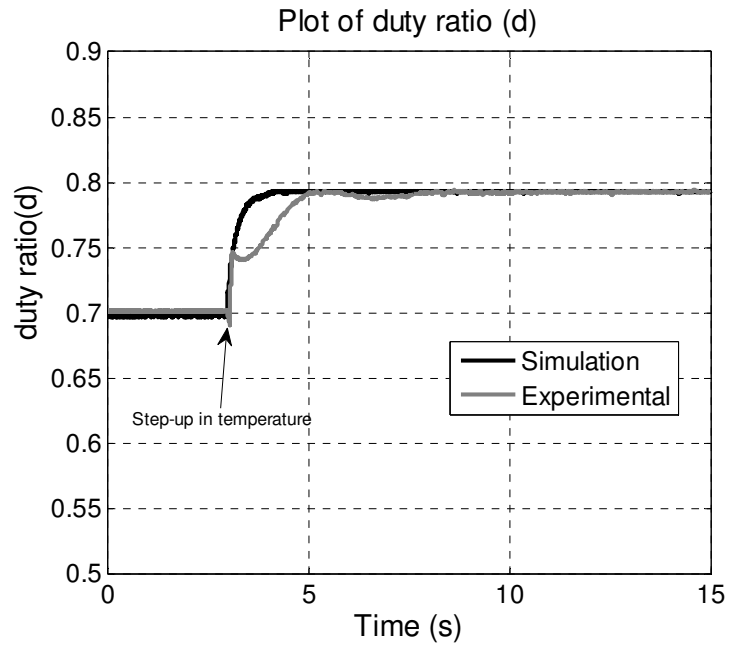


Figure 6.26: Comparison of duty ratio for step-up change in temperature.

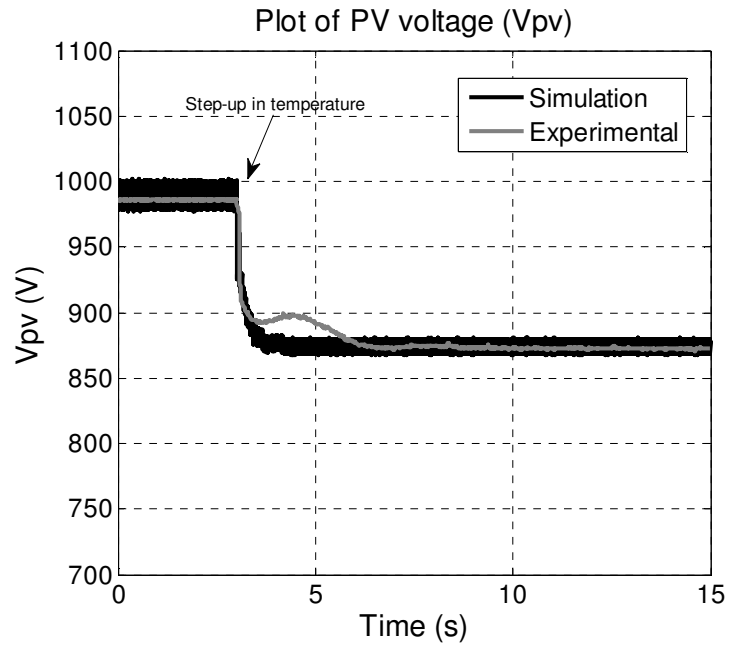


Figure 6.27: Comparison of PV voltage (V_{PV}) for step-up change in temperature.

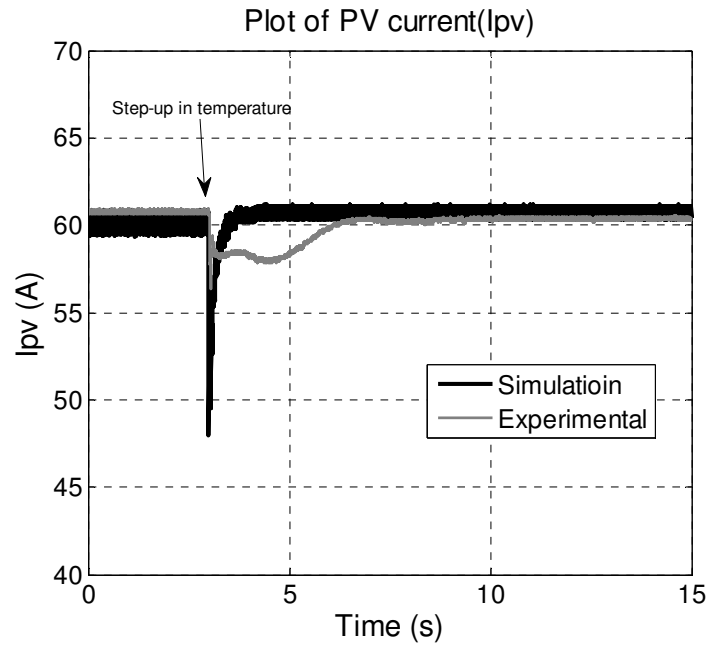


Figure 6.28: Comparison of PV current (I_{PV}) for step-up change in temperature.

6.3.4 Test 4: Step-down change in temperature level

In this test, simulation results are compared with the experimental results to verify the accuracy of the proposed controller under the step-down change in temperature. A comparison of the system response and performance under this disturbance is shown in Figure 6.29 – 6.32. PV power output (P_{PV}) is shown in Figure 6.29 which demonstrates the closeness between the practical and simulation results and show that the proposed controller tracks the MPP under the step-up change in temperature. Behavior of duty ratio is compared in Figure 6.30 and comparison for PV output voltage (V_{PV}) and current (I_{PV}) are illustrated in Figure 6.31 and 6.32 respectively. It can be noticed from all the graphs that the simulation results are in full agreement to the experimental results. This confirms the accuracy and potential of the proposed controller experimentally under the step-down change in irradiation condition

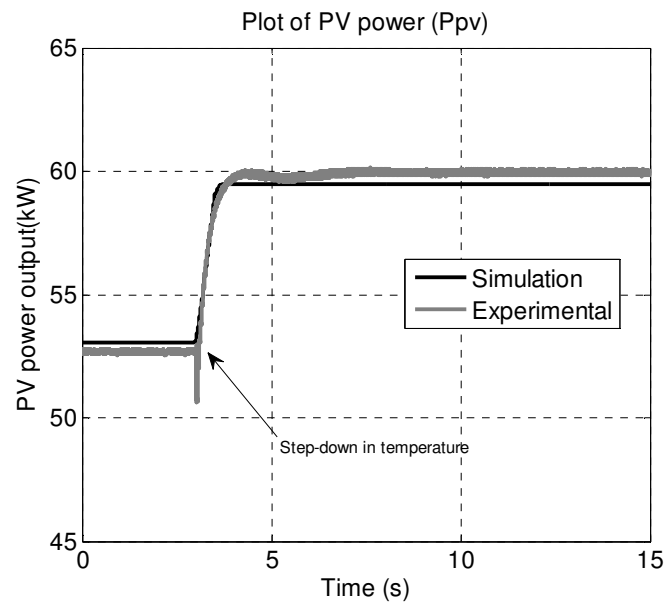


Figure 6.29: Comparison of PV power (P_{PV}) for step-down change in temperature.

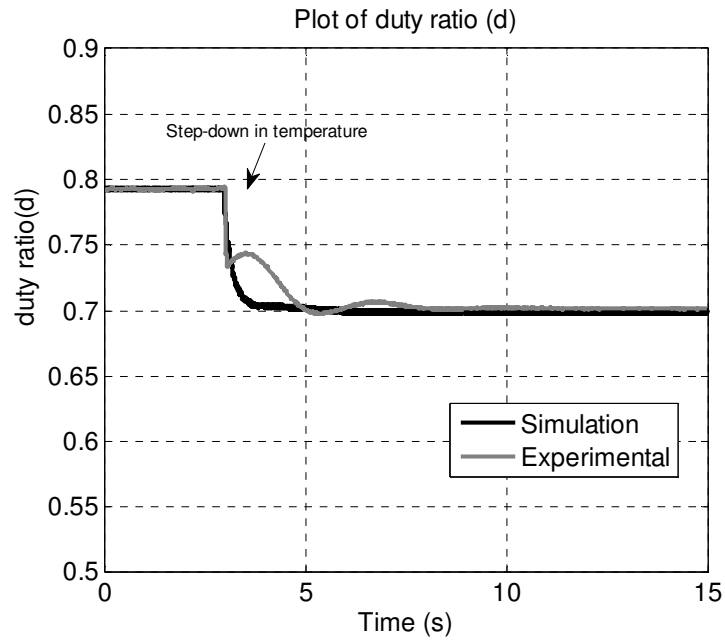


Figure 6.30: Comparison of duty ratio for step-down change in temperature.

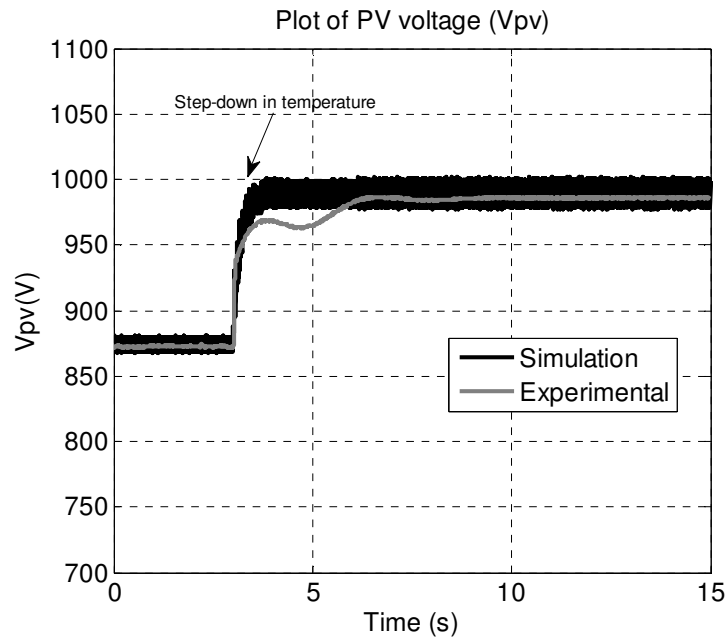


Figure 6.31: Comparison of PV voltage (V_{PV}) for step-down change in temperature.

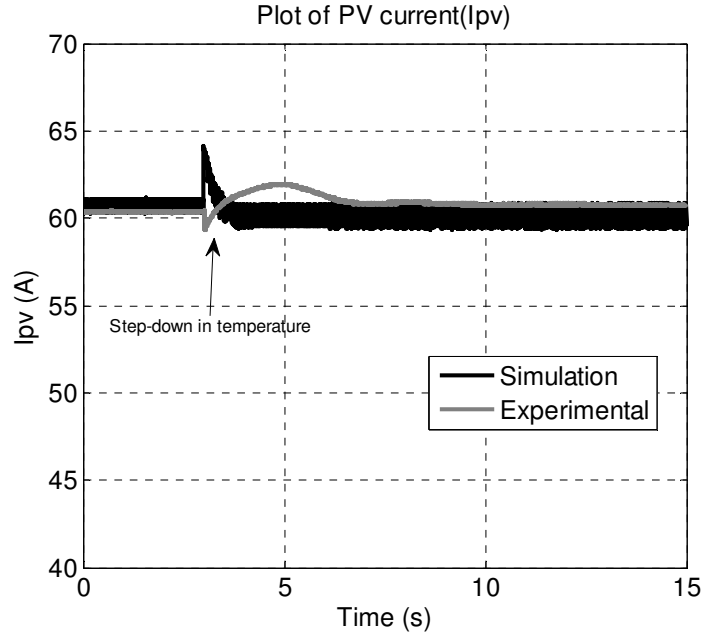


Figure 6.32: Comparison of PV current (I_{PV}) for step-down change in temperature.

6.4 CONCLUSION

In this chapter, experimental validation of the proposed ANFIS-based MPPT controller has been demonstrated under different disturbances. The performance of the proposed controller is compared with the conventional InCond method. Results and comparisons show that the proposed controller can track the MPP faster with less fluctuation in the steady state as compared with the conventional controller. Similarity between the experimental curves and the MATLAB/Simulink simulations results have also been shown to validate the accuracy and performance of the proposed controller practically.

CHAPTER 7 CONCLUSION AND FUTURE WORK

7.1 CONCLUSION

In this thesis a generalized PV array model simulator has been proposed and developed in the MATLAB/Simulink. Simulator has been designed based on the five parameters equivalent electric circuit model. The major challenge in the implementation of this model lies in the estimation of the five unknown model parameters. A novel ANFIS-based MPPT controller has also been proposed and the developed PV model has been utilized to evaluate the performance of the proposed ANFIS-based MPPT controller under different atmospheric conditions. Conventional MPPT techniques have some drawbacks like oscillation in the steady state, slow convergence and failure to track MPP in the rapidly changing conditions. All these factors causes considerable amount of power losses. It has been shown that the proposed controller can overcome the shortcoming of the conventional controllers.

7.1.1 Parameter Estimation for PV Electrical Model

- PV model parameters have been identified using the efficient stochastic optimization technique. Estimation problem is converted into optimization one where Differential Evolution (DE) as an efficient optimizing technique is

employed to estimate the model parameters at standard test condition (STC) (1000 W/m^2 and 25°C) using only the data provided by the manufacturer.

- The effectiveness of the proposed method has been analyzed by estimating the parameters of six PV panels of three different technologies (mono-crystalline, poly-crystalline and thin film) and comparing the determined I-V curves with the experimental curves given in the datasheets. Results and analysis have shown that the proposed method can simulate the output characteristics of all the three technologies efficiently.
- Precise PV simulator has been developed that is flexible enough to simulate any number of PV panels connected in series and parallel. The robustness of the proposed simulator is demonstrated under the partial shaded conditions. Additionally, the performance of the developed simulator is verified by interfacing it with the actual power electronics converter and maximum power point tracking (MPPT) controller.
- The proposed work will facilitate the power system design engineers to assess the behavior of the newly developed controllers and performance of the overall power system prior to any practical implementation.

7.1.2 Proposed ANFIS-Based MPPT controller

- A novel ANFIS-based MPPT controller has been proposed. The proposed controller hybridizes the principles of two efficient intelligent techniques; Fuzzy Inference systems (FIS) and Artificial Neural Network (ANN).

- A nonlinear time domain simulation has been carried out to assess the effectiveness of the proposed controllers under different disturbances. Results and comparison showed that the proposed ANFIS-based MPPT controller can fulfill the shortcomings of the conventional method and can track the MPP faster with less overshoots. The obtained results demonstrate that the proposed controller has better dynamic and steady state performance than the conventional method.
- Experimental setup has been put together to verify the effectiveness of the proposed controller practically. The ANFIS-based MPPT controller is developed in dSPACE DS1104 and PV system is designed in Real Time digital Simulator (RTDS). Results and analysis showed that the proposed ANFIS-based MPPT has fast response in the transient condition and has fewer oscillations in the steady state.
- Finally, comparison of experimental and MATLAB simulation results has been carried out to verify the accuracy of the proposed controller.

7.2 FUTURE WORK

The following subjects are recommended for future work.

1. The developed PV simulator can be modified by using two-diode PV model that will add two additional unknown parameters to optimize and comparison can be done between modified and proposed simulator to investigate their efficiencies.

2. Different optimization techniques can be used instead of DE to estimate the model parameters of PV, to study which optimizing technique is better.
3. Different objective function can be used to test the efficiency of the optimizing techniques.
4. Partial shading condition is one of the major issues and causes multiple peaks in the PV curve and made it difficult to track the global MPP. The proposed ANFIS-based MPPT controller is designed for uniform irradiation condition and it can be improved to work in the partial shading conditions.
5. In this thesis, step changes in irradiation and temperature has been applied to test the effectiveness of the proposed ANFIS-based MPPT. Of course, actual real data of irradiation and temperature can be used to verify its performance for real environmental conditions.
6. The developed PV system model and proposed MPPT controller can be interfaced with the power grid through inverter and effects of changing environmental conditions on power grid can be studied.
7. Practical setup of actual PV array with all necessary sensors and controllers can be installed to test the performance of proposed ANFIS-based MPPT controller.

APPENDIX-A: SOLAR PANEL DATASHEETS

SUNPOWER™

230 SOLAR PANEL

EXCEPTIONAL EFFICIENCY AND PERFORMANCE

BENEFITS

Highest Efficiency
SunPower™ Solar Panels are the most efficient photovoltaic panels on the market today.

More Power
Our panels produce more power in the same amount of space—up to 50% more than conventional designs and 100% more than thin film solar panels.

Reduced Installation Cost
More power per panel means fewer panels per install. This saves both time and money.

Reliable and Robust Design
Proven materials, tempered front glass, and a sturdy anodized frame allow panel to operate reliably in multiple mounting configurations.



SPR-230-WHT-U



The SunPower™ 230 Solar Panel provides today's highest efficiency and performance. Utilizing 72 all back-contact solar cells, the SunPower 230 delivers a total panel conversion efficiency of 18.5%. The panel's reduced voltage-temperature coefficient and exceptional low-light performance attributes provide outstanding energy delivery per peak power watt.

SunPower's High Efficiency Advantage - Up to Twice the Power

	Thin Film	Conventional	SunPower
Peak Watts / Panel	65	170	230
Efficiency	9.0%	13.0%	18.5%
Peak Watts / ft² (m²)	8 (90)	12 (130)	17 (185)

About SunPower

SunPower designs, manufactures and delivers high-performance solar electric technology worldwide. Our high-efficiency solar cells generate up to 50% more power than conventional solar cells. Our high-performance solar panels, roof tiles and trackers deliver significantly more energy than competing systems.



SUNPOWER™

230 SOLAR PANEL

EXCEPTIONAL EFFICIENCY AND PERFORMANCE

Electrical Data

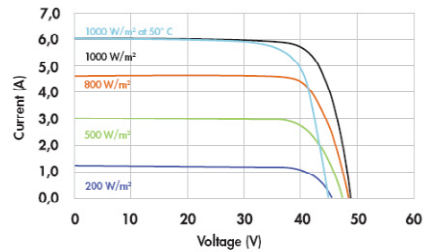
Measured at Standard Test Conditions (STC): irradiance of 1000W/m², AM 1.5, and cell temperature 25°C

Peak Power (+/-5%)	P _{max}	230 W
Rated Voltage	V _{mpp}	41.0 V
Rated Current	I _{mp}	5.61 A
Open Circuit Voltage	V _{oc}	48.7 V
Short Circuit Current	I _{sc}	5.99 A
Maximum System Voltage	UL	600 V
Temperature Coefficients		
	Power	-0.38% / K
	Voltage (V _{oc})	-132.5mV / K
	Current (I _{sc})	3.5mA / K
NOCT		45° C +/-2° C
Series Fuse Rating		20 A

Mechanical Data

Solar Cells	72 SunPower all-back contact monocrystalline
Front Glass	High transmission tempered glass
Junction Box	IP-65 rated with 3 bypass diodes Dimensions: 32 x 155 x 128 (mm)
Output Cables	1000mm length cables / MultiContact (MC4) connectors
Frame	Anodized aluminum alloy type 6063 (black)
Weight	33.1 lbs. (15.0 kg)

I-V Curve



Current/voltage characteristics with dependence on irradiance and module temperature.

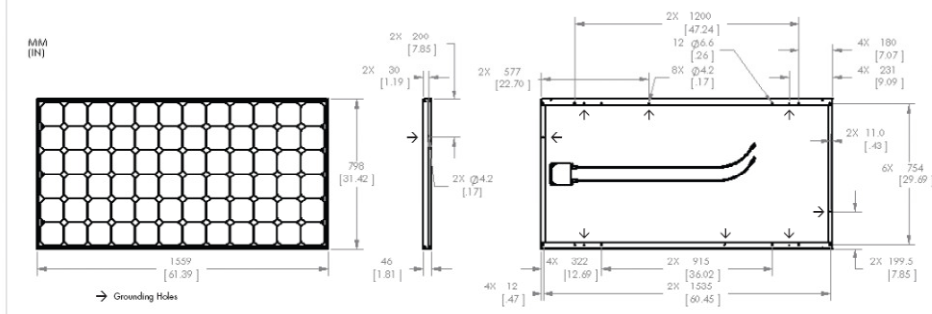
Tested Operating Conditions

Temperature	-40° F to +185° F (-40° C to +85° C)
Max load	113 psf 550kg/m² (5400 Pa) front – e.g. snow; 50 psf 245kg/m² (2400 Pa) front and back – e.g. wind
Impact Resistance	Hail 1 in (25 mm) at 52mph (23 m/s)

Warranties and Certifications

Warranties	25 year limited power warranty 10 year limited product warranty
Certifications	Tested to UL 1703, Class C Fire Rating

Dimensions



CAUTION: READ SAFETY AND INSTALLATION INSTRUCTIONS BEFORE USING THE PRODUCT.
Visit sunpowercorp.com for details

SUNPOWER and the SUNPOWER logo are trademarks or registered trademarks of SunPower Corporation.
© 2009 March SunPower Corporation. All rights reserved. Specifications included in this datasheet are subject to change without notice.

sunpowercorp.com
Document #001-42190 Rev"A" / UR_EN



English



The **leading** force
in **green** power



SunForte PM318B00

Mono-crystalline Photovoltaic Module

19.5%
EFF.

315W
318W

Power Range
315-318Wp



Back Contact Cells

No wiring in the front side enhances light conversion space



Highly Strengthened Design

Module complies with advanced loading tests to meet IEC61215 loading requirements

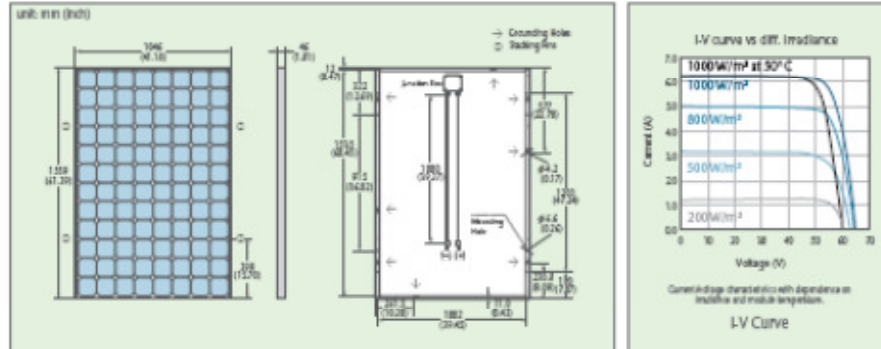
EFF. ↑
19.5%

19.5% Efficiency

The highest efficiency of 19.5%



SunForte PM318B00 (315-318 Wp)



Electrical Data

Typ. Nominal Power P_m	315 Wp	318 Wp
Typ. Module Efficiency	19.10%	19.50%
Typ. Nominal Voltage V_m (V)	54.70	54.70
Typ. Nominal Current I_m (A)	5.76	5.82
Typ. Open Circuit Voltage V_{oc} (V)	64.60	64.70
Typ. Short Circuit Current I_{sc} (A)	6.14	6.20
Maximum Tolerance of P_m	-3% / +5%	

* All data are for the 1000 W/m² irradiance and 25°C temperature (STC).
 * STC: Irradiance 1000 W/m², spectral distribution AM 1.5, temperature 25 ± 2°C, in accordance with IEC 60904-2.
 * The given electrical data are nominal values which account for basic manufacturing and manufacturing tolerance of ±10%, with the exception of P_m . The qualification is performed according to IEC 61215.

Temperature Coefficient

NOCT	45 ± 2° C
Typ. Temperature Coefficient of P_m	-0.38% / K
Typ. Temperature Coefficient of V_{oc}	-0.22% / K
Temperature Coefficient of I_{sc}	0.06% / K

* NOCT: Normal Operating Cell Temperature, measuring conditions: Irradiance 800 W/m², AM 1.5, air temperature 20° C, wind speed 1 m/s.

Mechanical Characteristics

Dimensions (L x W x H)	1559 x 1046 x 46 mm (61.39 x 41.18 x 1.81 inches)
Weight	18.6 kg (41.0 lbs)
Front Glass	High transmission tempered glass with AR-Tech, 3.2 mm (0.13 inches)
Cell	96 high efficiency back contact cells, 125 mm x 125 mm (5" x 5")
Cell Encapsulation	EVA
Back Sheet	Composite film
Frame	Anodized aluminum frame
Junction Box	Junction box with 3 bypass diodes
Cables	Length: each 1.0 m (39.37 inches)
Connector Type	MC4

Operating Conditions

Operating Temperature	-40...+80° C
Ambient Temperature Range	-40...+45° C
Maximum System Voltage	1000 V
IP Protection Level	IP 65
Serial Fuse Rating	15 A
Maximum Surface Load Capacity	Tested up to 5400 Pa according to IEC 61215 (advanced test)

Warranties and Certifications

Product Warranty	Maximum 5 years for material and workmanship
Performance Guarantee	Guaranteed output of 90% for 10 years and 80% for 25 years
Certifications	According to IEC 61215 and IEC 61730 guidelines*

* Please confirm other certifications with AUC office data.



AU Optronics Corporation

No. 1, U-Hsin Rd. 2, Hsinchu Science Park, Hsinchu 30078, Taiwan
 Tel: +886-3-590-8899 Email: solar@auo.com www.AUOsolar.com

AUO Green Solutions
 Printed with Soy Ink



© Copyright May 2011 AU Optronics Corp. All rights reserved. Information may change without notice.

230W Photovoltaic module

BP 3230N

BP 3230N-1 (01/10)



BP Solar has been manufacturing solar wafers, cells and modules for more than 35 years. This experience shows that the best way to optimize module life and electrical energy production is to attend to every detail in the design and manufacture of our products, our process controls and testing methods. BP Solar's Generation Endura photovoltaic modules offers the following benefits:



Strong, resistant, innovative design

The tubular frame is designed with Porsche Engineering to withstand heavy snow loads (5400Pa - 540kg/m²) in multiple mounting conditions. Shock absorbing corners, rounded profile and thick polyester back sheet protect the module against rough handling.



Excellent energy yields

High transmission ARC glass and margin allowance for LID effect maximize energy production. Increased distance between cells and frame and enhanced design that pushes the laminate to the front, reduce soiling losses.



More reliable connections, better cooling diodes

IntegraBus™ technology positions the bypass diodes and junction box away from the cells, ensuring cooler operation. Latching MC4 connectors for increased safety of the installation.



Flexible mounting, easy to handle

Using bolts or clamps, the Endura frame can be mounted in various configurations - even end-mounting; the rounded profile and low g/W ratio makes handling easier while reducing installation costs.

Enhanced warranty offer

BP Solar launches an industry leading warranty offer, with lower degradation rates on our modules manufactured beginning January 1st, 2010. Our internal testing standards that go well beyond international requirements back this innovative offer.



230W Photovoltaic module

BP 3230N



Electrical characteristics

	¹ STC (1000W/m ²)	² NOCT (800W/m ²)
Maximum power (P _{max})	230W	196.6W
Voltage at P _{max} (V _{mp})	35.7V	35.9V
Current at P _{max} (I _{mp})	7.00A	6.32A
Short circuit current (I _{sc})	8.40A	8.05A
Open circuit voltage (V _{oc})	38.7V	39.4V
Module efficiency	19.0%	
Tolerance	±4/+0%	
Nominal voltage	20V	
Efficiency reduction at 3000h/m ²	<0% (reduction coefficient 10.1%)	
Limiting reverse current	0.40A	
Temperature coefficient of I _{sc}	0.004 ± 0.010%/°C	
Temperature coefficient of V _{oc}	-0.30 ± 0.01%/°C	
Temperature coefficient of P _{max}	-0.3 ± 0.05%/°C	
³ NOCT	47±1°C	
Maximum series fuse rating	20A	
Application class according to EN 60904	Class A	
Maximum system voltage V _{sys} (V _{oc} max)	600V V _{oc} max < 1000V V _{oc} max < 1000V	

¹ Values at Standard Test Conditions (STC): irradiance 1000 W/m², air mass 1.5 and 25°C module temperature.
² Values at NOCT conditions: irradiance 800 W/m², ambient temperature 45°C and wind speed 1 m/s.
³ Nominal Cell Operating Temperature (NOCT) is the temperature at which the module operates at its maximum power under standard test conditions.

All electrical and mechanical characteristics are given at 25°C unless otherwise specified. The values are given for the module at 25°C. The values are given for the module at 25°C.

Mechanical characteristics

Solar cells	60 polycrystalline 6" x 6" cells (156x156mm) in series
Front cover	High transmission 3.2mm (1/8") alu glass
Encapsulant	EVA
Back cover	White polyester
Frame	Silver anodized aluminum
Diodes	Integration™ with 6 Schottky diodes
Junction box	Potted (IP 67), certified to meet UL 1709 flammability test
Output cables	4mm ² cable with locking MC4 connectors
Dimensions	Asymmetrical cable lengths: 1110mm (44.1") / 1180mm (46.9")
Weight	10.4kg / 42.0lbs

All dimensions are in mm (inches) unless otherwise specified.

Warranty

- Free from defects in materials and workmanship for 5 years
- 90% power output over 10 years
- 80% power output over 25 years

Certification

Certified according to the extended version of the IEC 61215:2016 (Crystalline silicon terrestrial photovoltaic modules - Design qualification and type approval)

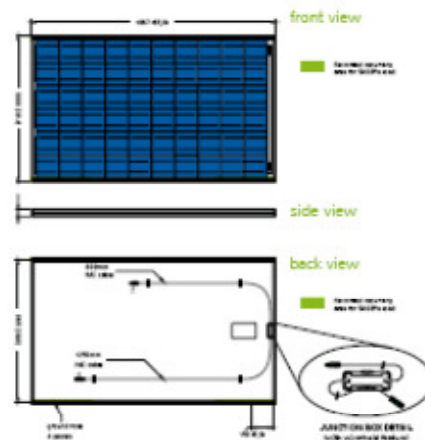
Certified according to IEC 61708-1 and IEC 61708-2 (Photovoltaic module safety qualification requirements for construction and testing)

Listed to UL 1703 (Standard for Safety by Intertek ETL Class C fire rating)

Manufactured in ISO 9001 and ISO 14001 certified factories

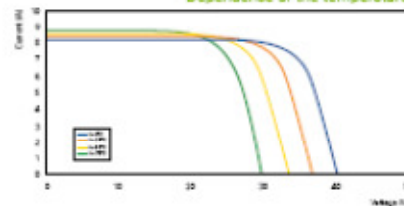
Module electrical measurements are calibrated to World metrologic reference via third party international laboratories

This data sheet complies with the EN 60904 requirements.
 The product is certified according to the requirements of the EN 60904 standard.

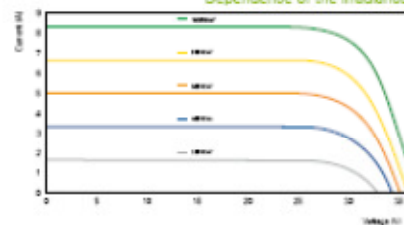


Dimensions in mm (in)

Dependence of the temperature



Dependence of the irradiance



Contact:

Use BP Solar website

Find more information on: www.bpsolar.com

12 10270-01/10 BP Solar 2010

LC120-12P

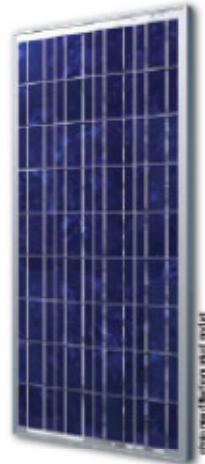
High-efficiency PV Module

Features

- high energy yields ensured by high conversion efficiency
- sturdy, clear-anodized aluminum frame with pre-drilled holes for quick installation
- advanced EVA encapsulation with triple-layer backsheet, meets the most stringent safety requirements for high-voltage operation
- pre-wired junction box equipped with connectors "plug'n'play"
- reliable bypass diodes to prevent overheating (hot spot effect) and to minimise power loss by shading
- manufactured in ISO 9001:2000-certified factory

Applications

- water pumping
- water purification systems
- remote village lighting
- solar home systems
- street and camp lights
- traffic signals
- medical facilities in remote areas
- microwave radio repeater stations
- battery charging
- etc.



Warranty

- Warranty: 2 years
- Performance guarantee:
up to 10 years (90% power output)
up to 20 years (80% power output)

Details according to warranty
issued by LORENTZ

Standards

LC120-12P is certified according to IEC 61215 and 61730 by TÜV Rheinland and meets the requirements for CE.



- Qualified, ISO 91016
- Safety tested, ISO 91730
- Periodic inspection

Specifications

Electrical Data

Peak power	P _{max}	[Wp]	120
Tolerance		[%]	+3/-3
Max. power current	I _{mp}	[A]	7.0
Max. power voltage	V _{mp}	[V]	17.1
Short circuit current	I _{sc}	[A]	7.7
Open circuit voltage	V _{oc}	[V]	21.8
Temperature co-efficient for P _{max}		[%/°C]	-0.50
Temperature co-efficient for V _{oc}		[%/°C]	-0.35
Temperature co-efficient for I _{sc}		[%/°C]	0.09
Max. system voltage		[V]	1,000

All technical data at standard test condition:
AM = 1.5, E = 1,000W/m², cell temperature: 25 °C

Cells

Number of cells in series	36
Number of cells in parallel	1
Cell technology	polycrystalline
Cell shape	rectangular

To find out more visit www.lorentz.de

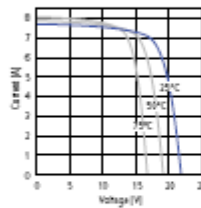
LORENTZ LORENTZ GmbH & Co. KG
Königsplatz 7, 24108 Hennebühl, Germany
Tel: +49 (0) 4102 7140-0, Fax: -20, www.lorentz.de
Errors assigned and possible alterations with out prior notice.

Sun. Water. Life.

Electrical Performance

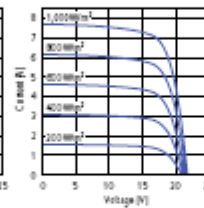
Electrical Performance

for different temperatures, at $\text{Irr} = 1 \text{ kW/m}^2$, $G = 1,000 \text{ Wh/m}^2$



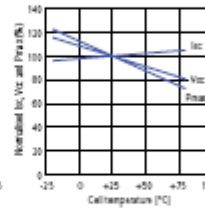
Electrical Performance

for different irradiances, at 25 °C



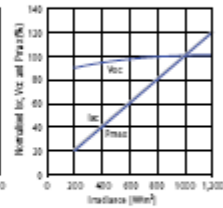
Temperature Dependence

of I_{sc} , V_{oc} and P_{max}

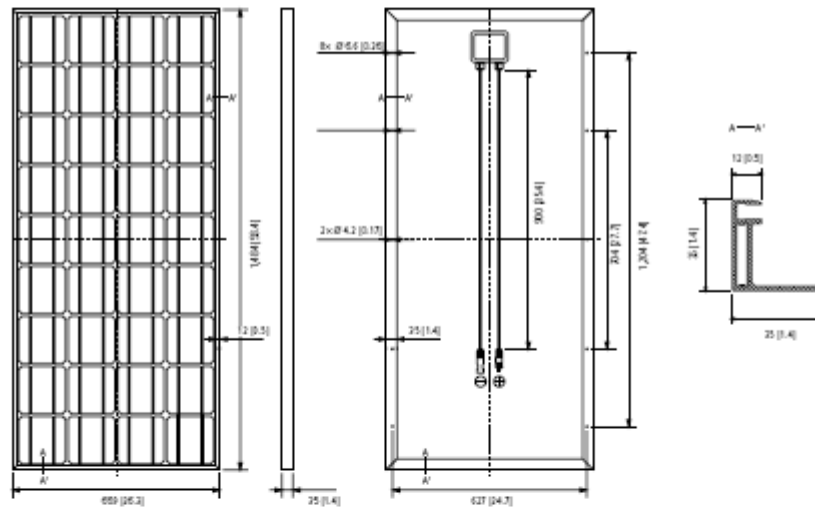


Irradiation Dependence

of I_{sc} , V_{oc} and P_{max} at 25 °C



Physical Specifications mm [in]



Weight	[kg]	13.5
Dimension	[mm]	660 x 1,484 x 35
Strength	[N/m²]	2,400
Cable		approx. 900mm / 35 in, 4mm² / AWG12
Connectors		NBZH PV-ZH02 or compatible

To find out more visit www.lorentz.de

LORENTZ GmbH & Co. KG
Königsplatz 7, 24150 Harsdorf-Uthung, Germany
Tel: +49 (0) 4102 77540-0, Fax: -20, www.lorentz.de
Errors excepted and possible alterations without prior notice.

Sun. Water. Life.

Kaneka

KANEKA HYBRID PV

Thin-film silicon hybrid solar panel

U-EA type

U-EA100/105/110/115/120



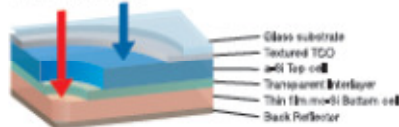
Decades of research and development have created HYBRID — the Next Generation innovation from Kaneka.

Kaneka's HYBRID solar panel has a tandem structure that absorbs both the blue and red ends of the light spectrum allowing it to convert even more of the sun's light into energy. This latest HYBRID innovation can deliver high power generation, kWh/kWp, and is environmentally friendly.

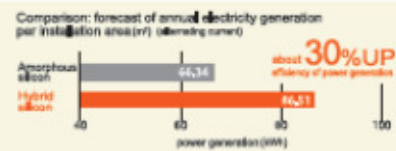
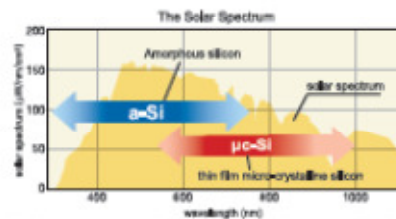
Kaneka's HYBRID technology combines the features of both amorphous silicon and micro-crystalline silicon to create higher energy production.

The words "solar panel" are often associated with crystalline solar panels, but Kaneka's HYBRID solar module offers some unique features over traditional crystalline. Its dual-layer structure of microcrystalline and amorphous silicon can capture both short and long wavelengths of the light spectrum, allowing the HYBRID to convert even more sunlight into electricity. This enhances the efficiency of power generation, and produces up to 30% higher power output than conventional thin-film amorphous silicon panels. The HYBRID delivers greater performance capabilities and offers a lower open circuit voltage for enhanced design flexibility. Kaneka's HYBRID panel is the future of solar power.

HYBRID absorbs both ultraviolet (short) rays and infrared (long) rays.



The Hybrid PV module comes with a 25 year warranty on power output.

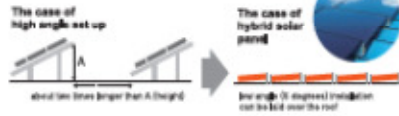


*Efficiency: At a case of (low angle (3 degrees) installation, due north). Based on Japanese power generation forecast.

U-EA type

HYBRID panels are ideal for low angle installations.

Because of HYBRID's cell structure, low angle (5 degree) roof installations are possible without a significant loss of power generation by shadow. Panels can be installed close together, allowing for more roof coverage and higher power output.



The HYBRID cell structure is shadow tolerant.

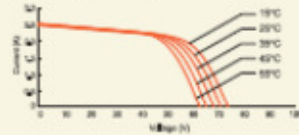
The HYBRID panel measures 1,210x1,008 mm. Unlike traditional crystalline panels, the HYBRID cells allow it to perform even if part of the panel is shaded.

The cell configuration allows it to prevent power output deterioration under shadow dropped conditions like picture below.

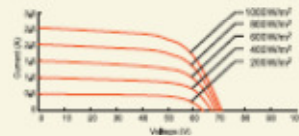


Electrical characteristics U-EA110 type

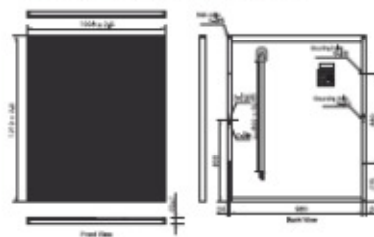
Current/Voltage characteristics at various cell temperature



Current/Voltage characteristics at various irradiance levels



U-EA100/U-EA106/U-EA110/U-EA116/U-EA120



Your local Kaneka dealer:
SunFields Europe

C/Lope Gómez de Marzoa, Edificio FEUGA, Oficina 12
15705 Santiago De Compostela (A Coruña)
Tel: +34 981 59 58 56 Email: contacto@sfe-solar.com

kaneka

<http://www.pv.kaneka.co.jp>

KANAKA BELGIUM N.V. GERMAN BRANCH
Othowen/Gütersloffen 13 D-48305 Wittenberg Germany
Phone: +494122460744 Fax: +494122460740

KANAKA TEXAS CORPORATION
8181, Unimex Road, Pasadena, Texas 77507, U.S.A.
Phone: +1-281-424-4800 Fax: +1-281-409-2223

KANAKA CORPORATION
3-4-1, Nakasendai, Kibaku, Osaka 536-0388, Japan
Phone: 81-6-6229-0515 Fax: 81-6-6229-0144

Products	U-EA100	U-EA106	U-EA110	U-EA116	U-EA120
Electrical Data (Standard Test Condition) ¹⁾	Maximum Power (P _{max}) [W]	160	166	174	176
	Efficiency	47.5%/10%	47.5%/10%	47.5%/10%	47.5%/10%
	Minimum value of P _{max} [W]	15.9	16.70	17.62	17.63
	Open circuit voltage (V _{oc}) [V]	71	71	71	71
	Short circuit current (I _{sc}) [A]	3.25	3.40	3.59	3.60
	Voltage at Power (V _{mp}) [V]	55.2	55.2	55.2	55.2
	Current at Power (I _{mp}) [A]	2.97	3.04	3.19	3.19
	Module Efficiency (%)	16.2	16.2	16.2	16.2
	Efficiency reduction at 2000h ²⁾	+0%	+0%	+0%	+0%
	Temperature (25°C/1)	45	45	45	45
Data at normal operating cell temperature (NOCT) ³⁾	Maximum Power (P _{max}) [W]	15.4	16.1	17.0	17.0
	Open circuit voltage (V _{oc}) [V]	49.2	49.2	49.2	49.2
	Short circuit current (I _{sc}) [A]	2.60	2.64	2.79	2.79
	Voltage at Power (V _{mp}) [V]	49.2	49.2	49.2	49.2
	Current at Power (I _{mp}) [A]	1.29	1.34	1.40	1.40
	Power (W)	4.20			
Temperature coefficients	Open circuit voltage (V _{oc}) [W]	-0.26			
	Short circuit current (I _{sc}) [W]	0.003			
	Power (W)	-0.20			
Mechanical characteristics Data	Cell Type	Thin film technology: Bi-Telluride thin crystalline Si			
	No. of cells	106 (10 in series) 2 in parallel			
	Dimension [mm]	911.214 × 1,108 × 34			
	Weight [kg]	15.0			
	Junction box (Dimension) [mm]	904 × 136 × 74.5			
	Output cable	2-core 2-core PV cable with MC4 Connect Plug and XT 3.0 connectors			
	Front panel	Low iron glass with silver Backsheet			
Life and Others	Frame material	anodized Alumin			
	Maximum system voltage [V]	600			
	Limiting reverse current [A]	0.5			
	Operating module temperature [°C]	-45~+60°C (module temperature)			
	Maximum load [W]	2,400			
	Application certification (IEC 61746-4)	A			
	Fire certification (IEC 61746-6)	Class C			
	Safety certification (IEC 61746-5)	B			

¹⁾ Standard 1000 W/m² spectrum Air Mass 1.5 and cell temperature 25°C

²⁾ Standard 800 W/m² and spectral test at cell temperature 25°C

IEC 61646/EN 1736 Safety Class II CE

Certification: IEC 61646-1, IEC 61746-1, Manufactured in ISO 9001 certified factories.



Shell Solar

Product Information Sheet

Shell ST36 Photovoltaic Solar Module

General

The Shell ST36 module is composed of a monolithic structure of series connected Copper Indium Diselenide (CIS) based solar cells.

The Shell ST36 can generate a peak power of 36 watts at 15.8 volts.

The Shell ST36 solar module has been designed for rural and industrial applications.

Qualifications and Certificates

The Shell ST36 solar module meets the following requirements:

- UL – Listing 1703

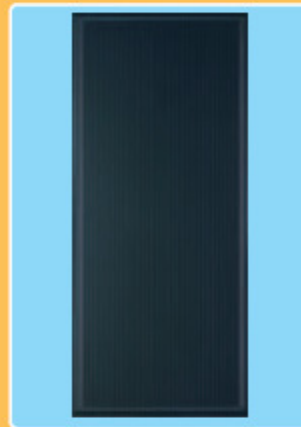


All Shell Solar modules are produced in B4 ISO 9001 certified factories.

Limited Warranties

- Peak Power for 10 years

Shell ST36 Module



Junction Box

The junction box provides a high quality, dust protected and splash proof IP44-rated housing. The housing contains a rigid connection block with screw terminals and by-pass diodes providing "hot spot" protection for the solar cells.

ProCharger™ – S Junction Box

Maximum conductor cross-section: 4 mm²
Type of protection: IP44



Benefits

- Exceptional performance under low light conditions, shade and high temperature tolerance that offers reliable power in adverse or changeable conditions.
- Class leading efficiency and stable output power delivering reliable high performance for many years.
- Highly transparent tempered glass delivering more power and ensuring high impact resistance and protection against hail, snow, ice, and storms.
- Uniform appearance ideal for applications where aesthetics are an important factor.
- 10 years research and over 3 years commercial manufacturing experience has been applied to the development of our CIS thin-film range to ensure that our products have a long and reliable service life backed by a 10 year warranty.



ELECTRICAL EQUIPMENT,
CHECK WITH YOUR INSTALLER

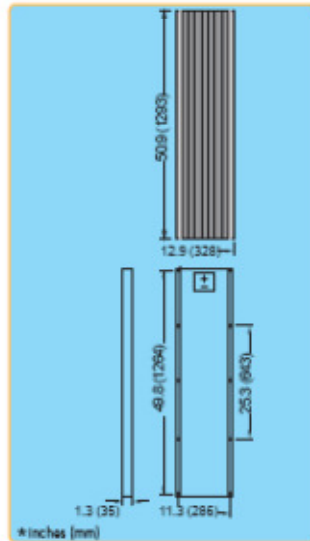
Due to continuous research and product improvement the specifications in this Product Information Sheet are subject to change without notice. Specifications can vary slightly. For installation and operation instructions, see the applicable manuals. No rights can be derived from this Product Information Sheet and Shell Solar assumes no liability whatsoever connected to or resulting from the use of any information contained herein.



Shell ST36 Photovoltaic Solar Module

Mechanical Specifications Module

A tension and corrosion-resistant anodized aluminum frame ensures dependable performance, even under harsh weather conditions. Pre-drilled mounting holes are provided for ease of installation.



Outside dimensions (in)	50.9 x 12.9
Thickness (inc. junction box) (in)	1.3
Thickness (exc. junction box) (in)	1.3
Weight (lb)	15.4

For installation instructions, please refer to the **Installation Manual** which is available from Shell Solar.

Electrical Characteristics

Data at Standard Test Conditions (STC)

STC: irradiance level 1000W/m², spectrum AM 1.5 and cell temperature 25°C

Rated power	P_r	36W
Peak power	P_{mpp}	36W
Peak power voltage	V_{mpp}	15.8V
Peak power current	I_{mpp}	2.28A
Open circuit voltage	V_{oc}	22.9V
Short circuit current	I_{sc}	2.68A
Series fuse rating		5A
Minimum peak power	$P_{mpp \text{ min}}$	32.4W

The abbreviation 'mpp' stands for Maximum Power Point.

Typical data at Nominal Operating Cell Temperature (NOCT) conditions

NOCT: 800W/m² irradiance level, AM 1.5 spectrum, wind velocity 1m/s, T_{amb} 20°C

Temperature	T_{NOCT}	47°C
Mpp power	P_{mpp}	24.6W
Mpp voltage	V_{mpp}	13.8V
Open circuit voltage	V_{oc}	20.2V
Short circuit current	I_{sc}	2.2A

Typical data at low irradiance

The relative reduction of module efficiency at an irradiance of 200W/m² in relation to 1000W/m² both at 25°C cell temperature and AM 1.5 spectrum is 5%.

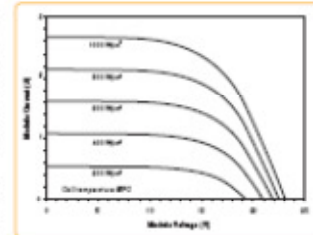
Temperature coefficients

αP_{mpp}	-0.6 %/°C
αV_{mpp}	-100 mV/°C
αI_{sc}	+0.32 mA/°C
αV_{oc}	-100 mV/°C

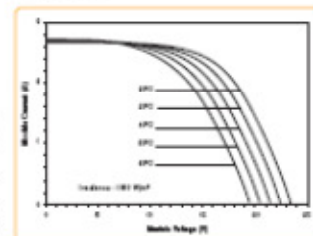
Maximum system voltage: 600 Vdc

Typical I/V Characteristics

The I/V graph below shows the typical performance of the solar module at various levels of irradiance.



The I/V graph below shows the typical performance of the solar module at various cell temperatures.



References in this Product Information Sheet to "Shell Solar" are to companies and other organizational entities within the Royal Dutch/Shell Group of Companies that are engaged in the photovoltaic solar energy business. Shell Solar was set up in 1999 and has its principal office in Amsterdam, the Netherlands.

For further information on all Shell Solar products contact:

Shell Solar
4650 Adèle Lane, Camarillo CA 93012
805-482-6800 Fax 805-388-6511
Web: www.shell.com/renewables

v2/st36/05/02/us



APPENDIX-B: DATA EXTRACT FROM PV PANEL DATASHEETS

Table B.1: Electrical data of selected PV panels at STC.

	Mono crystalline (mc-Si)		Poly crystalline (pc-Si)		Thin film	
	Sunpower 230W	SunForte PM318B00	Lorentz1 20W	PB solar	Kaneka U- EA110W (a-Si)	Shell ST36 (CIS)
Open circuit Voltage (V_{OC})	48.7V	64.7V	21.8V	36.7V	71V	22.9V
Short circuit current (I_{SC})	5.99A	6.2A	7.7A	8.4A	2.5A	2.68A
Maximum power Voltage (V_{MP})	41V	54.7V	17.1V	29.1V	54V	15.8V
Maximum power current (I_{MP})	5.61A	5.82A	7A	7.9A	2.04A	2.28A
Maximum Power (P_{MP})	230W	318W	70W	230W	110	36W
Number of Cells in series (NS)	72	96	60	60	106	42
ISC temperature coefficient (μ_{ISC})	3.5 mA/C	3.72 mA/°C	6.93 mA/°C	5.46 mA/°C	1.375 mA/°C	.32 mA/°C
Voc temperature coefficient (μ_{VOC})	-132.5 mV/°C	-174 mV/°C	-76 mV/°C	-132 mV/°C	-276.9 mV/°C	-100 mV/°C

Table B.2: Extracted I-V points for Sunpower 230W (mc-Si) PV panel

Condition		Key Point				
		SC	X	MPP	XX	OC
1000 W/m ² , 25°C	V (V)	0	20.4846	41	44.8678	48.7
	I (A)	5.99	5.96834	5.61	4.32705	0
800 W/m ² , 25°C	V (V)	0.00	20.2444	40.4888	44.3857	48.2827
	I (A)	4.78947	4.7753	4.47773	3.302	0
500 W/m ² , 25°C	V (V)	0	19.254	38.5073	42.767	47.0277
	I (A)	2.98988	2.9721	2.84818	2.19673	0
250 W/m ² , 25°C	V (V)	0	18.9234	37.8468	41.513	45.1783
	I (A)	1.20445	1.19028	1.11943	0.918542	0
1000 W/m ² , 50°C	V (V)	0	18.56	37.1202	40.9511	44.782
	I (A)	6.06478	6.05061	5.583	4.43972	0

Table B.3: Extracted I-V points for SunForte PM318B00 (mc-Si) PV panel

Condition		Key Point				
		SC	X	MPP	XX	OC
1000 W/m ² , 25C	V (V)	0	27.35	54.7	59.7	64.7
	I (A)	6.2	6.20014	5.82	4.2935	0
800 W/m ² , 25C	V (V)	0	27.007	54.0131	59.1518	64.2904
	I (A)	4.98221	4.95443	4.66513	3.45877	0
500 W/m ² , 25C	V (V)	0	26.21	52.4144	57.553	62.6917
	I (A)	3.15125	3.13593	2.90833	2.3123	0
200 W/m ² , 25C	V (V)	0	26.26	52.5285	56.468	60.4078
	I (A)	1.19573	1.19286	1.15215	0.97915	0
1000 W/m ² , 50C	V (V)	0	24.89	49.7879	54.755	59.7227
	I (A)	6.26512	6.24907	5.85936	4.31662	0

Table B.4: Extracted I-V points for BP Solar 3230N (pc-Si) PV panel

Condition		Key Point				
		SC	X	MPP	XX	OC
1000 W/m ² , 25C	V (V)	0	14.55	29.1	32.9	36.7
	I (A)	8.4	8.38	7.9	6.003	0
800 W/m ² , 25C	V (V)	0	14.5478	29.0955	32.5478	36
	I (A)	6.674	6.656	6.173	4.3658	0
600 W/m ² , 25C	V (V)	0	14.2276	28.4553	31.87	35.3
	I (A)	5.001	4.99	4.68787	3.56	0
400 W/m ² , 25C	V (V)	0	14.05	28.1352	31.223	34.3242
	I (A)	3.363	3.346	3.14911	2.2903	0
200 W/m ² , 25C	V (V)	0	13.7297	27.4593	30.18	32.9014
	I (A)	1.664	1.6461	1.52087	1.09	0
1000 W/m ² , 50C	V (V)	0	13.4122	26.8245	30.1529	33.4813
	I (A)	8.59	8.57415	7.77736	5.37099	0
1000 W/m ² , 75C	V (V)	0	11.5878	23.1262	26.3314	29.5365
	I (A)	8.74187	8.70351	7.99268	5.91164	0

Table B.5: Extracted I-V points for Lorentz120W LC120-12P (pc-Si) PV panel

Condition		Key Point				
		SC	X	MPP	XX	OC
1000 W/m ² , 25C	V (V)	0	8.55	17.1	19.45	21.8
	I (A)	7.7	7.60274	7	5.39726	0
800 W/m ² , 25C	V (V)	0	8.657	17.3139	19.417	21.521
	I (A)	6.14017	6.05479	5.47009	4.17808	0
600 W/m ² , 25C	V (V)	0	8.576	17.1521	19.175	21.1974
	I (A)	4.62222	4.53425	4.07521	3.0274	0
400 W/m ² , 25C	V (V)	0	8.087	16.0743	18.487	20.7997
	I (A)	3.07692	3.0274	2.78082	2.28767	0
200 W/m ² , 25C	V (V)	0	7.65	15.3069	17.99	20.6855
	I (A)	1.5453	1.50685	1.36986	1.16438	0
1000 W/m ² , 50C	V (V)	0	7.694	15.3888	17.333	19.2765
	I (A)	7.87156	7.76256	6.95837	5.13242	0
1000 W/m ² , 75C	V (V)	0	6.803	13.6069	15.227	16.8467
	I (A)	8.05505	7.90868	7.0108	5.16895	0

Table B.6: Extracted I-V points for Shell ST36 (CIS) PV panel

Condition		Key Point				
		SC	X	MPP	XX	OC
1000 W/m ² , 25C	V (V)	0	7.9	15.8V	19.35	22.9V
	I (A)	2.68A	2.6562	2.28A	1.45526	0
800 W/m ² , 25C	V (V)	0	7.9213	15.8426	19.0977	22.3528
	I (A)	2.14683	2.12873	1.8307	1.23391	0
600 W/m ² , 25C	V (V)	0	7.9412	15.8824	18.8166	21.7509
	I (A)	1.60894	1.59655	1.34472	0.913658	0
400 W/m ² , 25C	V (V)	0	7.7156	15.4312	18.085	20.7386
	I (A)	1.07577	1.05965	0.905915	0.654631	0
200 W/m ² , 25C	V (V)	0	6.943	13.8858	16.4914	19.097
	I (A)	0.542606	0.527473	0.471831	0.348509	0
1000 W/m ² , 20C	V (V)	0	8.3	16.6126	20.008	23.4037
	I (A)	2.67555	2.6562	2.28214	1.40345	0
1000 W/m ² , 30C	V (V)	0	7.67	15.3409	18.88	22.4297
	I (A)	2.68025	2.6562	2.30119	1.43642	0
1000 W/m ² , 40C	V (V)	0	7.373	14.7457	18.114	21.4827
	I (A)	2.68495	2.66562	2.22136	1.37049	0
1000 W/m ² , 50C	V (V)	0	6.872	13.7446	17.113	20.4816
	I (A)	2.68966	2.67504	2.20274	1.35636	0
1000 W/m ² , 60C	V (V)	0	6.37	12.7435	16.125	19.5076
	I (A)	2.69436	2.66562	2.18412	1.33752	0

Table B.7: Extracted I-V points for Kaneka U-EA110W (a-Si) PV panel

Condition		Key Point				
		SC	X	MPP	XX	OC
1000 W/m ² , 25C	V (V)	0	27	54	62.5	71
	I (A)	2.5	2.4065	2.04	1.33333	0
800 W/m ² , 25C	V (V)	0	27.176	54.3533	63.2	70.0462
	I (A)	2	1.9187	1.62602	0.96748	0
600 W/m ² , 25C	V (V)	0	26.76	53.5219	61.108	68.6952
	I (A)	1.50407	1.43089	1.22764	0.878049	0
400 W/m ² , 25C	V (V)	0	26.917	53.8337	60.38	66.9284
	I (A)	1	0.95935	0.813008	0.601626	0
200 W/m ² , 25C	V (V)	0	26.03	52.067	57.835	63.6028
	I (A)	0.495935	0.487805	0.422764	0.292683	0
1000 W/m ² , 15C	V (V)	0	27.904	55.8083	64.694	73.5797
	I (A)	2.49457	2.3259	2.07065	1.45694	0
1000 W/m ² , 35C	V (V)	0	25.98	51.963	60.07	68.1755
	I (A)	2.51087	2.35018	2.05905	1.36685	0
1000 W/m ² , 45C	V (V)	0	24	48.0139	56.743	65.4734
	I (A)	2.52717	2.37446	2.12391	1.44807	0
1000 W/m ² , 55C	V (V)	0	23.28	46.5589	54.665	62.7714
	I (A)	2.54348	2.39889	2.10748	1.39082	0

NOMENCLATURE AND SYMBOLS

$\mu_{I,sc}$	Temperature coefficient of short circuit current
$\mu_{V,OC}$	Temperature coefficient of open circuit voltage
a	Modified ideality factor
$a_{,ref}$	Modified ideality factor at STC condition
E_g	Band-gap energy
$E_{g,ref}$	Band-gap energy at STC condition
I_D	Diode current (A)
I_L	Light current (A)
$I_{L,ref}$	Light current at STC condition (A)
I_{mp}	Current at maximum power point (A)
$I_{mp,ref}$	Maximum power point current at STC condition (A)
I_o	Diode saturation current (A)
$I_{o,ref}$	Diode saturation current at STC condition (A)
I_{PV}	PV current (A)
I_{sc}	Short circuit current (A)
$I_{sc,ref}$	Short circuit current at STC condition (A)
I_{SH}	Current in shunt branch (A)
k	Boltzmann's constant (1.38e-23 J/K)
n	Ideality factor
N_{MAX}	Number of training data points
N_{pp}	Number of PV panel connected in parallel
N_S	Number of cells in PV panel

N_{ss}	Number of PV panel connected in series
P_{mp}	Power at maximum power point (W)
$P_{mp,ref}$	Power at maximum power point (W)
P_{pv}	Power of PV array (W)
q	Electronic charge (1.6021e-19 coulombs)
R_S	Series resistance (Ω)
$R_{s,ref}$	Series resistance at STC condition (Ω)
R_{SH}	Shunt resistance (Ω)
$R_{sh,ref}$	Shunt resistance at STC condition (Ω)
S_c	Operating irradiation (W/m^2)
S_{max}	Maximum range of irradiation for ANFIS MPPT controller (W/m^2)
S_{min}	Minimum range of irradiation for ANFIS MPPT controller (W/m^2)
S_{ref}	Reference irradiation (1000 W/m^2)
T_c	Operating temperature (degree C)
T_{max}	Maximum range of temperature for ANFIS MPPT controller (degree C)
T_{min}	Minimum range of temperature for ANFIS MPPT controller (degree C)
T_{ref}	Reference temperature (25 degree C)
V_{DC}	DC link voltage (V)
V_{mp}	Voltage at maximum power point (V)
$V_{mp,ref}$	Open circuit voltage at STC condition (V)
V_{oc}	Open circuit voltage (V)
$V_{oc,ref}$	Open circuit voltage at STC condition (V)
V_{PV}	PV Voltage (V)

ACRONYMS AND ABBREVIATIONS

<i>AIT</i>	Artificial Intelligence Techniques
<i>ANFIS</i>	Adaptive Neuro-Fuzzy Inference System
<i>ANN</i>	Artificial Neural Network
<i>a-Si</i>	amorphous silicon
<i>CdTe</i>	Cadmium Telluride
<i>CIGS</i>	Copper Indium Gallium Selenide
<i>CIS</i>	Copper Indium Selenide
<i>CP1104</i>	Connector Panel for DS1104
<i>DE</i>	Differential Evolution
<i>DG</i>	Distributed Generation
<i>DS1104</i>	dSPACE controller
<i>ECU</i>	Electronic Control Unit
<i>EPIA</i>	European Photovoltaic Industry Association
<i>FIS</i>	Fuzzy Inference System
<i>GA</i>	Genetic Algorithm
<i>GTAI</i>	Gigabit Transceiver Analogue Input
<i>GTAO</i>	Gigabit Transceiver Analogue Output
<i>HC</i>	Hill Climbing
<i>InCond</i>	Incremental Conductance
<i>LSE</i>	Least Square Error
<i>MAE</i>	Mean Absolute Error
<i>MBE</i>	Mean Bias Error

<i>mc-Si</i>	Mono- crystalline Silicone
<i>MPP</i>	Maximum Power Point
<i>MPPT</i>	Maximum Power Point Tracking
<i>N_{PP}</i>	Number of PV panel connected in parallel
<i>N_{SS}</i>	Number of PV panels connected in series
<i>OC</i>	Open Circuit
<i>P&O</i>	Perturb and Observe
<i>PCI</i>	Peripheral Component Interconnect
<i>pc-Si</i>	Poly-crystalline Silicone
<i>PSO</i>	Particle Swarm Optimization
<i>PV</i>	Photovoltaic
<i>RES</i>	Renewable Energy Sources
<i>RMSE</i>	Root Means Square Error
<i>RSCAD</i>	Software for RTDS
<i>RTDS</i>	Real Time Digital Simulator
<i>RTI</i>	Real Time Interface
<i>S</i>	Irradiation (W/m ²)
<i>SC</i>	Short Circuit
<i>SP</i>	Series Parallel
<i>STC</i>	Standard Test Condition
<i>T</i>	Temperature (degree C)
<i>TCT</i>	Total Cross Tied

REFERENCES

- [1] “International Energy Outlook, 2011,” *Energy Information Administration*, 2011. [Online]. Available: <http://www.eia.gov/forecasts/ieo/index.cfm>.
- [2] “U.S. energy-related CO₂ emissions in early 2012 lowest since 1992,” *Report*. [Online]. Available: <http://www.eia.gov/environment/emissions/carbon/>.
- [3] “Renewable Energy and Distributed Generation: International Case Studies on Technical and Economic Considerations,” *International Confederation of Energy Regulators 21 February 2012 Ref: I12-CC-17-03*. .
- [4] “Global Market Outlook For Photovoltaics Until 2016,” (*EPIA*) *Industry Association, European Photovoltaic*, 2012. [Online]. Available: http://www.epia.org/fileadmin/user_upload/Publications/Global-Market-Outlook-2016.pdf.
- [5] “Polar power.” [Online]. Available: <http://www.polarpowerinc.com/info/operation20/operation23.htm>. [Accessed: 10-Feb-2013].
- [6] J. V. Roger A. Messenger, *Photovoltaic Systems Engineering*, 2nd ed. 2003.
- [7] D. F. Menicucci and J. P. Fernandez, “User ’ s Manual for PVFORM: A Photovoltaic System Shulation Program For Stand-Alone and Grid-interactive Applications,” 1989.
- [8] Y. Hishikawa, Y. Imura, and T. Oshiro, “Irradiance-dependence and translation of the I-V characteristics of crystalline silicon solar cells,” in *Conference Record of the Twenty-Eighth IEEE Photovoltaic Specialists Conference - 2000 (Cat. No.00CH37036)*, 2000, pp. 1464–1467.
- [9] B. Marion, S. Rummel, and A. Anderberg, “Current-voltage curve translation by bilinear interpolation,” *Progress in Photovoltaics: Research and Applications*, vol. 12, no. 8, pp. 593–607, Dec. 2004.
- [10] D. King, J. Kratochvil, and W. Boyson, *Photovoltaic array performance model*. 2004.
- [11] Sandia National Laboratories, “Database of Photovoltaic Module Performance Parameters,” 2002. .

- [12] T. U. Townsend, "A method for estimating the long-term performance of directly-coupled photovoltaic systems," University of Wisconsin, Madison, 1989.
- [13] N. D. Benavides and P. L. Chapman, "Modeling the Effect of Voltage Ripple on the Power Output of Photovoltaic Modules," *IEEE Transactions on Industrial Electronics*, vol. 55, no. 7, pp. 2638–2643, Jul. 2008.
- [14] Y. T. Tan, D. S. Kirschen, and N. Jenkins, "A Model of PV Generation Suitable for Stability Analysis," *IEEE Transactions on Energy Conversion*, vol. 19, no. 4, pp. 748–755, Dec. 2004.
- [15] M. C. Glass, "Improved solar array power point model with SPICE realization," in *IECEC 96. Proceedings of the 31st Intersociety Energy Conversion Engineering Conference*, 1996, vol. 1, pp. 286–291.
- [16] Y. Kuo, T. Liang, and J. Chen, "Novel maximum-power-point-tracking controller for photovoltaic energy conversion system," *IEEE Transactions on Industrial Electronics*, vol. 48, no. 3, pp. 594–601, Jun. 2001.
- [17] W. G. Dunford and A. Capel, "A novel modeling method for photovoltaic cells," in *2004 IEEE 35th Annual Power Electronics Specialists Conference (IEEE Cat. No.04CH37551)*, 2004, pp. 1950–1956.
- [18] A. N. Celik and N. Acikgoz, "Modelling and experimental verification of the operating current of mono-crystalline photovoltaic modules using four- and five-parameter models," *Applied Energy*, vol. 84, no. 1, pp. 1–15, Jan. 2007.
- [19] F. González-Longatt, "Model of photovoltaic module in matlab," in *II CIBELEC*, 2005, pp. 1–5.
- [20] R. Chenni, M. Makhoulouf, T. Kerbache, and a. Bouzid, "A detailed modeling method for photovoltaic cells," *Energy*, vol. 32, no. 9, pp. 1724–1730, Sep. 2007.
- [21] K. Ishaque, Z. Salam, and H. Taheri, "Modeling and simulation of photovoltaic (PV) system during partial shading based on a two-diode model," *Simulation Modelling Practice and Theory*, vol. 19, no. 7, pp. 1613–1626, Aug. 2011.
- [22] W. De Soto, S. a. Klein, and W. a. Beckman, "Improvement and validation of a model for photovoltaic array performance," *Solar Energy*, vol. 80, no. 1, pp. 78–88, Jan. 2006.

- [23] C. Carrero, J. Amador, and S. Arnaltes, "A single procedure for helping PV designers to select silicon PV modules and evaluate the loss resistances," *Renewable Energy*, vol. 32, no. 15, pp. 2579–2589, Dec. 2007.
- [24] R. A. Dougal, "Dynamic multiphysics model for solar array," *IEEE Transactions on Energy Conversion*, vol. 17, no. 2, pp. 285–294, Jun. 2002.
- [25] M. G. Villalva, J. R. Gazoli, and E. R. Filho, "Comprehensive Approach to Modeling and Simulation of Photovoltaic Arrays," *IEEE Transactions on Power Electronics*, vol. 24, no. 5, pp. 1198–1208, May 2009.
- [26] J. a. Gow and C. D. Manning, "Development of a photovoltaic array model for use in power-electronics simulation studies," *IEE Proceedings - Electric Power Applications*, vol. 146, no. 2, p. 193, 1999.
- [27] N. Pongratananukul and T. Kaspafis, "Tool for automated simulation of solar arrays using general-purpose simulators," in *IEEE Workshop on Computers in Power Electronics, 2004. Proceedings.*, 2004, vol. 00, pp. 10–14.
- [28] S. Chowdhury, G. a. Taylor, S. P. Chowdhury, a. K. Saha, and Y. H. Song, "Modelling, simulation and performance analysis of a PV array in an embedded environment," in *2007 42nd International Universities Power Engineering Conference*, 2007, no. 1, pp. 781–785.
- [29] W. Herrmann, W. Wiesner, and W. Vaassen, "Hot spot investigations on PV modules-new concepts for a test standard and consequences for module design with respect to bypass diodes," in *Conference Record of the Twenty Sixth IEEE Photovoltaic Specialists Conference - 1997*, 1997, pp. 1129–1132.
- [30] H. Kawamura, K. Naka, N. Yonekura, S. Yamanaka, H. Kawamura, H. Ohno, and K. Naito, "Simulation of I–V characteristics of a PV module with shaded PV cells," *Solar Energy Materials and Solar Cells*, vol. 75, no. 3–4, pp. 613–621, Feb. 2003.
- [31] H. Patel and V. Agarwal, "MATLAB-Based Modeling to Study the Effects of Partial Shading on PV Array Characteristics," *IEEE Transactions on Energy Conversion*, vol. 23, no. 1, pp. 302–310, Mar. 2008.
- [32] H. Patel and V. Agarwal, "Maximum Power Point Tracking Scheme for PV Systems Operating Under Partially Shaded Conditions," *IEEE Transactions on Industrial Electronics*, vol. 55, no. 4, pp. 1689–1698, Apr. 2008.

- [33] M. Zagrouba, A. Sellami, M. Bouaïcha, and M. Ksouri, "Identification of PV solar cells and modules parameters using the genetic algorithms: Application to maximum power extraction," *Solar Energy*, vol. 84, no. 5, pp. 860–866, May 2010.
- [34] J. P. Charles, M. Abdelkrim, Y. H. Muoy, and P. Mialhe, "A practical method of analysis of the current-voltage characteristics of solar cells," *Solar Cells*, vol. 4, no. 2, pp. 169–178, Sep. 1981.
- [35] T. Ikegami, T. Maezono, F. Nakanishi, Y. Yamagata, and K. Ebihara, "Estimation of equivalent circuit parameters of PV module and its application to optimal operation of PV system," *Solar Energy Materials and Solar Cells*, vol. 67, no. 1–4, pp. 389–395, Mar. 2001.
- [36] J. a Jervase, H. Bourdouden, and A. Al-Lawati, "Solar cell parameter extraction using genetic algorithms," *Measurement Science and Technology*, vol. 12, no. 11, pp. 1922–1925, Nov. 2001.
- [37] W. Kim and W. Choi, "A novel parameter extraction method for the one-diode solar cell model," *Solar Energy*, vol. 84, no. 6, pp. 1008–1019, Jun. 2010.
- [38] M. G. Villalva, J. R. Gazoli, and E. R. Filho, "Modeling and circuit-based simulation of photovoltaic arrays," in *2009 Brazilian Power Electronics Conference*, 2009, pp. 1244–1254.
- [39] G. Walker, "Evaluating MPPT converter topologies using a Matlab PV model," *Journal of Electrical & Electronics Engineering, Australia*, vol. 21, no. 1, pp. 49–55, 2001.
- [40] A. Chatterjee, A. Keyhani, and D. Kapoor, "Identification of Photovoltaic Source Models," *IEEE Transactions on Energy Conversion*, vol. 26, no. 3, pp. 883–889, Sep. 2011.
- [41] M. T. Boyd, S. a. Klein, D. T. Reindl, and B. P. Dougherty, "Evaluation and Validation of Equivalent Circuit Photovoltaic Solar Cell Performance Models," *Journal of Solar Energy Engineering*, vol. 133, no. 2, p. 021005, 2011.
- [42] K. Ishaque and Z. Salam, "An improved modeling method to determine the model parameters of photovoltaic (PV) modules using differential evolution (DE)," *Solar Energy*, vol. 85, no. 9, pp. 2349–2359, Sep. 2011.
- [43] C. Carrero, D. Ramírez, J. Rodríguez, and C. a. Platero, "Accurate and fast convergence method for parameter estimation of PV generators based on three

main points of the I–V curve,” *Renewable Energy*, vol. 36, no. 11, pp. 2972–2977, Nov. 2011.

- [44] M. T. Elhagry, A. A. T. Elkousy, M. B. Saleh, T. F. Elshatter, and E. M. Abou-Elzahab, “Fuzzy modeling of photovoltaic panel equivalent circuit,” in *Proceedings of 40th Midwest Symposium on Circuits and Systems. Dedicated to the Memory of Professor Mac Van Valkenburg*, 2000, vol. 1, pp. 60–63.
- [45] F. Almonacid, C. Rus, L. Hontoria, M. Fuentes, and G. Nofuentes, “Characterisation of Si-crystalline PV modules by artificial neural networks,” *Renewable Energy*, vol. 34, no. 4, pp. 941–949, Apr. 2009.
- [46] Syafaruddin, E. Karatepe, and T. Hiyama, “Development of real-time simulation based on intelligent techniques for maximum power point controller of photovoltaic system,” *International Journal of Innovative Computing, Information and Control*, vol. 6, no. 4, p. 4198, 2010.
- [47] N. Moldovan, R. Picos, and E. Garcia-Moreno, “Parameter Extraction of a Solar Cell Compact Model using Genetic Algorithms,” in *2009 Spanish Conference on Electron Devices*, 2009, pp. 379–382.
- [48] M. Ye, X. Wang, and Y. Xu, “Parameter extraction of solar cells using particle swarm optimization,” *Journal of Applied Physics*, vol. 105, no. 9, p. 094502, 2009.
- [49] T. Esmar and P. L. Chapman, “Comparison of Photovoltaic Array Maximum Power Point Tracking Techniques,” *IEEE Transactions on Energy Conversion*, vol. 22, no. 2, pp. 439–449, Jun. 2007.
- [50] K. Ishaque and Z. Salam, “A review of maximum power point tracking techniques of PV system for uniform insolation and partial shading condition,” *Renewable and Sustainable Energy Reviews*, vol. 19, pp. 475–488, Mar. 2013.
- [51] A. Reza Reisi, M. Hassan Moradi, and S. Jamasb, “Classification and comparison of maximum power point tracking techniques for photovoltaic system: A review,” *Renewable and Sustainable Energy Reviews*, vol. 19, pp. 433–443, Mar. 2013.
- [52] B. Subudhi and R. Pradhan, “A Comparative Study on Maximum Power Point Tracking Techniques for Photovoltaic Power Systems,” *IEEE Transactions on Sustainable Energy*, vol. 4, no. 1, pp. 89–98, Jan. 2013.
- [53] C. Hua and J. Lin, “Fully digital control of distributed photovoltaic power systems,” in *ISIE 2001. 2001 IEEE International Symposium on Industrial Electronics Proceedings (Cat. No.01TH8570)*, 2001, vol. 1, pp. 1–6.

- [54] N. Kasa, T. Iida, and H. Iwamoto, "Maximum power point tracking with capacitor identifier for photovoltaic power system," *IEE Proceedings - Electric Power Applications*, vol. 147, no. 6, p. 497, 2000.
- [55] E. Koutroulis, K. Kalaitzakis, and N. C. Voulgaris, "Development of a microcontroller-based, photovoltaic maximum power point tracking control system," *IEEE Transactions on Power Electronics*, vol. 16, no. 1, pp. 46–54, 2001.
- [56] N. Femia, D. Granozio, G. Petrone, G. Spagnuolo, and M. Vitelli, "Predictive & Adaptive MPPT Perturb and Observe Method," *IEEE Transactions on Aerospace and Electronic Systems*, vol. 43, no. 3, pp. 934–950, Jul. 2007.
- [57] A. K. Abdelsalam, A. M. Massoud, S. Ahmed, and P. N. Enjeti, "High-Performance Adaptive Perturb and Observe MPPT Technique for Photovoltaic-Based Microgrids," *IEEE Transactions on Power Electronics*, vol. 26, no. 4, pp. 1010–1021, Apr. 2011.
- [58] N. Femia, G. Petrone, G. Spagnuolo, and M. Vitelli, "Optimization of Perturb and Observe Maximum Power Point Tracking Method," *IEEE Transactions on Power Electronics*, vol. 20, no. 4, pp. 963–973, Jul. 2005.
- [59] D. Sera, T. Kerekes, R. Teodorescu, and F. Blaabjerg, "Improved MPPT method for rapidly changing environmental conditions," in *2006 IEEE International Symposium on Industrial Electronics*, 2006, pp. 1420–1425.
- [60] D. Sera, T. Kerekes, R. Teodorescu, and F. Blaabjerg, "Improved MPPT Algorithms for Rapidly Changing Environmental Conditions," in *2006 12th International Power Electronics and Motion Control Conference*, 2006, pp. 1614–1619.
- [61] D. Sera, R. Teodorescu, J. Hantchel, and M. Knoll, "Optimized Maximum Power Point Tracker for Fast-Changing Environmental Conditions," *IEEE Transactions on Industrial Electronics*, vol. 55, no. 7, pp. 2629–2637, Jul. 2008.
- [62] K. Ishaque, Z. Salam, M. Amjad, and S. Mekhilef, "An Improved Particle Swarm Optimization (PSO)-Based MPPT for PV With Reduced Steady-State Oscillation," *IEEE Transactions on Power Electronics*, vol. 27, no. 8, pp. 3627–3638, Aug. 2012.
- [63] D. Peftitsis, G. Adamidis, A. Balouktsis, I. I. M. Athematical, and M. O. O. F. P. Hotovoltaic, "A New MPPT Method for Photovoltaic Generation Systems Based on Hill Climbing Algorithm," in *International Conference on Electrical Machines Paper*, 2008, no. 3, pp. 1–5.

- [64] W. G. Dunford, "A modified adaptive hill climbing MPPT method for photovoltaic power systems," in *2004 IEEE 35th Annual Power Electronics Specialists Conference (IEEE Cat. No.04CH37551)*, 2004, pp. 1957–1963.
- [65] K. H. Hussein, "Maximum photovoltaic power tracking: an algorithm for rapidly changing atmospheric conditions," *IEE Proceedings - Generation, Transmission and Distribution*, vol. 142, no. 1, p. 59, 1995.
- [66] D. P. Hohm and M. E. Ropp, "Comparative study of maximum power point tracking algorithms," *Progress in Photovoltaics: Research and Applications*, vol. 11, no. 1, pp. 47–62, Jan. 2003.
- [67] S. Qin, M. Wang, T. Chen, and X. Yao, "Comparative analysis of incremental conductance and perturb-and-observation methods to implement MPPT in photovoltaic system," in *2011 International Conference on Electrical and Control Engineering*, 2011, pp. 5792–5795.
- [68] A. Safari and S. Mekhilef, "Simulation and Hardware Implementation of Incremental Conductance MPPT With Direct Control Method Using Cuk Converter," *IEEE Transactions on Industrial Electronics*, vol. 58, no. 4, pp. 1154–1161, Apr. 2011.
- [69] C. Yang, C. Hsieh, F. Feng, and K. Chen, "Highly Efficient Analog Maximum Power Point Tracking (AMPPT) in a Photovoltaic System," *IEEE Transactions on Circuits and Systems I: Regular Papers*, vol. 59, no. 7, pp. 1546–1556, Jul. 2012.
- [70] D. Dondi, A. Bertacchini, D. Brunelli, L. Larcher, and L. Benini, "Modeling and Optimization of a Solar Energy Harvester System for Self-Powered Wireless Sensor Networks," *IEEE Transactions on Industrial Electronics*, vol. 55, no. 7, pp. 2759–2766, Jul. 2008.
- [71] O. Lopez-Lapena, M. T. Penella, and M. Gasulla, "A New MPPT Method for Low-Power Solar Energy Harvesting," *IEEE Transactions on Industrial Electronics*, vol. 57, no. 9, pp. 3129–3138, Sep. 2010.
- [72] M. A. Elgendy, B. Zahawi, and D. J. Atkinson, "Assessment of Perturb and Observe MPPT Algorithm Implementation Techniques for PV Pumping Applications," *IEEE Transactions on Sustainable Energy*, vol. 3, no. 1, pp. 21–33, Jan. 2012.
- [73] M. A. S. Masoum, H. Dehbonei, and E. F. Fuchs, "Theoretical and experimental analyses of photovoltaic systems with voltage and current-based maximum power-

- point tracking,” *IEEE Transactions on Energy Conversion*, vol. 17, no. 4, pp. 514–522, Dec. 2002.
- [74] K. Kobayashi, H. Matsuo, and Y. Sekine, “A novel optimum operating point tracker of the solar cell power supply system,” in *2004 IEEE 35th Annual Power Electronics Specialists Conference (IEEE Cat. No.04CH37551)*, 2004, pp. 2147–2151.
 - [75] B. Bekker and H. J. Beukes, “Finding an optimal PV panel maximum power point tracking method,” in *2004 IEEE Africon. 7th Africon Conference in Africa (IEEE Cat. No.04CH37590)*, 2004, vol. ol.1, pp. 1125–1129.
 - [76] S. Yuvarajan, “Photo-voltaic power converter with a simple maximum-power-point-tracker,” in *Proceedings of the 2003 International Symposium on Circuits and Systems, 2003. ISCAS '03.*, 2003, vol. 3, pp. III–399–III–402.
 - [77] M. a. Abido and N. a. Al-Ali, “Multi-Objective Optimal Power Flow Using Differential Evolution,” *Arabian Journal for Science and Engineering*, vol. 37, no. 4, pp. 991–1005, Apr. 2012.
 - [78] A. Mohamed and H. Shareef, “Hopfield Neural Network Optimized Fuzzy Logic Controller for Maximum Power Point Tracking in a Photovoltaic System,” *International Journal of Photoenergy*, vol. 2012, pp. 1–13, 2012.
 - [79] B. N. Alajmi, K. H. Ahmed, S. J. Finney, and B. W. Williams, “Fuzzy-Logic-Control Approach of a Modified Hill-Climbing Method for Maximum Power Point in Microgrid Standalone Photovoltaic System,” *IEEE Transactions on Power Electronics*, vol. 26, no. 4, pp. 1022–1030, Apr. 2011.
 - [80] Y. Zheng, C. Wei, and S. Lin, “A maximum power point tracking method based on tabu search for PV systems under partially shaded conditions,” in *IET Conference on Renewable Power Generation (RPG 2011)*, 2011, pp. 52–52.
 - [81] H. Taheri, Z. Salam, and K. Ishaque, “A novel Maximum Power Point tracking control of photovoltaic system under partial and rapidly fluctuating shadow conditions using Differential Evolution,” in *2010 IEEE Symposium on Industrial Electronics and Applications (ISIEA)*, 2010, no. Isiea, pp. 82–87.
 - [82] M. Kaliamoorthy and V. Rajasekaran, “A novel MPPT scheme for solar powered boost inverter using evolutionary programming,” in *2011 International conference on recent advancement in electrical , electronics and control engineering.*, 2011, pp. 346–351.

- [83] K. Ishaque, Z. Salam, H. Taheri, and A. Shamsudin, "Maximum Power Point Tracking for PV system under partial shading condition via particle swarm optimization," in *2011 IEEE Applied Power Electronics Colloquium (IAPEC)*, 2011, vol. 2, no. 2, pp. 5–9.
- [84] R. Ramaprabha, V. Gothandaraman, K. Kanimozhi, R. Divya, and B. L. Mathur, "Maximum power point tracking using GA-optimized artificial neural network for Solar PV system," in *2011 1st International Conference on Electrical Energy Systems*, 2011, no. 1, pp. 264–268.
- [85] M. S. Ngan and C. W. Tan, "Multiple Peaks Tracking Algorithm using Particle Swarm Optimization Incorporated with Artificial Neural Network," in *World Academy of Science, Engineering and Technology*, 2011, pp. 379–385.
- [86] F. Liu, S. Duan, F. Liu, B. Liu, and Y. Kang, "A Variable Step Size INC MPPT Method for PV Systems," *IEEE Transactions on Industrial Electronics*, vol. 55, no. 7, pp. 2622–2628, Jul. 2008.
- [87] S. Premrudeepreechacharn and N. Patanapirom, "Solar-array modelling and maximum power point tracking using neural networks," in *2003 IEEE Bologna Power Tech Conference Proceedings*, 2003, vol. 2, pp. 419–423.
- [88] K. Chao, M. Wang, and Y. Lee, "An extension neural network based incremental MPPT method for a PV system," in *2011 International Conference on Machine Learning and Cybernetics*, 2011, pp. 654–660.
- [89] M. Tsai, C. Tseng, G. Hong, and S. Lin, "A novel MPPT control design for PV modules using neural network compensator," in *2012 IEEE International Symposium on Industrial Electronics*, 2012, pp. 1742–1747.
- [90] M. A. Younis, T. Khatib, M. Najeeb, and M. Ariffin, "An Improved Maximum Power Point Tracking Controller for PV Systems Using Artificial Neural Network," in *Przeglad Elektrotechniczny (Electrical Review)*, 2012, no. 3, pp. 116–121.
- [91] C. Won, D. Kim, S. Kim, W. Kim, and H. Kim, "A new maximum power point tracker of photovoltaic arrays using fuzzy controller," in *Proceedings of 1994 Power Electronics Specialist Conference - PESC'94*, 1994, pp. 396–403.
- [92] A. El Khateb, N. A. Rahim, J. Selvaraj, and M. N. Uddin, "Fuzzy logic controller based SEPIC converter of maximum power point tracking," in *2012 IEEE Industry Applications Society Annual Meeting*, 2012, pp. 1–9.

- [93] A. Moreno, J. Julve, S. Silvestre, and L. Castaner, "A fuzzy logic controller for stand alone PV systems," in *Conference Record of the Twenty-Eighth IEEE Photovoltaic Specialists Conference - 2000 (Cat. No.00CH37036)*, 2000, pp. 1618–1621.
- [94] M. Godoy Simões and N. N. Franceschetti, "Fuzzy optimisation-based control of a solar array system," *IEE Proceedings - Electric Power Applications*, vol. 146, no. 5, p. 552, 1999.
- [95] N. Patcharaprakiti and S. Premrudeepreechacharn, "Maximum power point tracking using adaptive fuzzy logic control for grid-connected photovoltaic system," in *2002 IEEE Power Engineering Society Winter Meeting. Conference Proceedings (Cat. No.02CH37309)*, 2002, vol. 1, pp. 372–377.
- [96] Z. Cheng, H. Yang, and Y. Sun, "FPGA-based PV systems fuzzy MPPT control algorithm," in *2010 Seventh International Conference on Fuzzy Systems and Knowledge Discovery*, 2010, no. Fskd, pp. 1244–1248.
- [97] B. N. Alajmi, K. H. Ahmed, S. J. Finney, and B. W. Williams, "A Maximum Power Point Tracking Technique for Partially Shaded Photovoltaic Systems in Microgrids," *IEEE Transactions on Industrial Electronics*, vol. 60, no. 4, pp. 1596–1606, Apr. 2013.
- [98] T. L. Kottas, Y. S. Boutalis, and A. D. Karlis, "New Maximum Power Point Tracker for PV Arrays Using Fuzzy Controller in Close Cooperation With Fuzzy Cognitive Networks," *IEEE Transactions on Energy Conversion*, vol. 21, no. 3, pp. 793–803, Sep. 2006.
- [99] L. K. Letting, J. L. Munda, and A. Hamam, "Particle swarm optimized T-S fuzzy logic controller for maximum power point tracking in a photovoltaic system," in *2010 Conference Proceedings IPEC*, 2010, pp. 89–94.
- [100] N. Khaehintung, A. Kunakorn, and P. Sirisuk, "A novel fuzzy logic control technique tuned by particle swarm optimization for maximum power point tracking for a photovoltaic system using a current-mode boost converter with bifurcation control," *International Journal of Control, Automation and Systems*, vol. 8, no. 2, pp. 289–300, Apr. 2010.
- [101] a. Messai, a. Mellit, a. Guessoum, and S. a. Kalogirou, "Maximum power point tracking using a GA optimized fuzzy logic controller and its FPGA implementation," *Solar Energy*, vol. 85, no. 2, pp. 265–277, Feb. 2011.

- [102] J.-S. R. Jang, "ANFIS: adaptive-network-based fuzzy inference system," *IEEE Transactions on Systems, Man, and Cybernetics*, vol. 23, no. 3, pp. 665–685, 1993.
- [103] J.-S. R. Jang, "Neuro-fuzzy modeling and control," *Proceedings of the IEEE*, vol. 83, no. 3, pp. 378–406, Mar. 1995.
- [104] A. M. S. Aldobhani and R. John, "Maximum Power Point Tracking of PV System Using ANFIS Prediction and Fuzzy Logic Tracking," in *International MultiConference of Engineers and Computer Scientists (IMECS)*, 2008, vol. II, pp. 19–21.
- [105] F. Mayssa and L. Sbita, "Advanced ANFIS-MPPT control algorithm for sunshine photovoltaic pumping systems," in *2012 First International Conference on Renewable Energies and Vehicular Technology*, 2012, pp. 167–172.
- [106] H. Abu-Rub, A. Iqbal, S. Moin Ahmed, F. Z. Peng, Y. Li, and G. Baoming, "Quasi-Z-Source Inverter-Based Photovoltaic Generation System With Maximum Power Tracking Control Using ANFIS," *IEEE Transactions on Sustainable Energy*, vol. 4, no. 1, pp. 11–20, Jan. 2013.
- [107] J. A. Duffie and W. A. Beckman, *Solar Engineering of Thermal Processes*, 3rd ed. 2006.
- [108] J. Nelson, *The Physics of Solar Cells*. London: Imperial College Press, London, 2003.
- [109] U. Stutenbaeumer and B. Mesfin, "Equivalent model of monocrystalline, polycrystalline and amorphous silicon solar cells," *Renewable Energy*, vol. 18, no. 4, pp. 501–512, Dec. 1999.
- [110] R. Ramaprabha and B. L. Mathur, "A Comprehensive Review and Analysis of Solar Photovoltaic Array Configurations under Partial Shaded Conditions," *International Journal of Photoenergy*, vol. 2012, pp. 1–16, 2012.
- [111] "Shell ST36 Photovoltaic Solar Module," *Shell solar data sheet*. [Online]. Available: www.shell.com/renewables.
- [112] R. Storn, "Differential Evolution – A Simple and Efficient Heuristic for Global Optimization over Continuous Spaces," pp. 341–359, 1997.
- [113] D. L. King, "Photovoltaic module and array performance characterization methods for all system operating conditions," in *AIP Conference Proceedings*, 1997, vol. 394, pp. 347–368.

- [114] D. Guimard, P. P. Grand, N. Bodereau, P. Cowache, J.-F. Guillemoles, D. Lincot, S. Taunier, M. Ben Farah, and P. Mogensen, "Copper indium diselenide solar cells prepared by electrodeposition," in *Conference Record of the Twenty-Ninth IEEE Photovoltaic Specialists Conference, 2002.*, pp. 692–695.
- [115] "Sun Power 230 Solar Panel," *Sunpower data sheet*. [Online]. Available: www.sunpowercorp.com.
- [116] A. Mellit and S. a. Kalogirou, "Artificial intelligence techniques for photovoltaic applications: A review," *Progress in Energy and Combustion Science*, vol. 34, no. 5, pp. 574–632, Oct. 2008.
- [117] Z. Q. Bo, A. Klimek, Y. L. Ren, and J. H. He, "A Real Time Digital Simulation System for Testing of Integrated Protection Schemes," in *2008 Joint International Conference on Power System Technology and IEEE Power India Conference*, 2008, pp. 1–5.
- [118] S. Foo, "Real time simulation of power flow control strategies for fuel cell vehicle with energy storage by using Real Time Digital Simulator (RTDS)," in *2009 IEEE 6th International Power Electronics and Motion Control Conference*, 2009, pp. 2323–2327.
- [119] P. G. McLaren, R. Kuffel, R. Wierckx, J. Giesbrecht, and L. Arendt, "A real time digital simulator for testing relays," *IEEE Transactions on Power Delivery*, vol. 7, no. 1, pp. 207–213, 1992.
- [120] User's Manual, "DSpace DS1104," in <http://www.dspace.com/en/pub/home/products/hw/singbord/ds1104.cfm>.
- [121] The DSpace Foundation, "DSpace 1.5.2 Manual," 2009.

LIST OF PUBLICATIONS

The following papers are published from the work described in this thesis:

Conference

- [1] Muhammad Sheraz, M. A. Abido , “An Efficient Approach for Parameter Estimation of PV Model Using DE and Fuzzy Based MPPT Controller”, ISGT 2013, IEEE Power and Energy Society, Denmark, 6-9 October 2013.(Submitted)
- [2] Muhammad Sheraz, M. A. Abido, “An Efficient Fuzzy Logic Based Maximum Power point Tracking Controller for Photovoltaic Systems”, International Conference on Renewable Energies and Power Quality (ICREPQ'13), Bilbao Spain, 20-22 March, 2013.
- [3] Muhammad Sheraz, M. A. Abido , “An Efficient Maximum Power Point Tracking (MPPT) controller using Differential Evolution and Neural Network”, PECON 2012, IEEE international Power and Energy conference.
- [4] Muhammad Sheraz, M. A. Abido , “Assessment of Maximum Power Point Tracking Techniques for Photovoltaic Systems”, 15th STEM 2012, IEEE 15th Saudi Technical Exchange Meeting.

Journals

- [5] “An efficient Maximum Power Point Tracking Controller for PV systems using ANFIS” (ready to submit)
- [6] “A Novel Parameter Estimation Method for PV model using Differential Evolution” (under preparation)

VITAE

Name: Muhammad Sheraz Khalid

Date of birth: 4 March, 1988

Nationality: Pakistani

Present Address: KFUPM P.O. Box # 8606, King Fahd University of
Petroleum and Mineral, Dhahran - 31261, Saudi Arabia

Permanent Address: P.O. Box # 120389, Jeddah - 21322, Saudi Arabia

Email Address: isheraz@kfupm.edu.sa
sheraz_176@hotmail.com

Educational Qualification:

M.S (Electrical Power Engineering)

April, 2013

King Fahd University of Petroleum and Mineral,
Dhahran, Saudi Arabia.

B.Sc. (Electrical Engineering)

June, 2010

University of Engineering and Technology,
Lahore, Pakistan.

